AD-A008 533

GUIDE FOR THE DESIGN OF CONTROL STICKS IN VIBRATION
ENVIRONMENTS

William H. Levison, et al

Bolt Beranek and Newman, Incorporated

Prepared for:

Aerospace Medical Research Laboratory

February 1975

NOTICES

The experiments reported herein were conducted according to the "Guide for the Care and Use of Laboratory Animals," DHEW 73-23.

The voluntary informed consent of the subjects used in this research was obtained as required by Air Force Regulation 80-33.

This technical report has been reviewed and is approved for publication.

FOR THE COMMANDER

HENNING E. VON GIERKE
Director
Biodynamics and Bionics Division
Aerospace Medical Research Laboratory

AIR FORCE/56780/30 April 1975 — 100

1a

ACCESSION for		
NTIS	White Section	☑
DDC	Buff Section	☐
UNANNOUNCED		☐
JUSTIFICATION		
BY		
DISTRIBUTION/AVAILABILITY CODES		
Dist.	AVAIL. and/or SPECIAL	

Unclassified

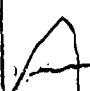| REPORT DOCUMENTATION PAGE		READ INSTRUCTIONS BEFORE COMPLETING FORM
1. REPORT NUMBER AMRL-TR-74-127	2. GOVT ACCESSION NO.	3. RECIPIENT'S CATALOG NUMBER AD-A008 533
4. TITLE (and Subtitle) GUIDE FOR THE DESIGN OF CONTROL STICKS IN VIBRATION ENVIRONMENTS		5. TYPE OF REPORT & PERIOD COVERED Final report
		6. PERFORMING ORG. REPORT NUMBER 6863
7. AUTHOR(s) William H. Levison Philip D. Houck, 1/Lt, USAF		8. CONTRACT OR GRANT NUMBER(s) F33615-74-C-4041
9. PERFORMING ORGANIZATION NAME AND ADDRESS Bolt Beranek and Newman, Inc 50 Moulton St. Cambridge, Mass 02138		10. PROGRAM ELEMENT, PROJECT, TASK AREA & WORK UNIT NUMBERS 62202F 7231 01 69
11. CONTROLLING OFFICE NAME AND ADDRESS Aerospace Medical Research Laboratory, Aerospace Medical Division, Air Force Systems Command, Wright-Patterson Air Force Base, Ohio 45433		12. REPORT DATE February 1975
		13. NUMBER OF PAGES ~~101~~ 154
14. MONITORING AGENCY NAME & ADDRESS(If different from Controlling Office)		15. SECURITY CLASS. (of this report) Unclassified
		15a. DECLASSIFICATION DOWNGRADING SCHEDULE

16. DISTRIBUTION STATEMENT (of this Report)

Approved for public release; distribution unlimited

17. DISTRIBUTION STATEMENT (of the abstract entered in Block 20, if different from Report)

18. SUPPLEMENTARY NOTES

19. KEY WORDS (Continue on reverse side if necessary and identify by block number)

Manual Control   Spring Gradient
Human Dynamic Response
Vibration
Control Stick Design

20. ABSTRACT (Continue on reverse side if necessary and identify by block number)
A set of manual control experiments was conducted to determine the effects of control-stick parameters on tracking performance in a vibration environment. Preliminary experimental variables were stick design parameters, stick location, and presence or absence of vibration. Stick parameters had little effect on rms tracking error under vibration conditions for the particular aircraft dynamics that were used in this study. Considerable effect on control activity was observed, however, which suggests that stick design parameters will significantly influence

DD FORM 1 JAN 73 1473   EDITION OF 1 NOV 65 IS OBSOLETE

i

overall performance in systems that respond at vibration frequencies. Stick location had no significant effect on either tracking or biodynamic performance measures. The vibration-correlated component of tracking error was relatively small, vibration effects were accounted for largely by changes in pilot model parameters related to visual resolution, time delay, and motor-related remnant. A model based guide for the design of control sticks in a vibration environment is described. This model is based on the state-variable model for pilot/vehicle systems. Effects of vibration are represented as additional model elements and by changes in pilot-related parameters of the tracking model.

PREFACE

The experiments were conducted at the vibration branch of
the Aerospace Medical Research Laboratory. They were made
possible by the conscientious and skilled efforts of Mr. Louis
Muhic, University of Dayton and T. Sgt. Philip McCain.
Mr. Charles Clauser of the AMRL kindly took the anthropometric
measurements of the subjects.

Lt. Philip D. Houck was the technical monitor for this
contract and project engineer for the AMRL experimental
program. Lt. Houck is the author of Section 2 of this
report.

TABLE OF CONTENTS

LIST OF FIGURES

LIST OF FIGURES (Continued)

LIST OF TABLES

1. INTRODUCTION AND SUMMARY

1.1   Objective of this Report

In recent years aircraft have been constructed such that
they can perform in environments that severely tax or exceed the
limits of human tolerance. Severe vibration is one such environ-
ment.

Whole-body vibration acts in a number of ways to cause
performance degradation of manned vehicle systems. Vibration
is transmitted to the seat of the pilot by the aircraft and
propagates through the pilot's torso and arm to the control
stick to produce control inputs that are linearly correlated
with the vibration input. Vibration also increases the
stochastic portion of the pilot's control activity (i.e.,
"remnant") due partly to visual interference effects (e.g.,
blurring due to relative eye-display motion) and, to a greater
extent, to motor interference effects such as noise injected
into proprioceptive feedback paths.

The effects of vibration on control performance are to
some extent influenced by the design of the control stick.
Accordingly, the Aerospace Medical Research Laboratory has
recently completed a series of man-in-the-loop experiments to
determine mathematically the relation between control-stick
design parameters and tracking performance in a vibration
environment. The objective of this report is to summarize the
results of this experimental study and to propose guidelines
for the design of control sticks in vibration environments.

1

1.2   Summary of Experimental Results

The primary variables of the experimental program were (a) stick design parameters, (b) stick location, and (c) presence or absence of whole-body vibration. Six stick configurations were explored: three "spring sticks" having relatively low spring gradients, and three "stiff sticks" having substantially larger spring gradients. Side and center stick locations were explored. A single z-axis sum-of-sines vibration environment was used in this program, and the biodynamic environment (pilot/seat interface, seat/platform interface, etc.) was kept as invariant as possible. Some of the important experimental results are summarized below.

Effects of Stick Parameters. Stick design had relatively little effect on tracking error under vibration conditions for the aircraft dynamics that were used, but considerably greater control activity was observed for the stiff sticks than for the spring sticks. This control activity could cause problems if the system or subsystem responds to those frequencies.

Vibration Feedthrough. Stick design parameters influenced primarily the vibration-correlated (i.e., "feedthrough") component of tracking error. These effects can be represented by an impedance model which includes the stick impedance plus two impedance functions, independent of stick design, that account for biodynamic response behavior.

Vibration Interference Effects. Feedthrough accounted for a small fraction (less than 10%) of the tracking error variance. In terms of the pilot/vehicle model employed in the analysis, the primary effects appear to be an increase in motor-related remnant and an increase in time delay. Visual effects appear to be secondary.

2

Model Results. Good agreement between model outputs and experimental measures were obtained for the six control stick configurations with a fixed set of model parameter values.

Stick Location. Stick location had no significant effect on rms tracking score, nor were significant effects observed on rms head, shoulder, or elbow accelerations.

Individual Differences. Individual differences with regard to biodynamic response measures, relative to mean performance, were generally no greater than subject-to-subject differences in tracking performance. Furthermore, not all such differences were statistically significant. Thus, it is reasonable to analyze performance of the "average man".

1.3 Nature of the Design Guide

If we were to follow traditional format, the design guide would consist of a set of tables and charts to allow rapid, straightforward optimization of control stick parameters for a variety of aircraft and for a variety of vibration and biodynamic environments. Perhaps the greatest obstacle to the development of a guide of this sort is the inability to extend existing results to other vibration and biodynamic environments. Comprehensive measures of tracking performance have not been obtained in a wide variety of such environments, and reliable theoretical models for biodynamic response behavior and for vibration-related interference effects are lacking to allow extrapolation of existing results.

Another potential problem is posed by the complexity of
the interaction between control task parameters, stick design,
vibration parameters, and biodynamic response mechanisms. All
these factors interact in ways that are not entirely linear to
influence tracking performance. Thus, it is not clear at this
point that a handbook-type guide could be provided for general
application without requiring an inordinate cataloguing of task
situations.

We therefore propose in this document a design guide based
on a rather extensive model with demonstrable predictive capabi-
lities. With such a model, the designer can not only optimize
the design of the control stick, but he can also explore the
effects of other important factors on pilot behavior and
overall system performance.

The model-based guide proposed in this report is built
around the state-variable, or "optimal-control" model for pilot/
vehicle systems. Vibration effects are accounted for by addi-
tional model elements and by changes in pilot-related parameters
of the tracking model. The procedure for using the proposed
model to predict the effects of stick parameters on tracking
performance is diagrammed in Figure 1 and is summarized below:

1. System dynamics are represented in state-variable
    format. Control-stick and display dynamics, as well
    as frequency-shaping of the tracking input, are
    included in this formulation.

2. Pilot-related model parameters not affected by
    vibration are assigned values from well-documented
    studies of pilot/vehicle performance in non-
    vibration environments.

4
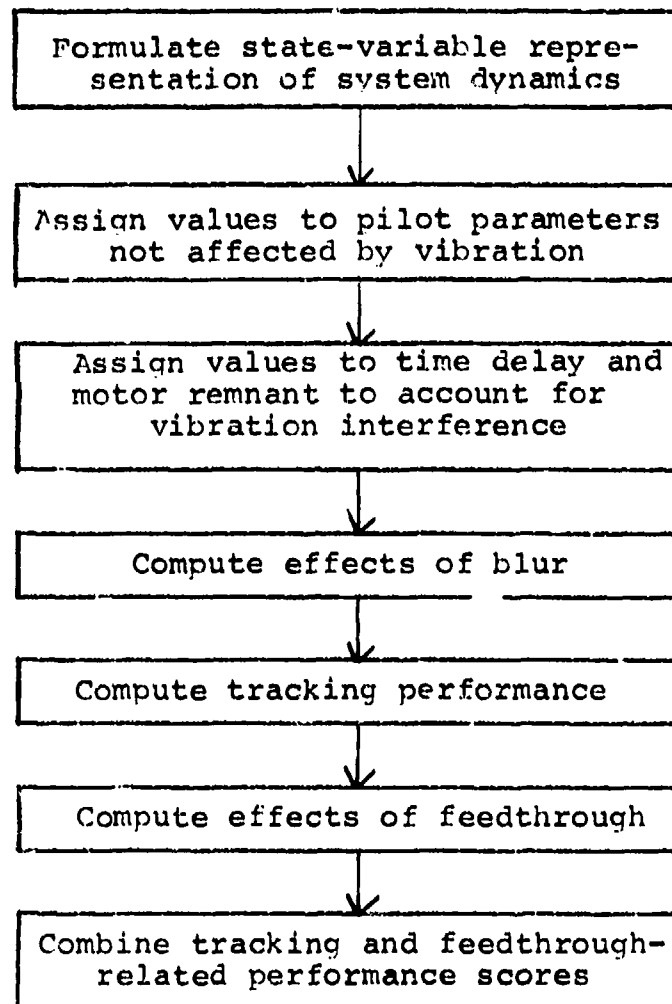
Figure 1. Procedure for Predicting Tracking Performance

3. Model parameters relating to pilot time delay and motor-related sources of pilot remnant are assigned values to reflect the effects of the vibration.

4. Describing functions relating head motion to platform acceleration are used to determine relative motion between the eye-point-of-regard and the display. This motion variable determines the value of a model parameter related to visual resolution limitations.

5. Having quantified all parameters of the pilot/vehicle model, predictions of tracking performance (including remnant) are now obtained.

6. The impedance model for stick feedthrough is analyzed to predict vibration-correlated stick motion for the stick configuration of interest, and the variance of the tracking error due to feedthrough is computed.

7. Error variance related to feedthrough is added to the variance score with the pilot/vehicle model to yield total error variance.

8. Since a change in stick parameters will generally affect both tracking performance as well as feedthrough, the entire procedure is repeated to explore the effects of changing one or more parameters of the control stick.

Once reliable theoretical models for biodynamic response mechanisms and vibration-related interference effects become available, it will be possible to use this model to explore the interactions between optimal stick design and factors such as vehicle dynamics, vibration parameters, and biodynamic environment. If some of these interactions are found to be unimportant, or if they can be accounted for in a simple manner, it may then be possible to define a set of guidelines in handbook format.

1.4   Limitations of the Design Guide

Because we lack reliable models for extrapolating existing results to other vibration and biodynamic environments, the design guide described in this report is intended to apply strictly to the biodynamic/vibration environment employed in the recent experimental study. Because of the demonstrated capability of the pilot/vehicle model to predict tracking performance in a variety of control situations, however, we expect the guide to be useful in exploring tracking tasks and stick designs beyond those studied in the laboratory. If the guide is to be extended to other biodynamic and/or vibration environments, "calibration" experiments will have to be performed to determine the effects of vibration on pilot parameters and to quantify relevant biodynamic response mechanisms.

The reader should be aware that the control-stick design influences primarily vibration feedthrough, which typically accounts for a small portion of the increment in tracking error due to vibration. Stick design is an important consideration nonetheless, for an inappropriate choice of parameters can result in much greater feedthrough than is necessary and/or require control forces or displacements that are outside the range of efficient tracking performance.

7

1.5   Suggested Areas for Further Research

The following areas of research are suggested for improving our understanding of the relationship between tracking performance and vibration and thereby allowing development of a more general design guide.

Biomechanical Models.   Considerable effort is required to develop reliable theoretical models for biomechanical response mechanisms so that the effects of vibration on head, body, and stick motions can be predicted for a variety of biodynamic and vibration environments.

Tracking Interference Effects.   Theoretical models are desired for predicting the effects of vibration on changes in pilot-related model parameters — particularly motor-related remnant parameters and time delay.   Further experimentation with different vibration spectra and different biodynamic environments would be needed to develop such models.

Further Development of Pilot/Vehicle Model.   The existing state-variable pilot/vehicle model is in a high state of development in that performance can be predicted for a variety of tracking situations with a consistent set of model parameters.   Nevertheless, further theoretical study is suggested to refine aspects of the model related to motor limitations; specifically, to isolate one or more parameters that account entirely for (and only for) degradation of motor-related sensory information.

Biodynamic Response Linearity. Experimental studies are needed to determine the extent to which biodynamic response mechanisms are linear. The existence of such linearity would greatly facilitate extension of the proposed design guide to additional vibration environments. Experimentation with various vibration spectra and amplitudes are required to explore linearity.

1.6 Organization of the Report

The main text of this report is devoted primarily to definition and illustration of the design guide; detailed exposition of experimental results is reserved for the Appendices.

The biodynamic/vibration environment to which the design guide applies is defined in Section 2, and other aspects of the experimental program are described. The model structure underlying the design guide is described as generally as possible in Section 3. Section 4 presents the design guide in more quantitative terms, and three numerical examples are presented. The guide is validated against data obtained in the experimental program, and design curves for stick gain and stick damping are presented for a specific tracking situation.

Analysis procedures used for data analysis are presented in Appendix A. Detailed discussions of experimental results are given in Appendices B (biodynamics response measures) and C (tracking performance). Some details of the model analysis are given in Appendix D, and we review methods for differentiating among potential vibration-related interference mechanisms. Anthropometric measurements of the test subjects are tabulated in Appendix E.

2. EXPERIMENTAL DESIGN

2.1 Purpose of These Experiments

The pilot controlling an aircraft in vibration environment shows degradation of performance due to noisy proprioceptive feedback and direct vibration feedthrough from the shoulder to the control stick. The primary interfacing of the pilot to the aircraft is through his motor control system and the control stick. The stiffness of the stick will determine how much of the vibration signal is allowed to enter the control loop and also gives the pilot proprioceptive feedback according to the "feel" of the stick. The purpose of these experiments was to find how pilot aircraft performance is effected by control stick parameters such as location, spring gradient, damping, and electrical gain. The objective is to provide the aircraft design community with control stick design criteria that will allow pilots in particular aircrafts to perform optimally in a vibration environment.

2.2 Experiment Design

The experiment that was conducted consisted of subjects flying a single axis compensatory tracking task with a simple integrator as the aircraft dynamics. The parameters of the experiment were whole-body vibration or absense of vibration and six control sticks varying from 2 lb/in to 600 lb/in in spring gradient. Each of the control sticks was arranged in both the side and center location. The control stick gain for each of the six sticks was held constant and is listed in

Table 4 (p. 54). The three spring sticks had a constant electrical displacement gain of 2.5 volts/in. Both the light and medium stiff sticks had the same electrical force gain of .9 volts/lb; whereas, the heavy stiff stick had a gain of only .5 volt/lb.

The 10 subjects participating in the experiment were members of the hazardous duty panel. Seven of the subjects participated in all of the experimental conditions and these subjects were used as the data base. The body structure of the subjects varied from large to small and covered most of the range of present aircrew. Since body size could influence transmission of the vibration signal to the control (e.g., a short man requires greater extension of his arm to reach the controls), the control configuration was fixed to allow investigation of the effects of body size. A table of anthropometric measurements obtained from the test subjects is given in Appendix E.

The following figures and diagrams describe the experimental set up. The tracking task is diagramed in Figure 2 and the control and subject orientation on the SIXMODE is demonstrated in Figures 2, 3-5. The bite bar that was held between the subjects' teeth was used to determine rotational and translational motion of the head so that a correlation could be made between visual degradation and head motion of the pilot. An accelerometer was also mounted on the subject's shoulder and elbow to measure the vibration transmitted through the body. All data was recorded without pre-processing on a 14-channel FM recorder. This system and the tracking simulation is shown in Figure 6.

11
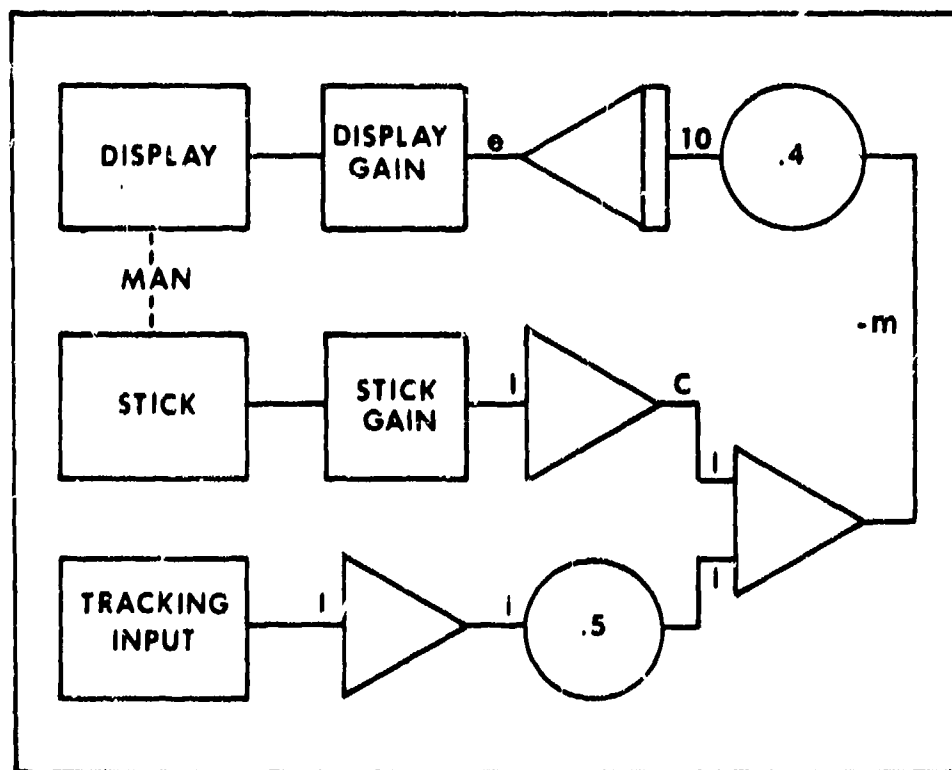
Figure 2. Tracking Task
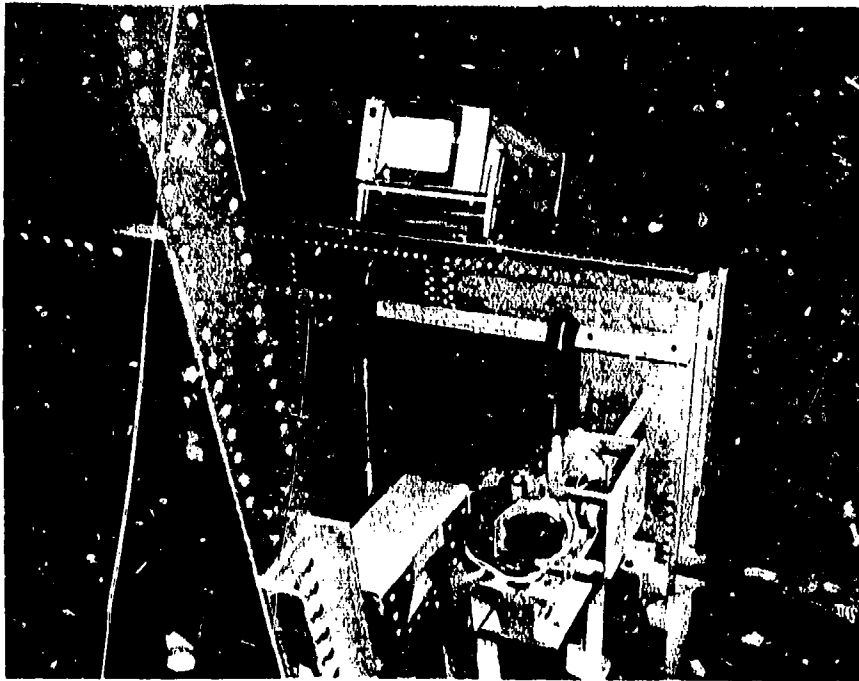
Figure 3. Control Stick and Display Configuration

Figure 4. Sixmode Vibration Table

13
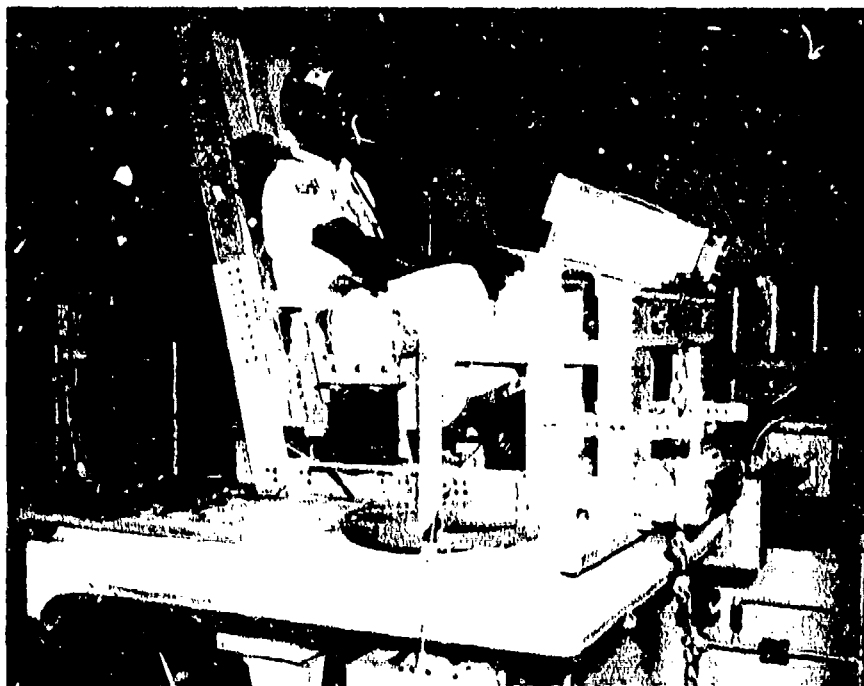
Figure 5. Subject Instrumentation
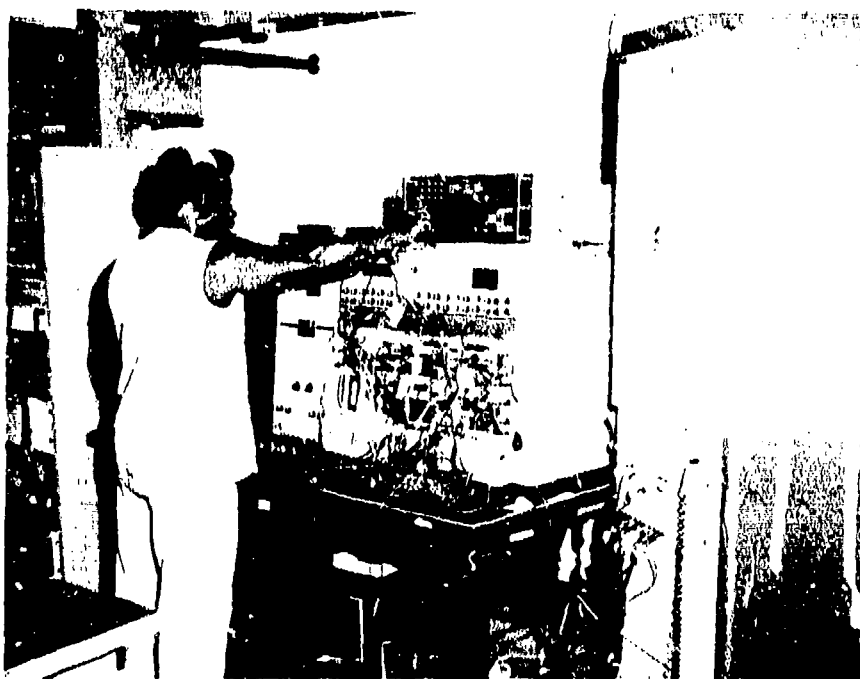
Figure 6. Data Recording and Task Simulation

14

The vibration environment was supplied by a large amplitude multi-degree of freedom hydraulic vibration table named the SIXMODE. It has six degrees of motion including x, y, z, roll, pitch and yaw. This table has a payload capacity of 1,000 lbs. and is capable of sinusoidal, sum of sines and random vibration. The experiment used a sum of five sines vibration with equal acceleration at 2, 3.3, 5, 7 and 10 hertz. The RMS level of table acceleration was approximately 0.3 g and had a crest factor of 3 giving the subject a maximum peak acceleration of about 1 g depending on how the sines added together. The acceleration input is very clean (for a hydraulic shaker) because of the elastomeric couplers, which filter out extraneous hydraulic inputs.

2.3   Vibration Feedthrough Example

Vibration feedthrough and its possible effects on control systems is demonstrated in the time traces of typical error and control signals shown in Figure 7. Static and vibration conditions are displayed for spring sticks and stiff sticks. The vibration feedthrough is quite evident in the stiff stick controller. The error signal contains a much smaller feedthrough component because of the filtering of the simulated vehicle dynamics (an integrator); nevertheless, some of the vibration peaks can be seen in the error signal. With the spring stick, the dynamics of the stick itself filters much of the vibration, giving by far a smoother signal. These considerations of vibration feedthrough are very important and should be considered in the development of all new systems.

15
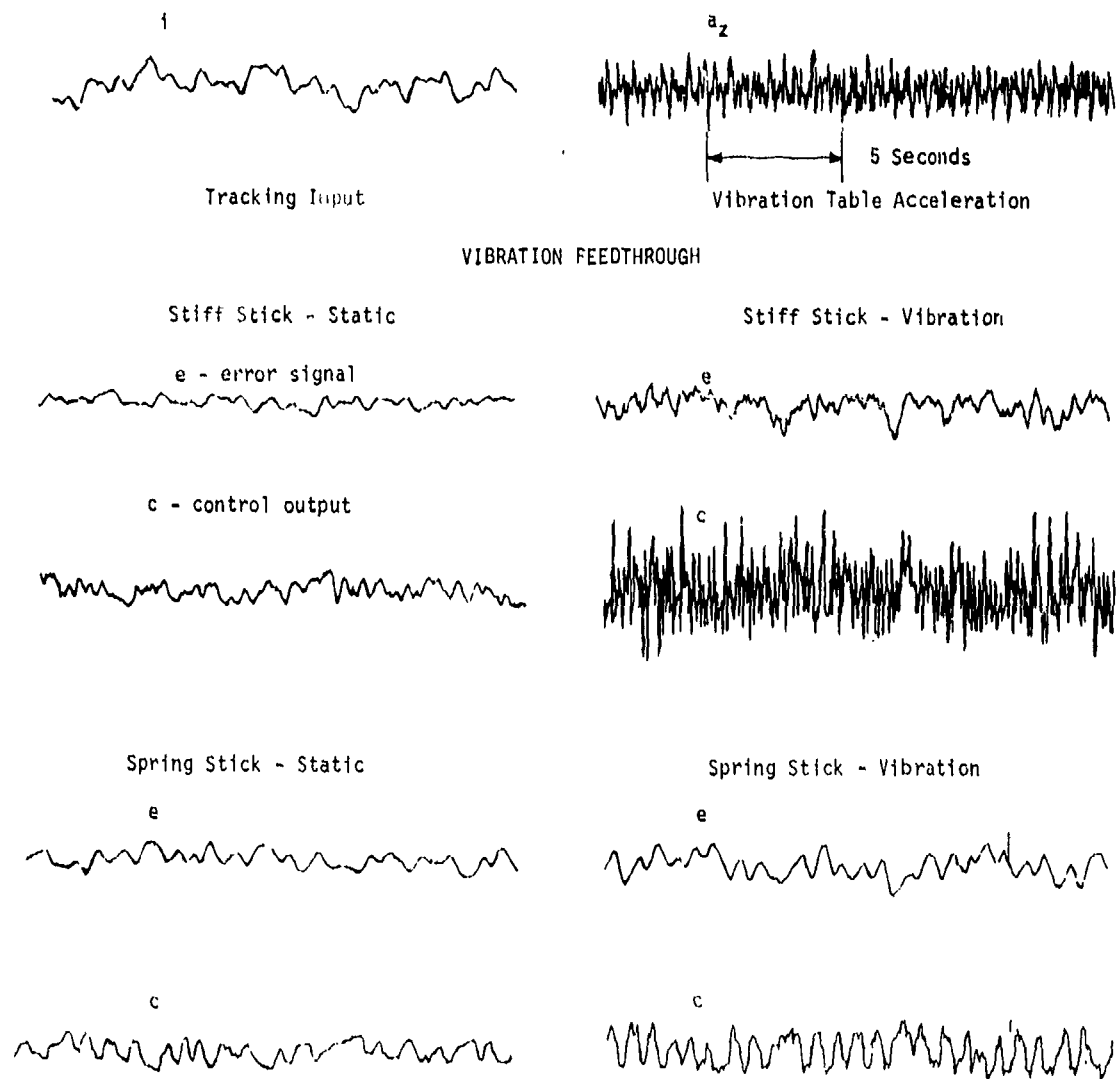
Figure 7. Time Traces of Error and Control Signals

2.4   Predictiveness of the Model

In addition to baseline experiments, another was performed to test the predictiveness of the model that was developed in this study. The results of the experiment and prediction are displayed in Table 1. For this case, the "light stiff" stick configuration defined in Table 4 was used, with the electrical gain reduced from 0.9 to 0.45 volt/lb.

Table 1

Comparison of Predicted and Measured Performance

"Light Stiff" Control Stick

Variable	RMS Performance Score	
	Measured	Predicted
a. Static Environment		
Error	.378	.341
Control	.344	.372
b. Vibration Environment		
Error	.463	.473
Control	.747	.708

3. MODEL STRUCTURE

3.1 Overview

Because tracking performance depends on the specifics of the tracking task, the properties of the control stick, and the nature of the vibration and biodynamic environments in a complex manner, some form of predictive model is mandatory if we are to analytically explore the effects of these parameters on performance. We have therefore derived a model-based guide for the design of control sticks in vibration environments. The models underlying the design guide are the subject of this section; the design guide itself is described in Section 4.

The key model element of the design guide is a pilot/vehicle model that relates system performance and pilot tracking behavior to elements of the control sy'tem such as plant dynamics, control-stick properties, and external tracking disturbances. The effects of vibration are represented partly as additional model components and partly as changes in values assigned to certain parameters of the basic pilot/vehicle model.

A skeletal outline of the model structure is shown in Figure 8. For simplicity of exposition, we consider a control situation of the type explored in the current study: namely, a single-input, single-output control system subject to vibration disturbances in a single axis. This model can be readily extended to include multi-input, multi-output systems.

The pilot is assumed to observe a compensatory display of tracking error and to manipulate a single control stick. Because the pilot will generally extract velocity as well as displacement

19
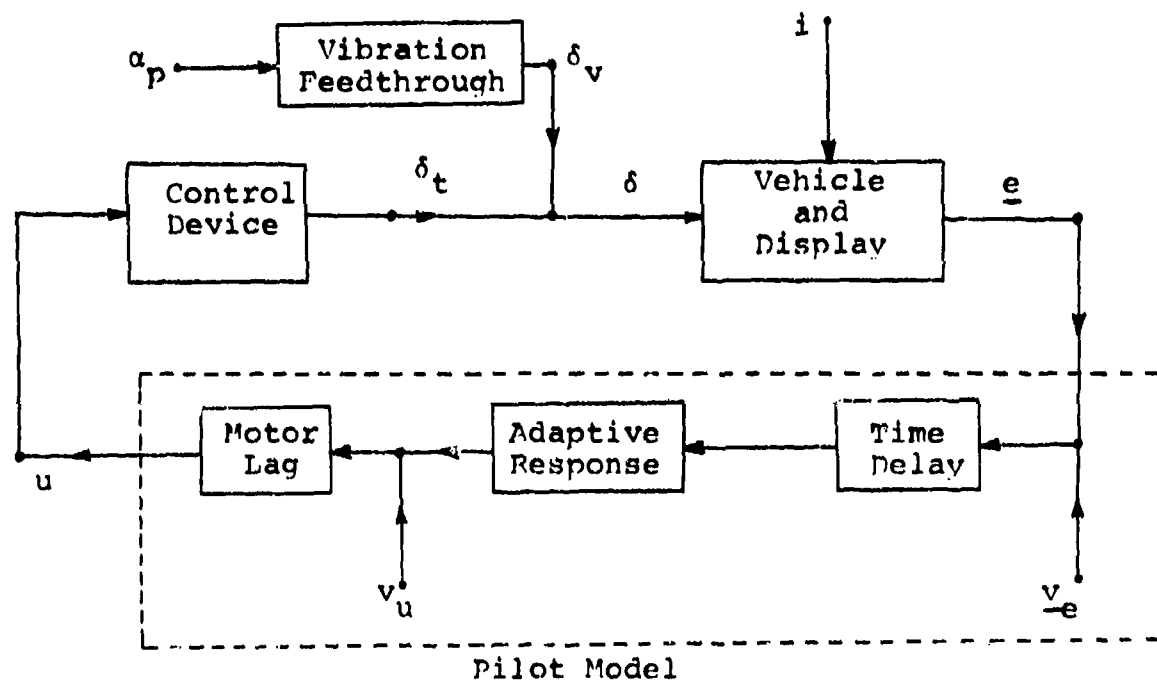
Figure 8. Outline of the Model Structure

information from the error indicator, tracking error is shown in Figure 8 as a vector quantity. The system is assumed to be disturbed by one or more zero-mean Gaussian random processes "i" which we designate as "tracking inputs" to differentiate from vibration inputs. In laboratory situations, tracking inputs are usually added in parallel with the pilot's control (to simulate wind gusts acting on the vehicle, for example) or in parallel with the vehicle output (i.e., as a command input).

We consider the control input "δ" to be the sum of two components: δ_t, the control input that is intended to minimize tracking error, and δ_v, an input correlated with the platform vibration input α_p that results from biomechanical vibration feedthrough. The signal δ_t includes both the response to the tracking error as well as wide-band stochastic behavior (i.e., "pilot remnant").

The control signal "u" that is actually generated by the pilot is converted to the electrical input "δ_t" in a manner determined by the mechanical and electrical properties of the control device. If the electrical output of the device is proportional to stick displacement, the following relationship obtains: $\delta(s) = K_c \cdot U(s)/ZS(s)$ where K_c is the constant of proportionality and $ZS(s)$ is the force/displacement characteristic of the control device in complex notation. Although not shown explicitly in Figure 3-1, vibration feedthrough is also influenced by the properties of the stick, as discussed shortly.

Pilot randomness is represented by a set of observation and motor noise processes. The pilot's perceptions of error displacement and error rate are assumed to be perturbed by white noise processes $\underline{v}_e$, and an additional motor noise process v_u is assumed to perturb control activity. Other pilot-related

21

limitations include an effective processing delay ("time delay" in Figure 8 associated for convenience with sensory inputs and a first-order low-pass filter ("motor lag") applied to the pilot's control response. Within the constraints imposed by the pilot's perception of the task and by the limitations mentioned above, the pilot will adapt his control strategy to achieve best performance.

Detailed discussion of the major components of the model follows. In Section 3.2 below, we review methods for predicting pilot behavior and system performance, and we describe the rationale for quantifying pilot limitations in non-vibration situations. The status of the biodynamic model elements is discussed in Section 3.3, and we discuss modifications to the basic pilot/vehicle model that are imposed by vibration environments.

3.2   Pilot/Vehicle Model

Predictions of pilot behavior and overall system performance are obtained with the aid of the state-variable (or "optimal-control") model for human estimation and control. The model is based on the assumption that the well-motivated, well-trained human operator behaves in a near optimal manner subject to his inherent constraints and limitations. Thus, once we have adequately described the control system, performance requirements, and pilot limitations, we can predict pilot behavior and system performance.

Detailed mathematical descriptions of the model, along with supporting experimental data, have been presented in the literature [1, 2]. Key features are reviewed below.

22

3.2.1 System Description

A linearized description of system dynamics is given by the
following state equation:

$$\dot{\underline{x}}(t) = \underline{A}\,\underline{x}(t) + \underline{B}\,u(t)\,\underline{E}\,\underline{w}(t)$$

where $\underline{x}(t)$ is the vector that describes the "state" of the vehicle,
$u(t)$ the pilot's (scalar) control input, and $\underline{w}(t)$ a vector of
wide-band ("white") driving noise processes. If the external
disturbances are rational noise spectra of first order or higher,
the resulting "input states" are included in the state vector $\underline{x}(t)$,
as are states that may be needed to represent dynamics of the
control device. In addition, tracking disturbances introduced
by linear mechanical feedthrough of the platform vibration can
be represented in this manner (provided, of course, that vibration
feedthrough can be described analytically).

The display variables used by the pilot are represented as
linear combinations of state variables as follows:

$$\underline{y}(t) = \underline{C}\,\underline{x}(t)$$

where the display vector $\underline{y}(t)$ typically includes both displacement
and rate variables for each physical display indicator. For a
single-variable tracking task in which system error $e(t)$ is the
only explicit display quantity, the (model) display vector contains
the two components:

$$y_1(t) = e(t)$$
$$y_2(t) = \dot{e}(t)$$

23

3.2.2 Performance Requirements

Performance requirements are specified in terms of a "cost" that is to be minimized. In the case of a single-variable tracking task, a good match between model and measured performance is obtained if we assume that the pilot is attempting to minimize a weighted sum of mean-squared tracking error plus mean-squared control rate. For a system perturbed by zero-mean disturbances, the cost [J] is defined as

$$J = \sigma_e^2 + G \, \sigma_{\dot{u}}^2$$

where G is the relative "cost weighting" associated with mean-squared control-rate activity. (We may assign a relative weighting of unity to mean-squared error with no loss of generality.) One of the consequences of assigning a cost weighting to control-rate, rather than to control displacement, is the introduction of a first-order lag in the predicted pilot describing function. We refer to the time constant of this lag network as the "motor time constant".

For a more realistic flight task in which the pilot manipulates a number of controls to regulate a number of flight variables, the cost will be defined as

$$J = \sum_{i=1}^{N_y} q_i \, \sigma_{y_i}^2 + \sum_{i=1}^{N_u} (r_i \, \sigma_{u_i}^2 + g_i \, \sigma_{\dot{u}_i}^2)$$

where N_y is the number of display variables; N_u the number of controls; and q_i, r_i, and g_i are the weighting coefficients associated with the various display, control, and control-rate variables, respectively.

24

Reasonable model predictions can be obtained if weighting coefficients are selected on the basis of maximum allowable deviations (or "limits") for problem variables [3]. A unit "cost" is associated with a given variable when the magnitude of the "error" (i.e., deviation from trim) is equal to the nominal limit. Thus, the weighting coefficient for each variable in the cost equation is computed simply as the inverse of the square of the corresponding limit.

3.2.3 Pilot Limitations

As noted above, model parameters that explicitly relate to pilot limitations are effective perceptual time delay, visual and motor noise processes, and, in the case of a single-variable task, the motor time constant. Numerical values for these parameters have been found to be remarkably invariant for a variety of tracking situations [1, 2]. Time delays have generally fallen within the range of 0.15 - 0.2 seconds, and motor time constants in the range of 0.08 to 0.1 seconds are typical.

A very simple model accounts for pilot remnant in situations where control gain is optimized and where visual threshold and saturation effects are negligible. In this case, both observation and motor noise processes appear to scale with the variance of the corresponding problem variables. Thus, in the single-variable tracking task, the variance of the injected white noise processes are

$$V_e = \sigma_e^2 \cdot P_e$$

$$V_{\dot{e}} = \sigma_{\dot{e}}^2 \cdot P_{\dot{e}}$$

$$V_u = \sigma_u^2 \cdot P_u$$

25

where P_e, $P_{\dot{e}}$, and P_u are the constants of proportionality (i.e., "noise/signal ratios") for error and error-rate perception and for motor output, respectively.

Consistent values have been found for these noise/signal ratios for a variety of laboratory tasks. Ratios of $.01\pi$ (i.e., -20 db) are typical for both P_e and $P_{\dot{e}}$, and a motor noise/signal ratio of $.003\pi$ (-25 dB) is typical. The relative invariance of these parameters in idealized laboratory situations suggests that the noise/signal ratios reflect fundamental limitations on human capability to process information.

The expression for observation noise variance is modified as follows to account for additional display-related limitations typical of realistic flight tasks:

$$V_{y_i} = \left[\frac{\sigma^2_{y_i}}{K^2(\sigma_i, a_i)} + \sigma^2_{y_{o_i}} \right] \cdot P_{y_i} \qquad (1)$$

where y_i denotes the i_{th} display variable, a_i is the effective perceptual threshold associated with the i_{th} variable, $K(\sigma_i, a_i)$ is the corresponding describing-function gain, and $\sigma^2_{y_{o_i}}$ is the variance of the "residual noise" [5]. The effect of the threshold-related gain is to increase the observation noise without limit as the signal deviation becomes small with respect to the "threshold", thus rendering information unobtainable from the display. The residual noise variance, on the other hand, represents a constant increment of observation noise resulting from non-threshold types of display limitations.

26

Laboratory studies indicate that an effective threshold of
from 0.05 - 0.1 degrees visual arc is typical for perception of
indicator displacement and a threshold of about 0.2 degrees/sec
visual arc is appropriate for velocity perception in a tracking
task [4].* If the pilot is required to maintain a display
indicator at some non-zero distance from a reference indicator,
the residual noise variance may be set equal to the square of
the distance (in experimental units) from the indicator to
reference [5].

3.2.4 Pilot Optimization

The pilot is assumed to adapt his control strategy, subject
to the limitations described above, to minimize the cost. The
adaptive portion of the pilot's strategy is represented by (a)
an optimal predictor that partially compensates for the inherent
time delay, (b) an optimal estimator to obtain the best estimate
of the state vector $\underline{x}(t)$, and (c) a set of optimal gains acting
on the best estimate of the state vector, the output of which
is a "commanded" control signal. This output is modified by a
first-order low-pass filter (whose time constant is the "motor
time constant" mentioned above) to reflect inherent limitations
on pilot bandwidth.

---

*These values have been derived mostly from studies of pilot
 remnant in single-variable tracking tasks and are intended to
 allow a valid statistical linearization of apparent threshold-
 related phenomena inherent in these experimental situations.
 The reader should not expect these "thresholds" to be
 necessarily identical to other measures of visual threshold
 that appear in the literature.

3.2.5 Model Outputs

The primary output varic. le of this pilot/vehicle model is the pilot's control signal, u(t). Once the characteristics of this signal have been determined, a set of relatively straightforward computations yields the pilot's describing function, remnant spectrum, and various measures of overall system performance (such as mean-squared error and mean-squared control activity).

3.3 Effects of Vibration

Whole-body vibration will generally cause unwanted control inputs due to biomechanical coupling between the vibration source and the control stick. In part, then, the effect of vibration may be reflected simply as an additional disturbance to the vehicle as diagrammed in Figure 8. In many situations, however, the dominant effect of vibration is to interfere with the sensory, central-processing, and motor response systems employed by the pilot in performing the tracking task. Effects of this sort are modeled as changes in model parameters related to pilot-limitations (i.e., time delay, motor lag, and visual and motor noise).

The treatment of various sources of vibration-related performance decrement are discussed below.

3.3.1 Vibration Feedthrough

Vibration-Correlated Control Inputs

"Vibration feedthrough" is the term we use to describe control inputs that arise from (basically linear) biomechanical coupling between the vibration source and the control stick.

28

Data analysis performed in this study (see Appendix B) indicates that the impedance model diagrammed in Figure 9 may be useful for predicting the interaction of control-stick dynamics and feedthrough.

We define the transfer impedance $ZT(j\omega)$ as the force transmitted to a rigid control stick. Thus,

$$ZT \equiv \frac{F_v}{\alpha_p} \Bigg|_{ZS = \infty}$$

where F_v is the resulting force, α_p is the platform acceleration, and ZS is the mechanical impedance of the control stick. (For ease of notation, we shall delete the argument $(j\omega)$ from frequency-domain models.) The output impedance ZO is defined as the ratio of the rigid-stick force to the free-stick displacement:

$$ZO \equiv \frac{\dfrac{F_v}{\alpha_p}\Bigg|_{ZS = \infty}}{\dfrac{C_v}{\alpha_p}\Bigg|_{ZS = 0}}$$

where C_v is stick displacement.

The impedance parameters ZT and ZO are assumed to reflect biodynamic properties of the pilot and of the pilot-cockpit interface and are assumed to be independent of control-stick characteristics as well as of parameters of the vibration inputs. The transfer functions for vibration feedthrough, relating stick force and stick displacement to platform vibration, are:

$$\frac{F_v}{\alpha_p} = \frac{ZT \cdot ZS}{ZO + ZS} \tag{2}$$

$$\frac{C_v}{\alpha_p} = \frac{ZT}{ZO + ZS} \tag{3}$$

29
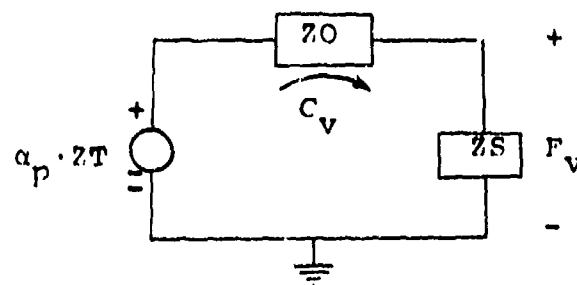
ZT = Transfer Impedance

ZO = Output Impedance

ZS = Stick Impedance

α_p = Platform Vibration

C_v = Stick Displacement

F_v = Stick Force

Figure 9.   Impedance Model for Vibration Feedthrough

In order to obtain numerical predictions of vibration feedthrough, we must have a means of deriving the feedthrough impedance functions ZT and ZO. These functions will in general depend on the structure of the pilot's seat, the interface between the pilot and the seat, the interface between the seat and the platform, and the physical characteristics of the pilot.

Efforts are currently underway to develop and refine models for predicting biodynamic parameters [6]. Existing models for vertical-axis vibration feedthrough range from simple second-order systems to high-order representations containing detailed models of the neuromuscular system [7-8]. At present, however, development of biodynamic models is not sufficiently advanced to allow reliable, numerical predictions of ZT and ZO. Accordingly, we must rely upon measurements obtained in the specific biodynamic environment of interest.

Once the impedance parameters ZT and ZO have been quantified and the vibration spectrum defined, the effects of vibration-correlated control inputs on tracking performance can be computed for various control-stick characteristics and for various plant dynamics as described below.

Effect on Tracking Performance

Vibration feedthrough will increase tracking error because of the unwanted inputs applied to the control system. Prediction of this error increment is particularly simple if the vibration spectrum contains most of its power at frequencies beyond the response bandwidth of the control system. In this case, the increment in tracking error is computed as the open-loop response of the control system to the feedthrough.

31

Assume that the control system is single-input, single-output with the transfer function Y_c, and let K_c represent the control gain in terms of electrical input to the system per unit of stick displacement. The error variance predicted by feedthrough is then

$$\sigma_{e_v}^2 = \int \left| \frac{ZT}{ZO + ZS} \right|^2 \quad K_c^2 \; |Y_c|^2 \; \Phi_{\alpha_p \alpha_p} \; d\omega \qquad (4)$$

Since the vibration input is assumed to be uncorrelated with the tracking input, this error term can be added to the error variance arising from the tracking disturbance to yield total error variance. This expression can also be used to predict various error terms of interest in a multi-output system, where the vehicle transfer function is now represented as Y_{c_i} to denote the response of the i_{th} output variable to the control input.

If the vibration spectrum contains significant power within the response bandwidth of the pilot/vehicle system, the pilot will be able to compensate for a portion of the feedthrough-related tracking error. In this case, feedthrough error would be less than that predicted by the open-loop approximation suggested above. An alternate method for predicting the effects of feedthrough would be to:

(a) Compute the spectrum of the feedthrough-related stick motion, given as

$$\Phi_{c_v \; c_v} = \left| \frac{ZT}{ZO + ZS} \right|^2 \cdot \Phi_{\alpha_p \alpha_p}$$

32

(b) Approximate this spectrum by filtered white noise and find a suitable state-variable representation for this process.

(c) Treat the feedthrough as an additional tracking input, and use the state-variable model described in Section 3.2 to predict response behavior simultaneously to the tracking and vibration inputs.

If the system under study is a moving-base simulation or an actual flight, prediction of feedthrough effects is further complicated if appreciable vehicle motions (for example, high-frequency bending modes) are induced by vibration-related control inputs. Such motions are likely to be fed back to the control stick through biomechanical coupling. To predict feedthrough-related error in this situation, the vehicle dynamics will have to be augmented to account for that additional loop closure.

3.3.2 Visual Effects

Calculation of Relative Eye-Display Motion

Platform vibration will in general produce relative motion between the head and the platform as well as front-back rotation of the head. Translation and rotation of the head will combine to produce relative motion between the head-point-of-regard and the display which, to the extent that the oculomotor system cannot compensate, will produce retinal motion of the display (i.e., blur).

33

Once the vibration environment has been specified and the biodynamic response properties of the head determined, rms relative displacement and velocity of the target image may be computed as follows. (Frequency-domain representation is implied.)

Let $\quad \alpha_h \equiv$ translational acceleration of the head (g)

$\quad \alpha_d \equiv$ translational acceleration of the display (g)

$\quad \alpha_\theta \equiv$ rotational acceleration of the head (rad/sec^2);

$\quad \alpha_p \equiv$ platform acceleration (g)

$\quad D \equiv$ viewing distance (inches)

Acceleration in inch/sec^2 of the head-point-of-regard, relative to the display, is then

$$\alpha_{dh} = 386.4 \ (\alpha_h - \alpha_d) + D \cdot \alpha_\theta$$

which may be expressed in terms of transfer functions as

$$\alpha_{dh} = \left[386.4 \ \left(\frac{\alpha_h}{\alpha_p} - \frac{\alpha_d}{\alpha_p} \right) + D \cdot \frac{\alpha_\theta}{\alpha_p} \right] \cdot \alpha_p$$

where the constant 386.4 represents the acceleration of gravity, at sea level, in inches/sec^2. Typical values for the display/platform transfer function are unity for a display rigidly attached to the accelerating platform (as was the case in this study), and zero for a completely isolated display (as is sometimes the case in laboratory experiments).

Since the oculomotor system will compensate for target motions at low frequencies, the above expression must be modified by a high-pass filter to provide an estimate of the relative acceleration of the eye point-of-regard. Thus,

$$\alpha_{de} = \alpha_{dh} \cdot T_{he}$$

The above expressions may be combined to yield the spectrum of the acceleration of the image motion:

$$\Phi_{\alpha_{de}\alpha_{de}} = \left| 386.4 \left(\frac{\alpha_h}{\alpha_p} - \frac{\alpha_d}{\alpha_p} \right) + D \cdot \frac{\alpha_\theta}{\alpha_p} \right|^2 \cdot \left| T_{he} \right|^2 \cdot \Phi_{\alpha_p\alpha_p}$$

Displacement and velocity variances are then given by the following integrations:

$$\sigma_{y_{de}}^2 = \int \frac{\Phi_{\alpha_{de}\alpha_{de}}}{\omega^4} \, d\omega \tag{5}$$

$$\sigma_{\dot{y}_{de}}^2 = \int \frac{\Phi_{\alpha_{de}\alpha_{de}}}{\omega^2} \, d\omega \tag{6}$$

As we do not presently have reliable theoretical models for relating head translation and rotation to platform acceleration, the quantities α_h/α_p and α_θ/α_p must be determined experimentally in biodynamic environments of interest. The transfer function α_d/α_p is determined by the interface between the display and the vibrating platform.

A simple model can be suggested for the transfer function T_{he}. Laboratory studies have shown that the eye can follow target motion that contains frequencies below 2 Hz. Response characteristics show a very rapid falloff between 2 and 4 Hz, and the tracking effectiveness of the eye at frequencies above 4 Hz is essentially nil [8-9]. Since the parameter T_{he} is the complement of the transfer function describing oculomotor response, T_{he} may be approximated reasonably well by a step function in the frequency domain that has zero gain from d-c to about 4 Hz and unity gain above 4 Hz.

Effect on Tracking Performance

Appropriate modifications to the parameters of the pilot/ vehicle model of Section 3.2 must be made in order to account for the effects of relative image motion on tracking performance. It is not clear from theoretical considerations, however, just what these modifications should be. If vibration-induced motion affected only the error indicator and not the reference indicator, we could treat image motion as a noise added to the error display; in this case, the mean-squared image displacement and velocity would be treated as residual noise variances and would be included in the expression for observation noise as indicated in equation (1).

Since vibration-induced blur causes simultaneous retinal motion of *both* the error indicator and the corresponding reference indicator, it is not obvious how blur degrades the pilot's ability to distinguish the position and velocity of the error indicator *relative to the reference indicator*. We must therefore rely on experimental results to serve as a guide for modeling the effects of blur.

The effect of vibration-related blur appears to depend on the nature of the vibration spectrum. In a study conducted by Allen et al. using sinusoidal vibration, the test subjects reported that their ability to allign error and reference lines seemed to be unimpaired by blurring [7]. Allen et al. commented that the luminous density of the blurred images of the error and reference lines were greatest near the extreme of travel, thereby providing sharp edges for allignment.

Since a quasi-random (sum of five sinusoids) vibration was used in the current study, the blurred images were expected to be somewhat more difficult to allign. Therefore, the effect of blur was approximated by setting the residual noise variance associated with error displacement equal to the displacement variance calculated by equation (5). Model predictions obtained with this treatment of blur were consistent with experimental results. On the other hand, setting residual noise on rate perception equal to image velocity as calculated by equation (6) yielded a predicted pilot remnant spectrum that differed appreciably from that observed experimentally. A better model match was obtained with image rate ignored; i.e., with rate residual noise set to zero.

Until we obtain a better theoretical understanding of how vibration-induced image motion influences perceptual processes used in tracking, we suggest that the effects of blur be accounted for by a residual noise variance associated with perception of error displacement. This variance is to be equal to the variance of the eye point-of-regard displacement relative to the display.

3.3.3 Motor Effects

In addition to inducing control motions correlated with the
vibration input as discussed above, whole-body vibration can
interfere with the pilot's ability to execute the desired response
to the tracking input. Interference of this sort has been thought
to arise largely from degradation of sensory feedback information
used in the regulation of control activity [7, 8, 10], leading to
measureable effects such as increased motor-related pilot remnant
and a more sluggish tracking response. Given the existing structure
of the state variable pilot/vehicle model, one would expect these
motor effects to be modeled by one or more of the following para-
meter modifications: (a) increased motor noise, (b) increased
time delay, and (c) increased motor time constant.

For the biodynamic environment explored in this study,
motor-related effects of vibration can be accounted for by increases
in the motor noise/signal ratio and in time delay; no change is
required for the motor time constant. (See Appendix D for
detailed discussion of the modeling performed in this study.)
We suspect that the increased motor noise reflects an increase
in the noise associated with proprioceptive and kinematic sensory
pathways, and that the pilot's adaption to this additional noise
results in describing-function changes that require an increased
time delay for adequate model-matching.* Further research is
needed to determine (a) how the injected motor noise varies with
vibration-related quantities in a vibration environment, and (b)
how the effective time delay relates to vibration and/or noise
parameters.

*The reader is reminded that "time delay" refers to a model para-
meter that may reflect the effects of a number of psychophysiological
phenomena. Increased time delay is required also by existing
frequency-domain models to adequately mimic the effects of vibra-
tion [8].

Analysis recently performed on manual tracking data obtained in a lateral vibration environment suggested that motor noise could be considered to scale with overall control activity; i.e., vibration feedthrough plus response to tracking error [10]. Analysis of longitudinal-axis vibration performed in the current study does not support this hypothesis, however. An alternative hypothesis more consistent with the existing data base is that the motor noise/signal ratio varies with limb (e.g., shoulder and/or elbow) motion.

Studies of tracking in a vibration environment -- including the study documented in this report — indicate that the following spring-mass-damper model is sufficient to relate shoulder motions to platform acceleration [7]:

$$\frac{\alpha_s}{\alpha_p}(s) \; = \; \frac{K + B_s}{K + B_s + M s^2}$$

$$= \; \frac{1 + (B/K)s}{1 + (B/K)s + (M/K)s^2}$$

(7)

where K, B, and M represent spring constant, damping factor and mass, respectively. Once the ratios B/K and M/K have been determined for pilots of a particular anthropometric structure situated in a specific biodynamic environment, the variance of the shoulder acceleration (or of any linear transformation of acceleration) can be predicted for various vibration spectra as follows:

$$\sigma_x^2 \; = \; \int \left| \frac{\alpha_s}{\alpha_p} \right|^2 \cdot \left| F \right|^2 \; \Phi_{\alpha_p \alpha_p} \; d\omega$$

where σ_x^2 is the variance of the quantity of interest (e.g., the first derivative of the acceleration) and F is the transformation process (e.g., differentiator) expressed as a transfer function.

39

In summary, current understanding of the effects of vibration on tracking behavior is not sufficient to allow us to specify analytic relationships between vibration parameters and changes in motor-related model parameters; we must therefore determine model-parameter changes from a "calibration experiment" performed in a specific biodynamic environment. Hopefully, the results of such an experiment will be valid for a variety of vibration environments and a variety of control-system response characteristics.

3.3.4 Central-Processing Effects

Long-term exposure to vibration can be expected to lead to stress effects such as fatigue, discomfort, anxiety, etc., which would further degrade the pilot's ability to process tracking information. Substantial research is needed to develop models for long-term effects, as studies of manual tracking in vibration environments have dealt primarily with tracking tasks of a few minutes duration. Consequently, we shall not attempt to account for these effects in the design guide presented in the following section.

4. DESIGN GUIDE

Guidelines for the design of control sticks in a vibration
environment can take a number of forms, depending on the intended
range of applicability. The more restricted the range, the easier
it is to present the design guide in a form that is immediately
unseable. For example, if we are concerned with the specification
of a single stick parameter (say, control gain) for a specific
tracking/vibration/biodynamic situation, the guide can consist of
a single curve of performance (e.g., mean-squared tracking error)
versus the parameter of interest. On the other hand, if the guide
is to apply to a range of tracking and biodynamic situations, it
will ideally take the form of an analytic model (or set of models)
having parameters that are either independent of the specifics of
the situation or that can be readily determined on a theoretical
basis. In this section we shall consider the proposed design guide
from both the general and restricted views.

The proposed design guide is based on the model structure
outlined in the preceding section of this report. In the most
general sense, the model itself *is* the guide; that is, the model
is to be applied in a specific situation of interest to explore
the consequences of one or more candidate control-stick configu-
rations.

The status of biodynamic modeling prohibits a fully general
design guide at this time. In many cases, analytic forms for
biodynamic response mechanisms cannot reliably be presented.
Furthermore, where such forms exist, we do not know how to quantify
parameters without the benefit of experimental data obtained in the
specific biodynamic/vibration environment. In addition, we do not
know the functional relationship between vibration parameters and

41

changes in parameters of the pilot/vehicle model. Consequently, the design guide discussed here must be restricted to the bio-dynamic and vibration environments explored in this study as described in Section 2. Nevertheless, the highly analytic pilot/vehicle model incorporated in the design guide should allow one to explore tracking tasks and control configurations that have not been studied experimentally.

Quantification of model parameters for the design guide is discussed below in Section 4.1. Numerical examples are presented in Section 4.2 to validate the model and to provide simple quantitative guidelines for the selection of specific control parameters in specific situations.

4.1   Quantification of Model Parameters

Model parameters are categorized as follows for convenience of discussion: (1) data-dependent parameters, (2) problem variables, and (3) remaining pilot parameters.

For the most part, parameters of the design guide that relate directly to the vibration and biodynamic environments are empirical parameters that have been quantified on the basis of the experimental study described in Section 2. These parameters are considered to be data-dependent; that is, we have no theoretical basis for reliably predicting how parameter values will change for different biodynamic/vibration environments. On the other hand, parameters that describe the tracking task and the control configuration can be considered as variables of the design guide. The remaining pilot-related model parameters are either relatively invariant or can be determined on a theoretical basis.

42

Data dependent parameters, problem variables, and remaining
pilot parameters are discussed separately below. The reader is
assumed to be familiar with the model structure and parameter
definitions presented in Section 3 of this report.

4.1.1 Data-Dependent Parameters

Vibration Environment

This design guide applies to a z-axis vibration disturbance
of about .26 g rms consisting of the sum of five sinusoids. The
average vibration spectrum measured in this experimental study is
shown below in Table 2.*

Table 2

Experimental Vibration Spectrum

| Frequency | | Power |
(Hz)	(rad/sec)	(dB)
2	12.5	-17.7
3	21.0	-18.1
5	31.7	-19.2
7	43.8	-19.7
10	63.3	-20.1

Feedthrough Impedance Parameters

Stick displacement is assumed to be correlated with platform
vibration as follows:

*See Appendix A for a definition of spectral quantities.

43

$$\frac{C}{\alpha_p}(s) \approx \frac{ZT}{ZO + ZS} \qquad (8)$$

where the transfer impedance ZT and the output impedance ZO are as shown in Figure 10 for center and side stick locations. An amplitude-ratio of 0 dB signifies 1 lb of stick force per g of platform acceleration for ZT and 1 lb of stick force per inch of stick displacement for ZO.

Relative Eye-Display Motion

The spectrum of relative motion between the eye-point-of-regard and the display may be estimated as follows:

$$\phi_{\alpha_{de}\alpha_{de}} = \left| 386.4 \left(\frac{\alpha_h}{\alpha_p} - \frac{\alpha_d}{\alpha_p} \right) + D \cdot \frac{\alpha_\theta}{\alpha_p} \right|^2 \cdot \left| T_{he} \right|^2 \cdot \phi_{\alpha_p\alpha_p} \qquad (9)$$

where the transfer functions relating vertical head acceleration to platform acceleration (α_h/α_p) and head rotation to platform acceleration (α_θ/α_p) are as shown in Figure 11. The expression (α_h/α_p) is dimensionless, whereas α_θ/α_p has units of rad/sec^2)/g. The filter function T_{he} is assumed to have zero transmission from d.c. to 4 Hz (25 rad/sec) and unity transmission for frequencies above 4 Hz.

Viewing distance D and display/platform transfer may be treated as problem variables, if desired. For the data analysis performed in this study, D was assumed to be 30 inches, and the transfer function (α_d/α_p) was unity to reflect the fact that the display was rigidly attached to the platform.

44
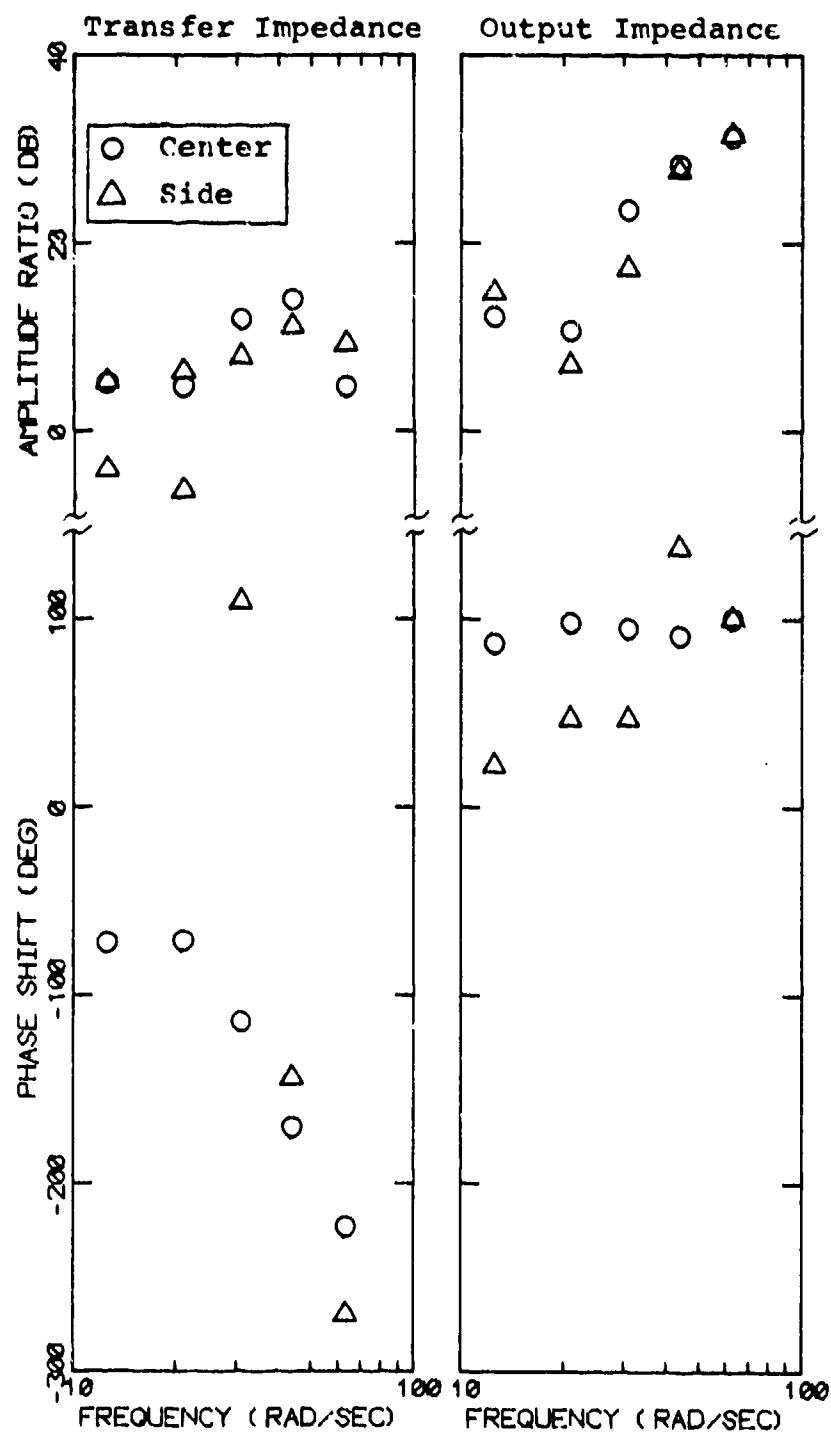
Figure 10. Transfer and Output Impedances

45
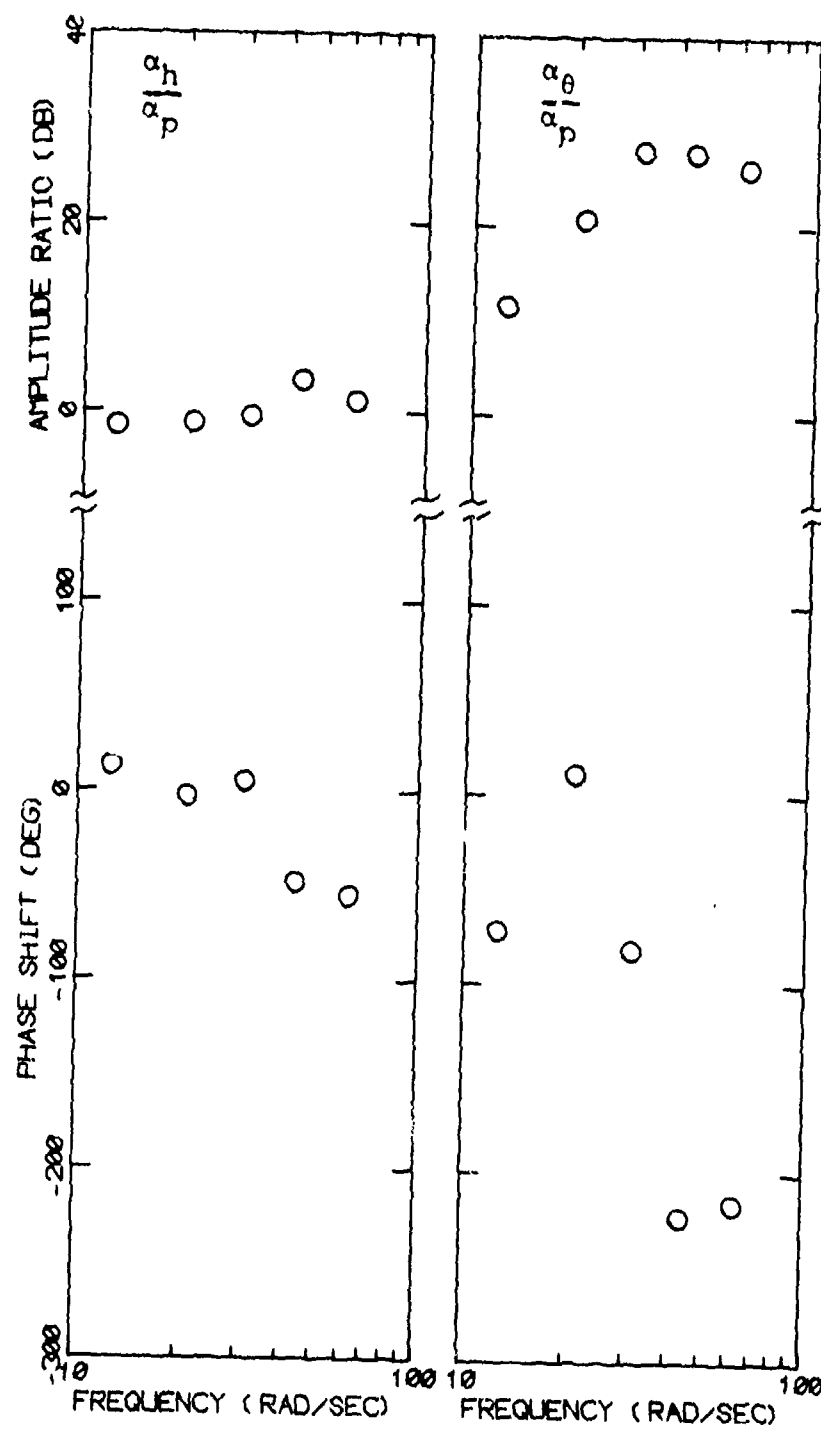
Figure 11.   Head Motion Measurements

46

Once the spectrum of eye-display motion is computed, the integration defined by equation (3-5) may be performed to yield the variance of the relative motion between the display and the eye-point-of-regard. The residual noise variance associated with perception of tracking error (a model parameter) is set equal to this derived measure.

Vibration-Related Pilot Parameters

A time delay of 0.2 seconds and a motor noise/signal ratio of 0.04 (relating the variance of the injected white motor noise to the variance of the predicted control force) are assigned on the basis of measurements obtained in this study. These parameter values are suggested only for the vibration and biodynamic environments described in this report. (Values of 0.15 seconds and 0.004 are suggested for static environments.)

4.1.2 Problem Variables

Task Parameters

Previous application of the pilot/vehicle model has shown that a good match between model outputs and experimental measurements can be obtained with a consistent set of pilot-related parameters for a variety of laboratory tracking tasks [1, 2]. On this basis, we shall assume that the design guide described here can be expected to give reasonably accurate predictions for tracking tasks using vehicle dynamics and input spectra other than those explored in this study. Application is restricted, however, to the static situation and to the vibration/biodynamic environment explored in this study.

47

Display-Related Parameters

The design guide should be valid for a variety of display designs. Display dynamics are included in the description of system dynamics as discussed in Section 3.2.1. Limitations of visual resolution may also be treated by appropriate selection of effective "thresholds". Typically, position and rate information will be obtained from each moving display element. On the basis of previous studies of pilot remnant [4], we suggest that threshold levels be computed as follows:

$$\left.\begin{array}{l} a_y = \dfrac{D}{G} \cdot \dfrac{0.05}{57.3} \\[2em] a_{\dot{y}} = \dfrac{D}{G} \cdot \dfrac{0.2}{57.3} \end{array}\right\} \quad (10)$$

where a_y and $a_{\dot{y}}$ are the thresholds associated with displacement and rate, expressed in the desired experimental units (e.g., volts); D is the distance to the display (e.g., inches), and G is the display gain expressed as units of display deflection per experimental unit (e.g., inches/volt).

Application of the design guide is suggested for situations in which the display format is symbolic, rather than pictorial, and in which saturation effects are not important.

Control-Stick Parameters

The design guide is intended especially to explore the effects of control-stick parameters on performance in the vibration/biodynamic environment described in Section 2. Application to stick configurations not explored in this study is demonstrated in Section 4.2.

48

Although any linear relationship between stick force and stick displacement may be considered, we suspect that the following second-order impedance functions will be adequate in most cases:

$$ZS(s) = \frac{M_s}{386.4} s^2 + B_s s + K_s \tag{11}$$

where ZS is the impedance relating force in pounds to displacement in inches; K_s is the spring gradient in lbs/inch; B_s is the damping in lbs/(in/sec); and M_s is the effective mass of the stick in pounds. Stick dynamics are included in the description of system dynamics as demonstrated in Section 4.2.

4.1.3 Remaining Pilot Parameters

For a well-trained test subject, the observation noise/signal ratio appears to reflect the level of attention to the tracking task. For single-variable tracking tasks, this parameter appears for the most part to be independent of the specifics of the tracking tasks and is unaffected by the presence or absence of vibration (at least for the short exposure intervals that have been studied experimentally). A value of about -20 dB (i.e., 0.01π) is typical, although a value of -21 dB was found to provide a better match to the data explored in this study.

The observation noise/signal ratio will generally be increased if the pilot has to share attention among a number of tasks and/or among a number of display variables within a given task. A reasonable model for the effect of attention is to let the noise/signal ratio vary as follows:

$$P_{y_i} = P_o / f_i \tag{12}$$

where P_{y_i} is the noise/signal ratio associated with the i_{th} display variable, f_i is the fraction of attention devoted to that variable, and P_o is the nominal value associated with single-variable tracking (say, -20 dB) [11].

In most single-variable laboratory situations that we have studied, the "cost" that the pilot is assumed to minimize appears to represent a limitation on pilot bandwidth rather than objective performance requirement. Typically, the expression for the cost is a weighted sum of mean-squared tracking error and mean-squared control-rate, where the relative weighting is chosen to provide an effective "motor time constant" of about 0.1 second.

If excessive control forces or displacements are required, an additional weighting coefficient on control force (or displacement) is needed. The following expression for cost was found to match the data (both static and vibration conditions) analyzed in this study:

$$J = 1.0 \ \sigma_e^2 + .03 \ \sigma_u^2 + g \ \sigma_{\dot{u}}^2 \tag{13}$$

where σ_e^2 is the mean-squared error in volts^2, σ_u^2 is the mean-squared force in pounds^2, and (g) is selected to provide a motor time constant of 0.1 seconds. Since the display gain used in this study was approximately 0.19 inches/volt, the relative weightings assigned to error and to control force imply that the test subjects considered the presence of a 1-inch tracking error as "costly" as the requirement to generate about 30 pounds of control force.

As discussed in Section 3.2.2, a more elaborate cost
expression will be required to adequately model performance in
a realistic multi-variable flight situation. In this case,
weighting coefficients reflect objective performance requirements
and hardware limitations as well as pilot preference [3].

Suggested values for pilot-related parameters of the
tracking model are summarized in Table 3. The absence of
numeric entries indicates that parameter values are to be
computed as described above.

4.2   Numerical Examples

Three examples are presented to demonstrate application
of the design procedure and to serve as guidelines for possible
additional experimentation to be performed by AMRL with the same
set of control devices in a similar laboratory setting. The
primary control variables explored in the following examples
are, in order, (1) spring gradient, (2) electrical stick gain,
and (3) stick damping.

4.2.1 Spring Gradient

For our first illustrative example of the design procedure,
we compare model predictions with the results of the experimental
study described in Section 2 of this report. The reader will
recall that the spring gradient was one of the major experimental
variables, along with stick location and presence or absence of
vibration. Because of equipment constraints, however, stick
damping and electrical gain also had to be varied as spring
gradient war changed. Since, in general, performance will be
affected by a change in any one of these stick parameters, this

51

Table 3

Suggested Values for Pilot-Related Model Parameters

Parameter	Parameter Value	
	Static	Vibration*
Cost**	$J = \sigma_e^2 + \left(\frac{1}{30}\right)^2 \sigma_u^2 + g\,\sigma_{\dot{u}}^2$	
Time Delay	0.15 sec	0.20 sec
Motor Noise/Signal Ratio	0.004	0.04
Observation Noise/Signal Ratio	0.01π	
Visual Threshold	***	
Visual Residual Noise	***	

*Valid only for the vibration/biodynamic environment described in Section 2.

**Tracking error in inches, force in pounds, and g selected to provide a motor time constant of 0.1 seconds.

***Value calculated as described in text.

example will not lead to a simple curve of performance versus spring gradient. We begin with this example, nevertheless, as it affords the best means for quantitatively validating the design procedure.

The relevant control-stick parameters are shown in Table 4. Spring gradient and electrical gains were determined in this experimental study; stick damping, stick mass, and effective hand mass were obtained from documentation of the preceding study performed at AMRL [7]. Vehicle transfer functions relating system error (E) to disturbance input (I) and control input (C) are reviewed below, with all variables in volts:

$$\frac{E}{I}(s) = \frac{2}{s} \tag{14a}$$

$$\frac{E}{C}(s) = \frac{4}{s} \tag{14b}$$

Since the lowest vibration frequency (2 Hz, or 12.5 rad/sec) was beyond the gain-crossover frequency of the pilot/vehicle system (less than 5 rad/sec), tracking response and vibration feedthrough were analyzed separately and the results combined to yield predictions of system performance in the vibration environment.

Response to Tracking Input

The force-feel properties of the pilot/stick interface must be accounted for in order to model adequately the effects of control-stick parameters on tracking performance in static and vibration environments. This interaction was modeled by the following impedance function relating stick output C (in volts) to force input F (in lbs):

53

Table 4

Control Stick Parameters

	Parameter	Spring			Stiff		
		Light	Med	Heavy	Light	Med	Heavy
K_c	Electrical gain, volts/lb	1.25	.36	.21	.9	.9	.5
K_e	Electrical gain, volts/inch	2.5	2.5	2.5	34.2	117	300
K_s	Spring gradient, lbs/inch	2	7	12	38	130	600
B_s	Stick damping, lbs/(inch/sec)	.027	.027	.027	.0103	.0103	.0103
M_s	Stick mass, lbs	0.7	0.7	0.7	0.7	0.7	0.7
M_h	Mass of hand end of arm, lbs	2.7	2.7	2.7	2.7	2.7	2.7
M_T	$M_s + M_h$, lbs	3.4	3.4	3.4	3.4	3.4	3.4

54

$$\frac{C}{F}(s) = \frac{K_e}{\dfrac{M_T}{386.4} s^2 + B_s s + K_s}$$ (15)

where the parameters of the impedance and their units are as expressed in Table 4. Note that the force F is not necessarily the force applied to the control stick, but rather the force needed to drive the combination of the stick plus the inertia of the forearm.

The vehicle transfer functions and the force-feel impedance were combined to yield the effective control system shown in the flow diagram of Figure 12. The reader is referred to Appendix D for a state-variable representation of this system.

Since the model analysis described in this application of the design guide was performed with the benefit of having experimental data in hand, pilot-related model parameters were selected to provide a good match overall to the various experimental conditions. To this extent, model results given here are not true "predictions". Since model parameters were kept fixed for all six control-stick configurations, however, the *differences* in performance measures that the model exhibits for the different configurations represent actual predictions. Furthermore, model parameters not directly affected by the presence of vibration have numerical values quite similar to those found in previous studies of tracking in non-vibration environments.

Parameters relating to cost functional, time delay, and motor noise were as indicated in Table 3 for the vibration environment. A somewhat lower observation noise/signal ratio (-21 dB) than that shown in Table 3 was used, as it provided

55
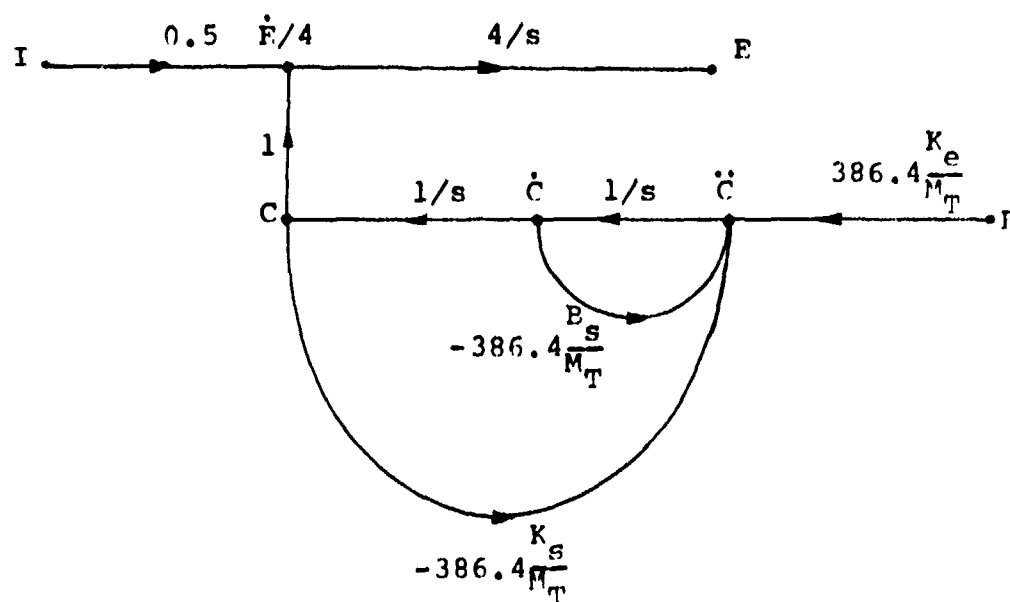
I = Tracking Disturbance, volts

F = Tracking Error, volts

C = Control Input, volts

F = Applied Force, pounds

K_e = Electrical Stick Gain, volts/inch

K_s = Spring Gradient, pounds/inch

B_s = Stick Damping, pounds/(in/sec)

M_T = Combined Mass of Stick and Forearm, pounds

Figure 12.   Linear Flow Diagram of Control System

56

a better match to both static and vibration data obtained in this study. "Threshold" levels of approximately 0.14 and 2.7 volts were computed from equation (4-3) for displacement and rate perception, respectively. A display gain of 0.1875 inches/volt and viewing distance of 30 inches were used for this calculation. Computations equivalent to those implied by equation (4-2) led to an rms residual noise on error displacement of 0.44 volts.*

Once the system was described analytically and pilot parameters quantified, the pilot/vehicle model was then able to predict measures of system performance for the various control configurations in the absence of vibration feedthrough. Errors and control motions due to feedthrough were computed separately, as discussed below.

Vibration Feedthrough

Vibration-correlated error and control scores were computed separately for the side and center stick locations, with the results then averaged together. With the vehicle dynamics given as in equation (14b) vibration-correlated error was predicted as

$$\sigma_{e_V}^2 = \sum_{i=1}^{5} \left| \frac{ZT}{ZO + ZS} \right|^2 \frac{16}{\omega^2} K_e^2 \cdot \phi_{\alpha_i \alpha_i} \tag{16}$$

*See Appendix B for detailed discussion of the computation of relative motion between eye-point-of-regard and display.

57

where $\Phi_{\alpha_i\alpha_i}$ represents the power (in g^2) contained in the i_{th} sinusoidal component of the vibration input (Table 2), K_e the electrical gain of the stick (Table 4), ZT and ZO the feed-through impedance functions defined in Figure 10, and ZS the stick impedance. The stick impedance was defined as

$$ZS(s) = \frac{M_s}{386.4} s^2 + B_s s + K_s \tag{17}$$

with parameters M_s, B_s, and K_s as defined in Table 4. An expression identical to equation (16), but minus the quantities related to vehicle dynamics, was used to predict vibration-correlated control scores.

Performance Predictions

Predictions of tracking-related and vibration-correlated error and control scores are shown separately and combined in Table 5. The feedthrough component of tracking error is small, accounting for less than five percent of the predicted total error in all cases. Feedthrough is a much more prominent aspect of the control score, however. For two of the control-stick configurations — light and medium stiff — vibration feedthrough accounts for about half the predicted mean-squared control displacement.

Predicted rms error and control scores are compared with measured performance scores in Figure 13. Each experimental data point in this figure represents the average performance of seven test subjects, with the brackets indicating $\pm$ 1 standard deviation due to inter-subject variability.

58

Table 5

Predicted Error and Control Scores for the Experimental Control-Stick Configurations

| | Control-Stick Configuration | | | | | |
| | Spring | | | Stiff | | |
Variable	Light	Med	Heavy	Light	Med	Heavy
$\sigma^2_{e_t}$, (volts^2)	.250	.229	.233	.227	.229	.222
$\sigma^2_{e_v}$, (volts^2)	.002	.001	.000	.009	.010	.003
$\sigma^2_{e_{total}}$, (volts^2)	.252	.230	.233	.236	.239	.225
$\sigma_{e_{total}}$, (volts)	.502	.480	.482	.485	.489	.475
$\sigma^2_{c_t}$, (volts^2)	.231	.273	.198	.473	.541	.443
$\sigma^2_{c_v}$, (volts^2)	.045	.016	.008	.448	.434	.148
$\sigma^2_{c_{total}}$, (volts^2)	.276	.289	.206	.921	.975	.591
$\sigma_{c_{total}}$, (volts)	.525	.538	.455	.960	.988	.970
$\sigma^2_{u_t}$ (pounds^2)	.102	1.19	2.89	.228	.231	.683

The subscript "t" indicates correlation with tracking input.

The subscript "v" indicates correlation with the platform vibration.
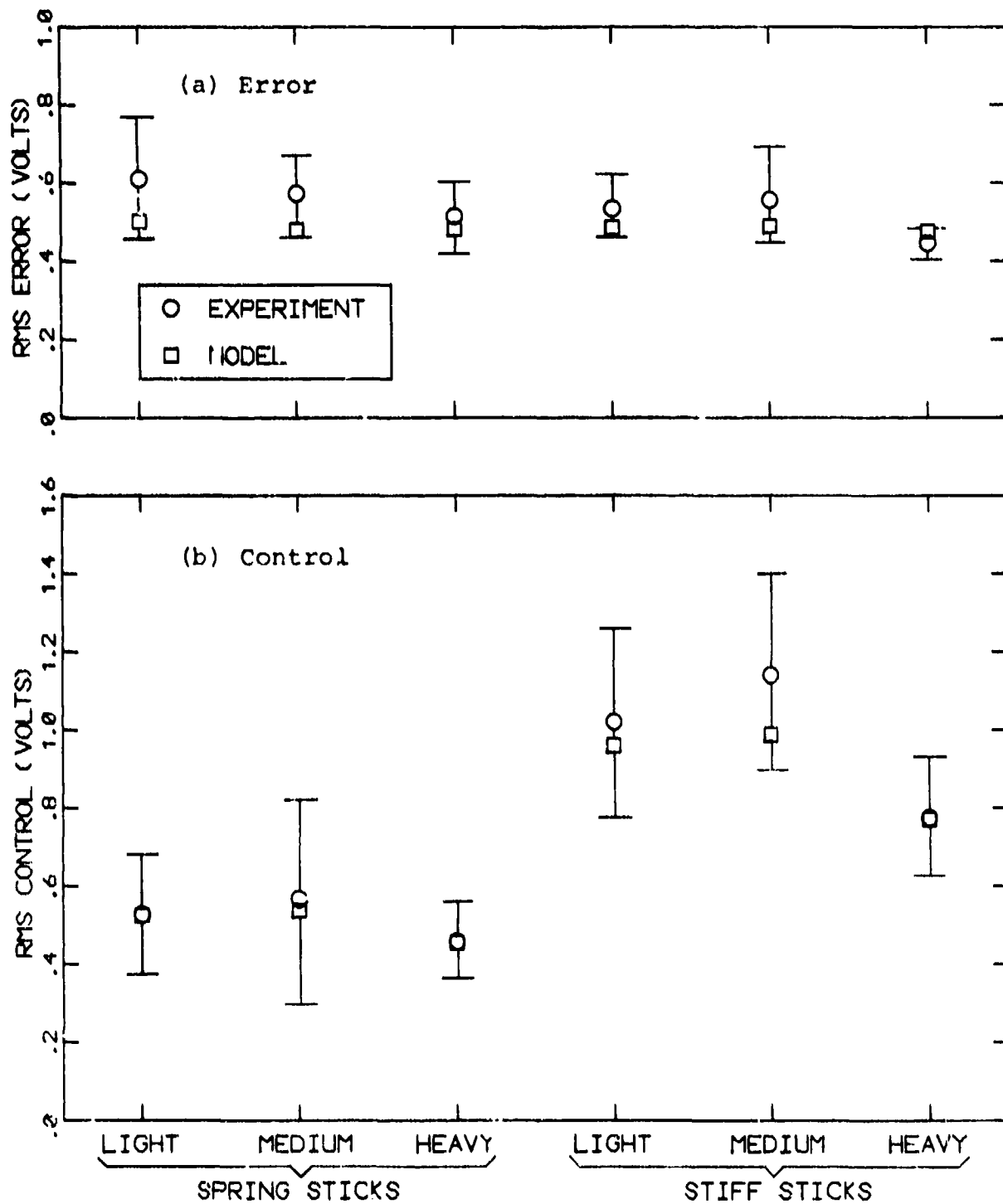
Figure 13. Comparison of Measured and Predicted RMS Performance Scores

60

The model predicts essentially no change in rms error score across the control-stick configurations. The experimental scores exhibit some variability (which is statistically significant), but no consistent trend. Since model predictions fall within one standard deviation of the corresponding experimental measurements, we consider the agreement between model and measurement to be adequate for the rms error score.

Agreement is much closer between "predicted" and measured rms control scores, however, and stiff-stick scores are shown to be more than double, on the average, than the spring-stick scores. This result implies the spring sticks would be the better choice if the vehicle exhibited resonances at frequencies where vibration power was significant, given the control-stick configurations explored in this particular study.

The relative insensitivity of predicted rms error with control-stick configuration shown in Figure 13 is somewhat misleading in that the effects of vibration have, to some extent, counterbalanced the basic performance differences across control sticks. As shown in Appendix C, model predictions as well as experimental measurements show improved performance with the stiff sticks in the absence of vibration. Vibration causes a greater percentage increase in rms error with the stiff sticks, however, which tends to equalize error scores across spring and stiff sticks when vibration is present.

4.2.2 Optimization of Electrical Gain

In this example we demonstrate application of the design method to the optimization of a single control-stick parameter in a particular tracking situation. Specifically, we consider the

tracking task and biodynamic/vibration environment defined in the preceding example, and we optimize the electrical gain of the "light-stiff" stick as defined in Table 4. Because we are keeping constant all remaining parameters of the task, we can derive a design curve that indicates the range of control gains that may be considered optimal.

As in the preceding example, vibration feedthrough and tracking response are computed separately and combined. From equation (16) we note that the variance of the vibration-correlated tracking error is proportional to the square of the stick gain when all other system parameters are held fixed. We may thus use the results of Table 5 to predict vibration-correlated error scores (as well as control scores, if desired) to any control gain as follows:

$$\sigma_{e_V}^2 = \sigma_{e_O}^2 \cdot \left(\frac{K_e}{K_O}\right)^2 \tag{18}$$

where $\sigma_{e_O}^2$ is the error score computed previously for the gain K_O.

Since we are considering a "stiff" stick in which stick force, rather than stick displacement, is considered the control quantity of interest, it is perhaps more appropriate to specify stick gain in units of volts/lb rather than volts/inch. We note from Table 5 that feedthrough accounted for an error score of 0.009 volts^2 for the light stiff stick. As this prediction was obtained for a stick gain of 0.9 volts/lb, we may now restate equation (18) as

$$\sigma_{e_V}^2 = .011 \ K_c^2 \tag{19}$$

where K_c is the stick electrical gain in volts/lb. This relationship is shown in Figure 14 by the dotted line.

The pilot/vehicle model is used to predict the effect of stick gain on the portion of the tracking error variance correlated with the tracking input. Except for the stick gain, problem variables and pilot-related parameters are as described in the preceding example for the light-stiff stick configuration. The relationship between input-related error score and stick gain is shown by the dashed curve in Figure 14.

The solid curve shown in Figure 14 shows the total error variance score as a function of stick gain. Minimum error variance is predicted for a gain of about 6 volts/lb. If we consider as "optimal" any stick gain that allows an error score within 10% of the theoretical minimum, then the range of optimal gain extends between approximately 0.2 and 1.3 volts/lb for the particular tracking/biodynamic/vibration situation explored in this example.

The range of optimal stick gains predicted here is considerably less than that usually associated with tracking under static conditions. Although stick gain was not explored in this study, a recent study of tracking under vibration conditions confirms the prediction that considerably less lattitude is allowed in selecting stick gains for vibration environments [8].

Theoretically, analysis via the pilot/vehicle model would be sufficient to determine the range of acceptable stick gains in the absence of vibration (or in vibration situations where feedthrough is negligible). In this situation, however, the model would have to be augmented to account for the upper bound on stick gain that arises from neuromuscular tremor and other souces

63
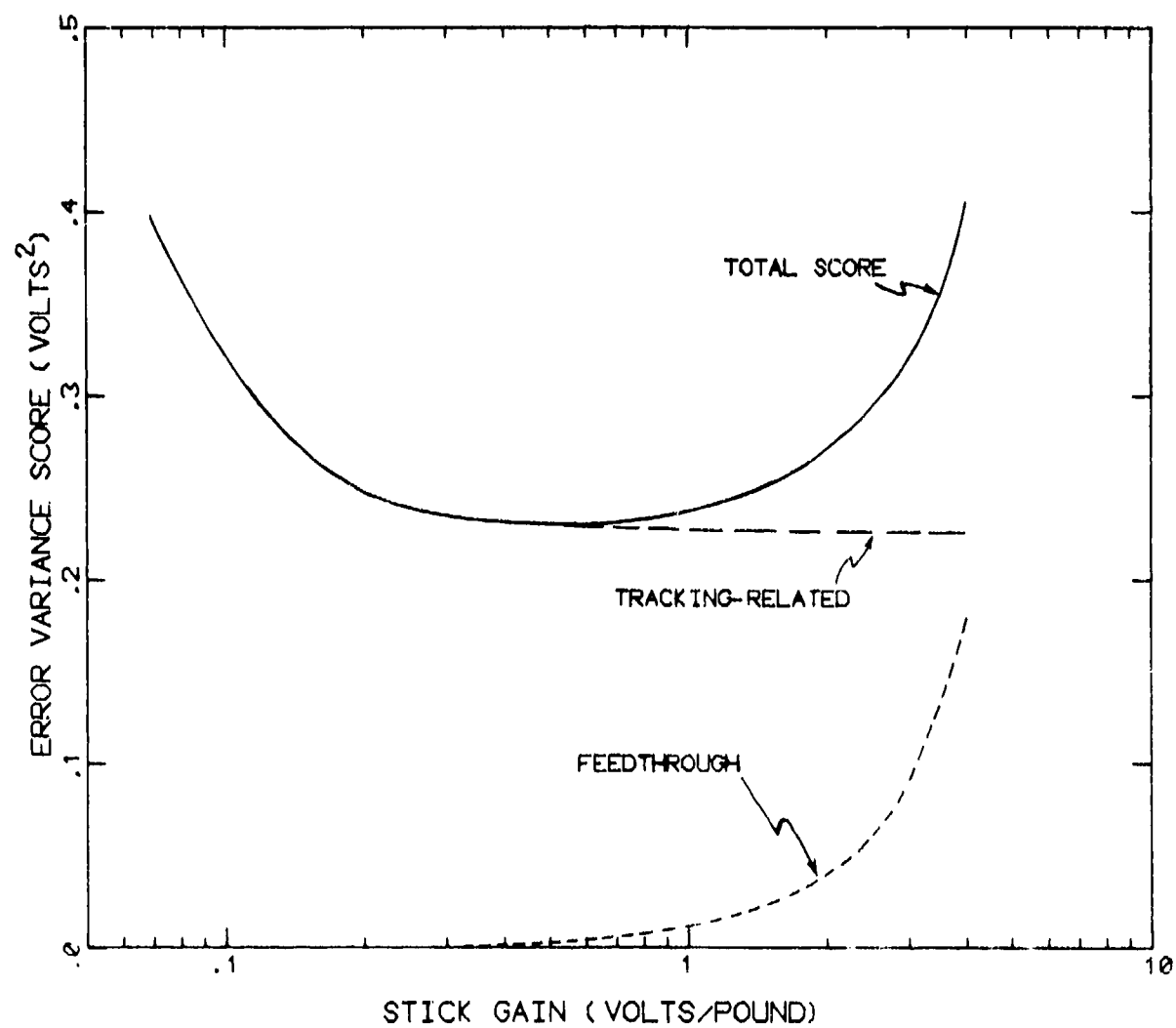
Figure 14.   Effect of Stick Gain on Predicted Error Variance
            (Light Stiff Stick)

64

of irreducible random control activity. We suspect that a "residual motor noise" — akin to the residual observational noise parameters now included in the model formulation — would serve this purpose. Additional research would be needed to quantify this model parameter.

4.2.3 Effect of Stick Damping

In this final example we use the design procedure to explore the effects of stick damping on performance. We again restrict analysis to the light stiff stick in the task situation defined in the initial example, and the results are presented as a design curve showing the relation between error variance and stick damping.

Analysis proceeds essentially as in the preceding two examples. Since stick damping — and thus stick impedance — is a variable of the analysis, the expression of equation (16) predicts the relation between vibration-correlated error and stick damping. Except for the variable stick damping, all problem parameters are the same as defined for the light-stiff configuration in the initial numerical example. The effects of stick damping on vibration-correlated error score, are displayed by the dotted curve in Figure 15.

Model analysis allows us to predict the effects of stick damping on the tracking-related component of the error variance score. Except for stick damping, model parameters and problem variables are as defined in the initial example. The results of this analysis are displayed by the dashed curve.

65
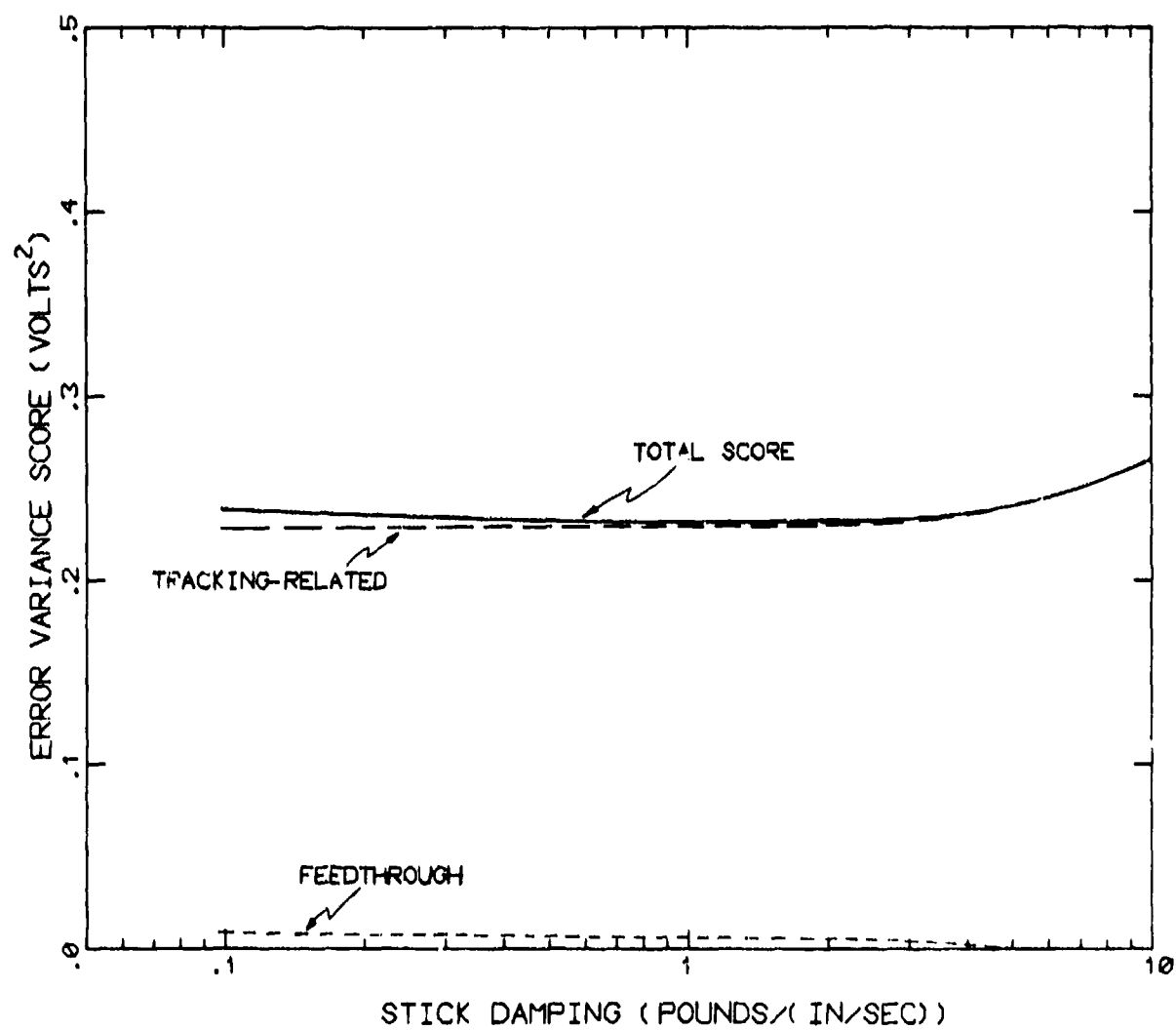
Figure 15. Effect of Stick Damping on Predicted Error Variance
(Light Stiff Stick)

The effects of damping on total performance is shown by
the solid curve. Because of the small contribution of feedthrough
to the error score, only a slight reduction in score can be
achieved by increasing the damping. As damping is increased
beyond about 2 lb/(in/sec), the mechanical impedance of the
stick begins to impair tracking efficiency, causing an increase
in the overall error variance score.

APPENDIX A

COMPUTATIONAL TECHNIQUES

A.1   Amplitude Statistics

Standard deviation scores were computed for all tracking and biodynamic variables. These scores were computed over a 100-second measurement interval that commenced approximately 15 seconds after initiation of the tracking run. As all variables had essentially zero mean, we have used the term "rms performance score" elsewhere in this report to signify the standard deviation scores.

Mean performance scores were computed across subjects, and the standard deviation (SD) of the individual scores was computed to provide a measure of subject-to-subject variability. Also computed was the standard error (SE) associated with the mean to provide an estimate of the repeatibility of the experiment. The SD and SE scores were computed as follows:

$$SD = \left[\frac{1}{N-1} \sum_{i=1}^{N} (\sigma_i - \bar{\sigma})^2 \right]^{1/2}$$

$$SE = \frac{SD}{\sqrt{N}}$$

where σ_i is the average performance score for the i_{th} subject performing a given experimental task, $\bar{\sigma}$ is the mean of the σ_i, and N is the number of test subjects.

A.2   Power Spectra

Power sp ctra were computed using fast-Fourier transform
techniques based on the Cooley-Tukey method of computing trans-
forms [12]. Spectra were computed from data covering a 100-
second measurement interval beginning approximately 15 seconds
after the initiation of the tracking run. This measurement
interval allowed the fundamental analysis frequency of about
0.0628 rad/sec to be an integral sub-multiple of the theoretical
base frequency (about 0.126 rad/sec' used in constructing the
sums-of-sinusoids tracking input.

The procedure for differentiating between input-correlated
and remnant-related components of a given spectrum was similar
to that used in the past [4], except that correction was made
for non-ideal inputs. Let us first describe the procedure used
with ideal inputs, then discuss the modifications needed in this
study.

We define "ideal" inputs as consisting of a number of
undistorted sinusoids that are harmonics of some fundamental
frequency. Sinusoidal components of the tracking input and
vibration input would have the same fundamental. A measurement
interval for the FFT would be chosen equal to the reciprocal of
the fundamental input frequency (or an integral multiple thereof).
Under these circumstances, signal power measured at a frequency
not coincident with a component of either the tracking or vibration
input would be defined as "remnant"; power measured at a component
frequency of the tracking input would be assumed to be correlated
with the tracking input (provided the remnant power at neighboring
measurement frequencies was sufficiently small); and power
measured at a component frequency of the vibration input would be
considered correlated with the vibration source (again, provided a
favorable signal/noise ratio).

A-2

The input signals obtained from the data tapes were non-ideal; that is, the component sinusoids were "smeared" to the extent that appreciable signal power was observed over two or three measurement frequencies on either side of the nominal input frequency. Possible sources of such distortion include (a) imperfections in the devices used to generate the inputs at experiment time, (b) speed fluctuations of the analog tape drive during recording and/or playback, (c) inaccuracies or fluctuations in sampling rate during digitization. In any event, it was necessary to modify the analysis program so that signal power appearing at measurement frequencies close to the nominal input frequency would be properly decomposed into input-correlated and remnant power, rather than being considered entirely as remnant power.

The correction procedure is based on the following two assumptions: (a) signal power measured at a nominal input frequency is not significantly corrupted by noise and can be considered to be entirely correlated with the input signal; (b) the linear transfer characteristic relating the response of a particular signal to the input is essentially invariant over a small range of frequency (say, $\pm$ 0.2 rad/sec). As we show below, the first assumption can be tested in a given measurement situation. If the assumption is violated, we consider the measurements unreliable and proceed accordingly. We cannot directly test the second assumption in a specific situation. However, analysis of previous experimental data (including model analysis) indicates that describing functions and spectra vary smoothly with frequency and can thus be considered constant over the small range of frequency we are considering here.

Let X_k be the Fourier transform of the signal $x(t)$ as computed for the k_{th} input frequency. According to the first assumption,

$$X_k \simeq T_k \cdot I_k$$

where I_k is the transform of the k_{th} input component, and T_k is the linear transfer characteristic relating the two signals. At neighboring frequencies, where both input-correlated and remnant power may be important, the following relationship applies:

$$X_{k+j} = X_{i_{k+j}} + X_{r_{k+j}} \tag{A-1}$$

where the subscripts "i" and "r" denote input-correlated and remnant-related signal components. Since the transfer characteristic is assumed invariant for small values of the index "j", the correlated power may be written as

$$X_{i_{k+j}} = T_k \cdot I_{k+j}$$

or, in terms of measurable quantities:

$$X_{i_{k+j}} = \left[\frac{X_k}{I_k}\right] \cdot I_{k+j} \tag{A-2}$$

Equations (A-1) and (A-2) may be combined to yield the following computation for the remnant-related component of the signal:

$$X_{r_{k+j}} = X_{k+j} - \left[\frac{X_k}{I_k}\right] I_{k+j}$$

A-4

We now define the "corrected" measure of input-correlated power to be

$$\Phi_{x_i x_{i_k}} = \frac{1}{2} \sum_{j=-J}^{+J} |X_{i_{k+j}}|^2$$

and the remnant power associated with the k_{th} input component is

$$\Phi_{x_r x_{r_k}} = \frac{1}{2J} \cdot \frac{1}{2} \sum_{j=-J}^{+J} |X_{r_{k+j}}|^2$$

Since pilot remnant appears to be a continuous function of frequency, the estimate of remnant power is normalized by the factor 2J to yield average power per measurement interval. No such normalization is performed on the estimate of input-correlated power, as the theoretical input signal has power at only a few widely-separated frequencies.

A.3   Describing Functions

Estimates of pilot describing functions at input frequencies were obtained by dividing the transform of the control signal by the transform of the error signal. Similar manipulations of transforms were performed to provide estimates (at vibration frequencies) of the transfer characteristics relating (a) shoulder acceleration to platform acceleration, (b) inboard bitebar acceleration to platform acceleration, (c) outboard bitebar to inboard bitebar accelerations, and (d) elbow to shoulder accelerations.

A-5

A.4   Measurement Reliability

Measurement reliability is determined by the ratio of "signal"
power to "noise" power at a given measurement frequency. Two signal/
noise ratios must be considered when analyzing measures of tracking
performance: the ratio of total power to remnant power estimated at
a given frequency, and the ratio of remnant power to system (other
than pilot) noise.

As noted above, reliable estimates of the input-correlated
stick and error power are needed to obtain reliable estimates of
the pilot describing function. The best estimate of the input-
correlated power at a given input frequency is the difference
between the total power at that frequency and the average of the
remnant power at neighboring frequencies. There is some un-
certainty associated with the estimate of input-correlated power,
however, since, at a given frequency, the remnant-related signal
may combine positively or negatively with the input-correlated
signal. If we assume that the phase relation between remnant
and input-correlated power is uniformly distributed between 0
and 360 degrees, the standard deviation of the error (in dB)
associated with the estimate of input-correlated power is related
to the signal/noise ratio as shown in Table A-1. In this case,
"signal" refers to input-correlated power and "noise" to remnant
power.

Since vibration influences tracking performance primarily
through an increase in pilot remnant, reliable estimates of the
remnant spectrum are desired to test models of pilot performance
in vibration environments. Table A-1 can be used to determine
the reliability of the remnant estimate as well, where we now
interpret the remnant as "signal" and system noise as "noise".

Table A-1

Error in Estimating Signal Power

Ratio of Total Power to Noise Power (dB)	Standard Deviation of Error in Estimate of Signal Power (dB)
4	4.7
6	3.4
8	2.6
10	2.0
12	1.6
14	1.2
16	1.0
18	0.8
20	0.6

Note that system noise can only be obtained in an experiment in which there is no tracking, or in which tracking is performed by an appropriate electronic feedback network.

For the data analyzed in this study we adopted a signal/ noise criterion of 3 dB, which corresponds to approximately a 7 dB ratio of total power to noise power. That is, spectral and describing function measurements were considered unreliable and disregarded in further analysis wherever total signal power failed to be at least 7 dB greater than the estimated noise power. "Corrected" (as described above) estimates of remnant power were used in making this test.

Vibration spectra from one experimental run were examined in considerable detail to determine the fidelity of the platform vibration spectrum and to assess the utility of deriving linear models for biodynamic response mechanisms. The spectrum of the platform acceleration was examined in the vicinity of the nominal vibration frequencies to explore for possible distortion in the component sinusoids. The spectrum appeared to be very clean for the particular data examined. Power was down by at least 20 dB outside a band of $\pm$ 0.2 rad/sec about each nominal input frequency. Furthermore, there were no significantly large "spikes" of power between input frequencies. Thus, power at non-input frequencies was relatively smoothly distributed over frequency, at least in the frequency region spanned by the five vibration input frequencies.

Detailed inspection of the spectra for shoulder and bitebar signals showed that the fall-off about the nominal vibration frequency was about the same as the fall-off of the platform spectrum. Furthermore, the ratio of vibration-correlated to remnant power (measured in the vicinity of vibration input frequencies) was generally quite large for all biodynamic quantities.

Biodynamic data from selected experiments were analyzed to determine the fraction of total response power not correlated with the platform acceleration. As shown in Table A-2, the fractional remnant power was, on the average, about 20%. Head and limb motions were thus largely due to linear coupling with the platform, and emphasis was accordingly placed on measuring biodynamic describing functions.

A.5   Equivalent Continuous Spectra

The 100-second measurement interval yielded line spectra with a spacing of approximately 0.0623 rad/sec between successive lines. These line spectra were transformed into equivalent continuous spectra for comparison with model results. Remnant-related spectra were transformed simply by dividing the power at each measurement frequency by the "measurement window" of 0.0623 rad/sec.

Because the power in the tracking input was basically concentrated at five frequencies instead of being distributed continuously over frequency, input-correlated spectral measurements could not be transformed into equivalent continuous density functions by normalizing with respect to the measurement sindow. Instead, a "box car" approximation was made to the input spectrum.

Table A-2

Average Fractional Remnant Power of Biodynamic
Acceleration Variables

Variable	Experimental Condition	
	Light Spring Stick Center	Light Stiff Stick Side
Shoulder	.084	.115
Elbow	.126	.351
Inboard Bitebar	.286	.254
Outboard Bitebar	.196	.181
Average	.199	

That is, each sinusoidal component of the input was considered to represent the integral of a constant power density extending over the region of fr.quency space bounded by the geometric midpoints of the component frequency and the two neighboring frequencies. Input·correlated power measurements were then normalized with respect to the frequency interval spanned by the corresponding segment of the box-car input.

A.6 Some Definitions

We use the term "spectrum" to refer both to discrete spectral measurements as well as to continuous power spectral density functions. Spectra are defined as being nonzero over positive frequencies only, and signal variance is related to the "spectrum" as follows:

$$\sigma_x^2 = \int_0^\infty \phi_{xx}(\omega)\,d\omega$$

where $\phi_{xx}(\omega)$ is the spectrum of the signal $x(t)$ and σ_x^2 is the variance of $x(t)$. In the case of a discrete spectrum, the integration over frequency is to be interpreted as a summation.

Tracking inputs and vibration inputs are assumed to be linearly uncorrelated. By definition, "remnant" power is not linearly correlated with either of these signals. Therefore, the spectrum of any tracking or biodynamic variable may be considered to be the sum of three component spectra:

$$\phi_{xx} = \phi_{x_i x_i} + \phi_{x_v x_v} + \phi_{x_r x_r}$$

where the subscripts "i", "v", and "r", designate components of
signal power that are correlated with the tracking input,
correlated with the vibration input, and remnant-related.
Similarly, signal variance may be considered as the combination
of three components:

$$\sigma_x^2 = \sigma_{x_i}^2 + \sigma_{x_v}^2 + \sigma_{x_r}^2$$

where each component variance is equal to the integral over
positive frequencies of the corresponding component spectrum.

APPENDIX B
ANALYSIS OF BIODYNAMIC RESPONSE DATA

There are a number of biodynamic response mechanisms that act to degrade tracking performance when the pilot/vehicle system is subjected to vibration environments. Direct mechanical coupling between the vibration input and the control stick (i.e., vibration feedthrough) will introduce a control input that is linearly correlated with the system. Such an input can have a significant effect on performance, especially if the vehicle has resonant characteristics at vibration frequencies (e.g., aircraft bending modes). Feedthrough may also increase the level of wide-band pilot remnant by interfering with neuro-muscular feedbacks needed for precise control of the stick. Similarly, vibration of the limbs may also interfere with these feedbacks.

Relative motion between the eye point-of-regard and the display may induce blurring and thus degrade visual inputs needed for effective control. Since the oculomotor system will not allow the eye to compensate for relative motions at frequencies above 4 Hz, visual interference effects can be inferred to a large extent from a study of vibration-induced head motion. Finally, exposure of long duration to substantial vibration can be expected to induce fatigue and and a general feeling of ill-being, thereby leading to further degradation in tracking performance.

A comprehensive set of biodynamic response measures was obtained in the experimental program so that the relative importance of various vibration-related interference mechanisms could be assessed. Acceleration of the vibrating platform was recorded

along with shoulder and elbow acceleration. Accelerometers mounted on a bitebar provided measures indicative of linear and rotational head motion. In addition, the Fourier analysis techniques described in Appendix A allowed us to identify the portion of the pilot's control response linearly related to the platform vibration. From these measures were obtained linear models (i.e., describing functions) relating body, head, and limb motions to the vibration input. These models were then used to infer measures that were not directly obtained (such as relative motion between the eye fixation point and the display).

Response measures obtained for the various biodynamic mechanisms are presented below, and special analysis procedures used in obtaining these measures are described. We begin presentation of the experimental results with a description of the data base.

B.1.1 Data Base for Biodynamic Measurements

As noted in Section 2, not all test subjects participating in the experimental program participated in each sub-experiment. In addition, as explained later in this Appendix, certain biodynamic measures obtained in the early experiments could not be calibrated reliably for analysis.

The data base for the results presented in this Appendix is indicated in Table B-1. An "X" in the column labeled C (or S) indicates that a reliable measure was obtained with the stick located in the center (or side) position.

Table B-1

Data Base for Biodynamic Measurements

Stick	Subject													
	CBH		PH		RM		DM		JP		AP		DS	
	C	S	C	S	C	S	C	S	C	S	C	S	C	S

a. Shoulder, Elbow, and Bitebar Accelerations

Stick	C	S	C	S	C	S	C	S	C	S	C	S	C	S
Light Spring	X	X	X	X	X			X			X	X		X
Medium Spring		X		X				X		X		X		X
Heavy Spring		X		X		X		X		X		X		X
Light Stiff	X	X	X	X		X	X	X	X			X	X	X
Medium Stiff	X		X		X		X		X		X		X	
Heavy Stiff	X		X		X		X		X		X		X	

b. Vibration-Correlated Component of Control Response

Stick	C	S	C	S	C	S	C	S	C	S	C	S	C	S
Light Spring	X	X	X	X	X			X			X	X	X	X
Medium Spring	X	X	X	X	X			X		X	X	X	X	X
Heavy Spring		X		X		X		X	X			X		X
Light Stiff	X	X	X	X		X	X	X	X			X	X	X
Medium Stiff	X	X	X	X	X	X	X		X		X	X	X	X
Heavy Stiff	X		X		X		X		X		X		X	

C: Indicates reliable data available for center stick location

S: Indicates reliable data available for side stick location

B.1.2 Rms Acceleration Scores

As noted in Table B-1, only the light spring and light stiff stick configurations yielded reliable measures of all biodynamic varia'les for both center and side locations. Rms acceleration scr es for shoulder, elbow, inboard bitebar, and outboard bitebar accelerometers are shown for both locations in Table B-2a. Scores (in units of g) are shown for each of five test subjects, and the mean performance of these subjects is given.

A summary of the analysis of variance of these scores is given in Table B-2b. Entries show the level of significance of performance differences. No significant primary effects due to stick location or stick configuration are found for any of the four biodynamic measures, and significant differences across subjects are shown only for the bitebar accelerations. Since stick location has no significant effect on these measures, further analysis of biodynamic data is based (here possible) on measures averaged across side and center stick locations.

Rms acceleration scores are shown for seven test subjects in Table B-3. Also shown are mean performance as well as standard deviations and standard errors computed acorss subjects.*
Wherever possible, data have been averaged across side and center stick locations.

*See Appendix A for a definition of statistical measures.

a) <u>Effect of Stick Location on Rms Acceleration Scores</u>

Stick	Location	Subject					
		CBH	PH	DM	AP	DS	Mean

a. Shoulder

Stick	Location	CBH	PH	DM	AP	DS	Mean
Light Spring	Center	.238	.328	.275	.314	.337	.298
Light Spring	Side	.230	.268	.274	.347	.305	.285
Light Stiff	Center	.300	.307	.275	.378	.336	.319
Light Stiff	Side	.240	.254	.308	.275	.260	.267

b. Elbow

Stick	Location	CBH	PH	DM	AP	DS	Mean
Light Spring	Center	.291	.331	.316	.338	.255	.306
Light Spring	Side	.912	.282	.277	.236	.302	.402
Light Stiff	Center	.412	.363	.304	.327	.284	.338
Light Stiff	Side	.272	.708	.446	.380	.297	.421

c. Inboard Bitebar

Stick	Location	CBH	PH	DM	AP	DS	Mean
Light Spring	Center	.308	.232	.342	.394	.280	.311
Light Spring	Side	.344	.271	.367	.365	.350	.339
Light Stiff	Center	.384	.260	.391	.362	.327	.345
Light Stiff	Side	.410	.234	.346	.347	.296	.327

d. Outboard Bitebar

Stick	Location	CBH	PH	DM	AP	DS	Mean
Light Spring	Center	.265	.216	.280	.329	.248	.268
Light Spring	Side	.311	.239	.314	.229	.314	.301
Light Stiff	Center	.325	.244	.323	.321	.293	.301
Light Stiff	Side	.306	.219	.287	.296	.262	.274

b) <u>Summary of Analysis of Variance</u>

Source of Difference

Variable	Location	Stick	Subject	Location X Stick	Location X Subject	Stick X Subject
Shoulder	-	-	-	-	-	-
Elbow	-	-	-	-	-	-
Inboard Bitebar	-	-	.01	.-	-	-
Outboard Bitebar	-	-	.01	.01	-	-

Entries show level of significance

Table B-3

Rms Acceleration Scores

Stick	Individual Subjects							Statistics		
	CBH	PH	RM	DM	JP	AP	DS	Mean	SD	SE

a. Shoulder

Stick	CBH	PH	RM	DM	JP	AP	DS	Mean	SD	SE
Light Spring	.234	.298	.175	.274	.404	.330	.321	.291	.073	.028
Medium Spring	.343	.275		.323	.313	.290	.233	.296	.039	.016
Heavy Spring	.276	.260	.272	.194	.256	.298	.269	.261	.032	.012
Light Stiff	.270	.280	.200	.292	.394	.276	.298	.287	.057	.022
Medium Stiff	.286	.314	.301	.326	.362	.268	.239	.299	.040	.015
Heavy Stiff	.288	.317	.257	.286	.233	.286	.282	.278	.027	.010

b. Elbow

Stick	CBH	PH	RM	DM	JP	AP	DS	Mean	SD	SE
Light Spring	.602	.306	.269	.296	.308	.287	.278	.335	.119	.045
Medium Spring	.794	.780		.414	.326	.220	.428	.494	.239	.098
Heavy Spring	.302	.353	.323	.837	.365	.524	.347	.436	.191	.072
Light Stiff	.342	.536	.269	.375	.318	.354	.290	.355	.088	.033
Medium Stiff	.354	.353	.696	.408	.336	.256	.424	.404	.140	.053
Heavy Stiff	.415	.435	.364	.374	.388	.366	.376	.388	.027	.010

c. Inboard Bitebar

Stick	CBH	PH	RM	DM	JP	AP	DS	Mean	SD	SE
Light Spring	.326	.252	.346	.354	.280	.380	.315	.322	.044	.017
Medium Spring	.335	.292		.360	.275	.352	.422	.339	.053	.022
Heavy Spring	.342	.296	.372	.327	.302	.324	.295	.323	.028	.011
Light Stiff	.397	.247	.283	.368	.255	.354	.312	.317	.058	.022
Medium Stiff	.322	.274	.450	.388	.280	.361	.369	.349	.062	.024
Heavy Stiff	.354	.275	.344	.308	.345	.369	.273	.324	.039	.015

d. Outboard Bitebar

Stick	CBH	PH	RM	DM	JP	AP	DS	Mean	SD	SE
Light Spring	.288	.228	.300	.297	.261	.329	.281	.283	.032	.012
Medium Spring	.312	.277		.317	.256	.315	.368	.308	.038	.016
Heavy Spring	.165	.227	.246	.212	.212	.406	.301	.253	.079	.030
Light Stiff	.316	.232	.238	.305	.242	.308	.278	.274	.036	.014
Medium Stiff	.306	.267	.494	.330	.261	.323	.327	.330	.078	.029
Heavy Stiff	.195	.285	.249	.245	.237	.492	.195	.271	.102	.039

All scores are in g's.

Table B-4 contains a summary of the analysis of variance performed on the scores contained in Table B-3. Because of the missing data point for Subject RM, this analysis is performed on data provided by the remaining six subjects. Since there is only one entry per subject per stick configuration (center, side, or the average of the two), we can compute only main effects.

Table B-4 shows that there are no main effects for the shoulder and elbow accelerations and that only inter-subject differences are significant for the bitebar accelerations. We therefore conclude that limb and head vibrations are essentially invariant with regard to the specifics of the control stick. Furthermore, the lack of inter-subject differences (at least as far as shoulder and elbow response is concerned) justifies consideration of the "average man" that is defined by the average response behavior of the test subjects.

B.2   Vibration Feedthrough

B.2.1   Analysis Procedures

Vibration feedthrough is defined as the component of the pilot's control response that is linearly related to the vibration input. Describing functions relating control response to vibration were obtained using the Fourier analysis procedure described earlier. These measures were averaged across subjects for purposes of model analysis. In order that the effects of stick location be observable, however, averaging was not performed across center and side conditions.

B-7

Table B-4

Analysis of Variance of Data in Table B-3

Variable	Source of Difference	
	Stick	Subject
Shoulder	—	—
Elbow	—	—
Inboard Bitebar	—	.001
Outboard Bitebar	—	.01

Entries show level of significance

As expected, the feedthrough describing function varied with the control-stick characteristics. In order to characterize these results in a manner that would allow extrapolation to control-stick designs not studied in this program, a regression analysis was performed to identify portions of the response mechanism independent of control-stick parameters.

The following model structure was assumed:

$$X(j\omega) \equiv \frac{C}{\alpha}(j\omega) = \frac{ZT(j\omega)}{ZO(j\omega) + ZS(j\omega)} \qquad (B-1)$$

where   C = stick response in inches

α = table vibration in g's

ZT = the effective biodynamic transfer impedance of the pilot in lb/g,

ZO = the effective biodynamic output impedance of the pilot in lb/in,

ZS = the mechanical impedance of the control stick in lb/in.

The parameters ZT and ZO are intended to reflect the biodynamical properties of the pilot and the interface between the pilot and the cockpit. For this model form to have maximum predictive capability, ZT and ZO should be independent of the mechanical and electrical properties of the control stick. (Location of the control stick will in general affect these parameters, however, since stick location influences positioning of the body and limbs.)

Two sets of transfer characteristics were determined: one set for center stick location and one for side. A non-parametric regression analysis was performed, that is, no analytic form was assumed for the frequency dependency of ZT and ZO. Instead, independent regression analysis was performed on the data obtained at each vibration frequency.

The algorithm for the regression analysis is developed as follows. Let $X_i(j\omega_1)$ be the stick/table transfer function measured at a particular frequency ω_1 with the i_{th} control configuration, and let $\hat{X}_i(j\omega_1)$ be the transfer that is predicted by the model of equation (B-1) for the "best" values of ZT and ZO. From equation (B-1) we obtain

$$\hat{X}_i = \frac{ZT}{ZO + ZS_i} \qquad\qquad (B-2a)$$

$$\frac{1}{\hat{X}_i} = \frac{1}{ZT}[ZO + ZS_i] \qquad\qquad (B-2b)$$

where the argument $(j\omega_1)$ is omitted for compactness.

We now define $ZTI \equiv 1/ZT$
$$ZOT \equiv ZO/ZT \qquad\qquad (B-3)$$

which allows equation (B-2b) to be rewritten as

$$\frac{1}{\hat{X}_i} = ZOT + ZTI \cdot ZS_i$$

The fractional error in $1/\hat{X}_i$ (which is approximately equal in magnitude to the fractional error in $\hat{X}_i$ for small errors) is

$$e_i \equiv \frac{\frac{1}{\hat{X}_i} - \frac{1}{X_i}}{\frac{1}{X_i}} = \frac{X_i}{\hat{X}_i} - 1$$

$$e_i = ZOT \cdot X_i + ZTI \cdot Z_i \cdot ZS_i - 1$$

B-10

The expression for the modeling error may be given in the
following matrix form

$$
\begin{bmatrix} e_1 \\ \cdot \\ \cdot \\ \cdot \\ \cdot \\ e_n \end{bmatrix}
=
\begin{bmatrix} \hat{X}_1 & \hat{X}_1 \cdot XS_1 \\ \cdot & \cdot \\ \cdot & \cdot \\ \cdot & \cdot \\ \hat{X}_n & \hat{X}_n \cdot ZS_n \end{bmatrix}
\begin{bmatrix} ZOT \\ ZTI \end{bmatrix}
-
\begin{bmatrix} 1.0 \\ \cdot \\ \cdot \\ \cdot \\ \cdot \\ 1.0 \end{bmatrix}
$$

which we may express by the shorthand notation

$$
\underline{E} = \underline{A} \cdot \underline{Z} - \underline{B}
$$

Note that the matrix $\underline{A}$ consists of measured (X_i) and known (ZS_i)
quantities, both of which will generally be complex.

ZOT and ZTI can be determined if measurements are obtained
for two or more stick configurations. The values that minimize
the sum of the squared modeling errors are given by the expression

$$
\begin{bmatrix} ZOT \\ ZTI \end{bmatrix}
=
(\overset{*}{\underline{A}}{}' \ \underline{A})^{-1} \cdot \overset{*}{\underline{A}}{}' \ \underline{B}
$$

where $\overset{*}{\underline{A}}{}'$ denotes the complex conjugate of the transposed matrix.
The parameters ZT and ZO are then derived from the identities of
equation (B-3).

If measurements are obtained for only two stick configura-
tions, values for ZT and ZO can be found to provide a perfect
match to the stick/table transfer function at each measurement
frequency. If measurements are obtained for more than two stick
configurations, a good match to the data will be possible only if

B-11

the basic assumption underlying the regression analysis is valid;
namely, that there are identifiable components of the vibration
feedthrough mechanism that are independent of control-stick para-
meters.

B.1.2 Experimental Results

Average stick/platform transfer functions are given in
Figures B-1 and B-2 for each of the six control stick configurations.
Measures for both center and side locations, where available, are
shown separately. Amplitude ratios (expressed in dB) represent the
vibration-correlated control response in inches per g of platform
acceleration.

The amplitude ratios reveal no consistent differences
between center and side locations. Location does have a noticeable
effect on phase shift, however. A less negative phase shift is
consistently shown for the center location, especially at the
lower vibration frequencies. In addition, the curves for the
side location show an increase in phase shift occurring between
the 5 and 7 Hz (31 and 44 rad/sec) vibration . equencies — a
trend not revealed for the center location.*

The transfer and output impedances derived from these
measurements are shown in Figure B-3. Also shown for comparison
are the mechanical impedances for each of the six control sticks.
Amplitude ratios indicate pounds/g for the transfer impedance
and pounds/inch for the output and stick impedances. Again,

---

*Since phase shift is a circular measure, it is possible that some
 of the phase measures shown in these figures are in error by 360°.
 Additional measures in the region of 5-7 Hz (or alternatively, a
 reliable theoretical model) are required to shed further light on
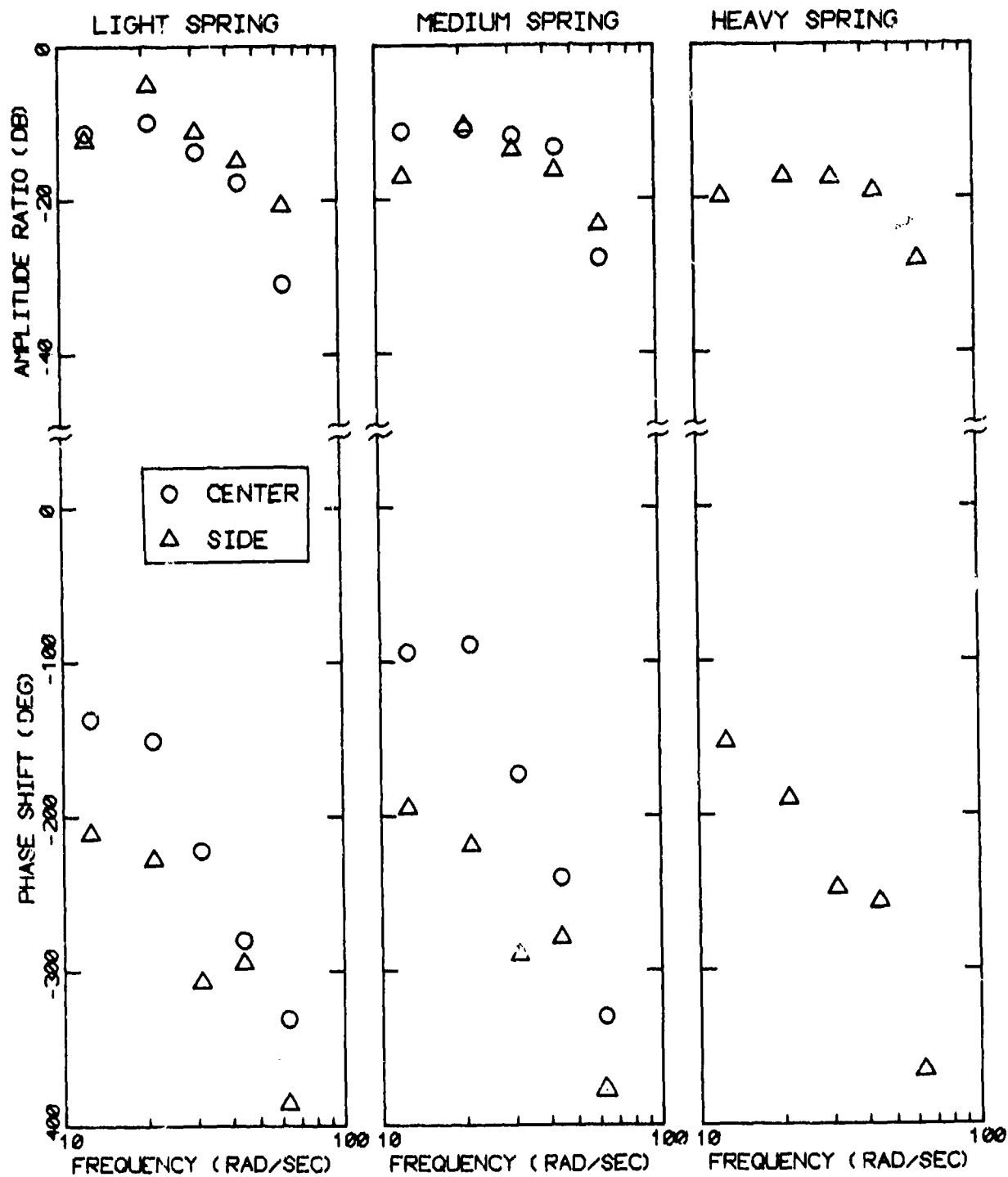 the frequency dependency of the phase shift response.

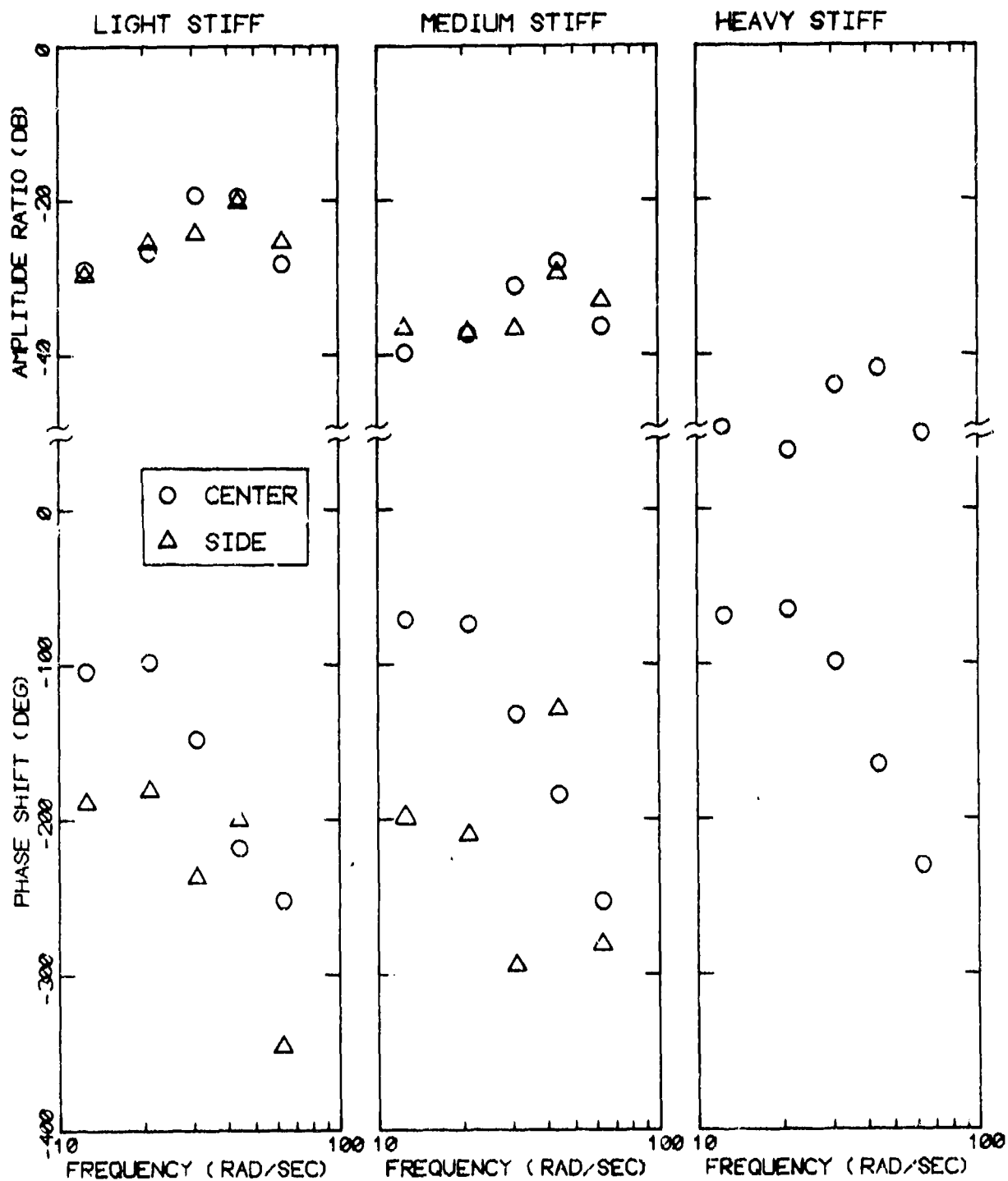Figure B-1. Average Stick/Platform Describing Functions, Spring Sticks

B-13

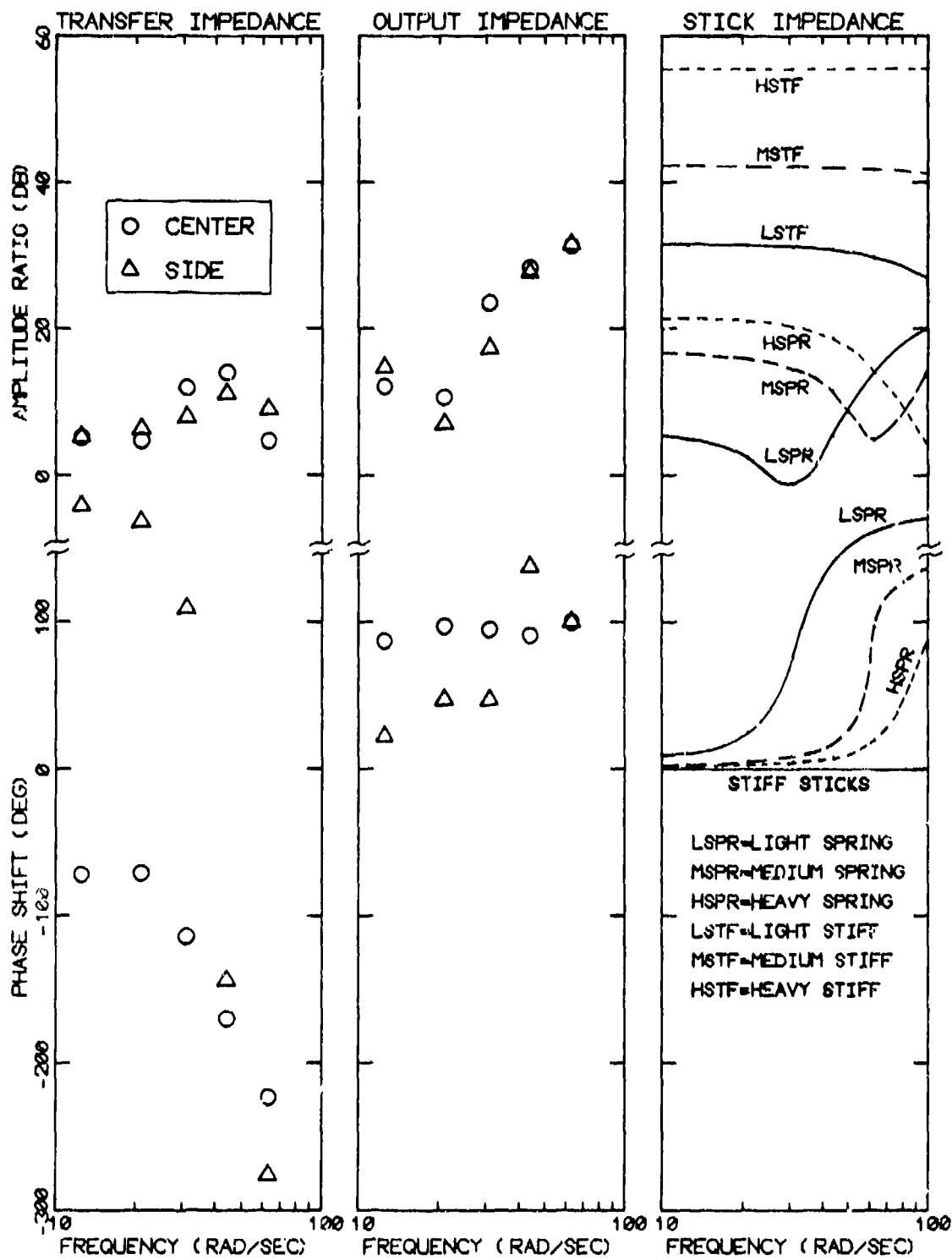Figure B-2. Average Stick/Platform Describing Functions, Stiff Sticks

B-14

Figure B-3.   Transfer, Output, and Stick Impedances

stick location has an appreciable effect on phase shift and a
negligible effect on amplitude ratio.

The impedance functions help explain the way in which the
stick/platform transfers (particularly the amplitude ratio) change
with stick parameters. For stick configurations which yield a
stick impedance less than the output impedance ZO, one would
expect the stick/platform transfer to be largely independent of
stick impedance. Conversely, as the stick impedance become much
larger than ZO, the stick/platform transfer should begin to vary
inversely with stick impedance.

The transfers shown in Figures B-1 and B-2 largely confirm
these predicted trends. The light spring and medium spring sticks
show similar stick/platform transfers. On the other hand, the
stiff sticks yield stick/platform amplitude ratios that appear to
decrease inversely with the stick impedance.

Considerable effort was made to find simple analytic
approximations to the transfer and output impedances. While good
second-order fits were obtained for the amplitude ratios for both
side and center locations, a good match to the phase-shift behavior
was not obtained. Accordingly, we have refrained from presenting
smooth approximations to these impedance functions.

In order to assess the validity of summarizing vibration
feedthrough mechanisms in terms of the impedance functions ZT and
ZO, we have used these derived measures to "predict" the vibration-
correlated component of the control scores by carrying out the
following computation:

$$\sigma_{c_v}^2 \; (volts^2) \;\; = \;\; \sum_{i=1}^{5} \left| \frac{ZT}{ZO \, + \, ZS} \right|^2 \, K_e^2 \; \phi_{\alpha_p \alpha_p}$$

These predicted scores are compared with the corresponding experimental measurements in Figure B-4. For the most part, there is good agreement between predicted and measured vibration-correlated scores over a large dyramic range. Thus, we are justified in using the impedance concept; we can, with reasonable confidence, extrapolate the results of this experiment to situations involving other control configurations, provided we restrict the problem situation to one having the same biodynamic and vibration environments explored in this study.

B.3   Shoulder and Elbow Response

B.3.1   Analysis Procedures

Describing functions relating shoulder and elbow acceleration to platform acceleration were computed as described in Appendix A. Because of the constraints of the computer program that was used to digitize the analog data, however, special effort was required to calibrate acceleration variables. Since reliable calibrations could not be obtained for all experiments, some biodynamic data had to be omitted from analysis because of scale-factor uncertainties. Calibration methods are discussed below.

The computer program that was available for digitizing the experimental data required that two different but constant signal levels be provided for each analog variable. Given these two signal levels, and provided with the interpretation of each signal level in terms of experimental units, the program was then able to compute for each problem variable the linear relationship between signal level in experimental units and volts received at the A/D converter.
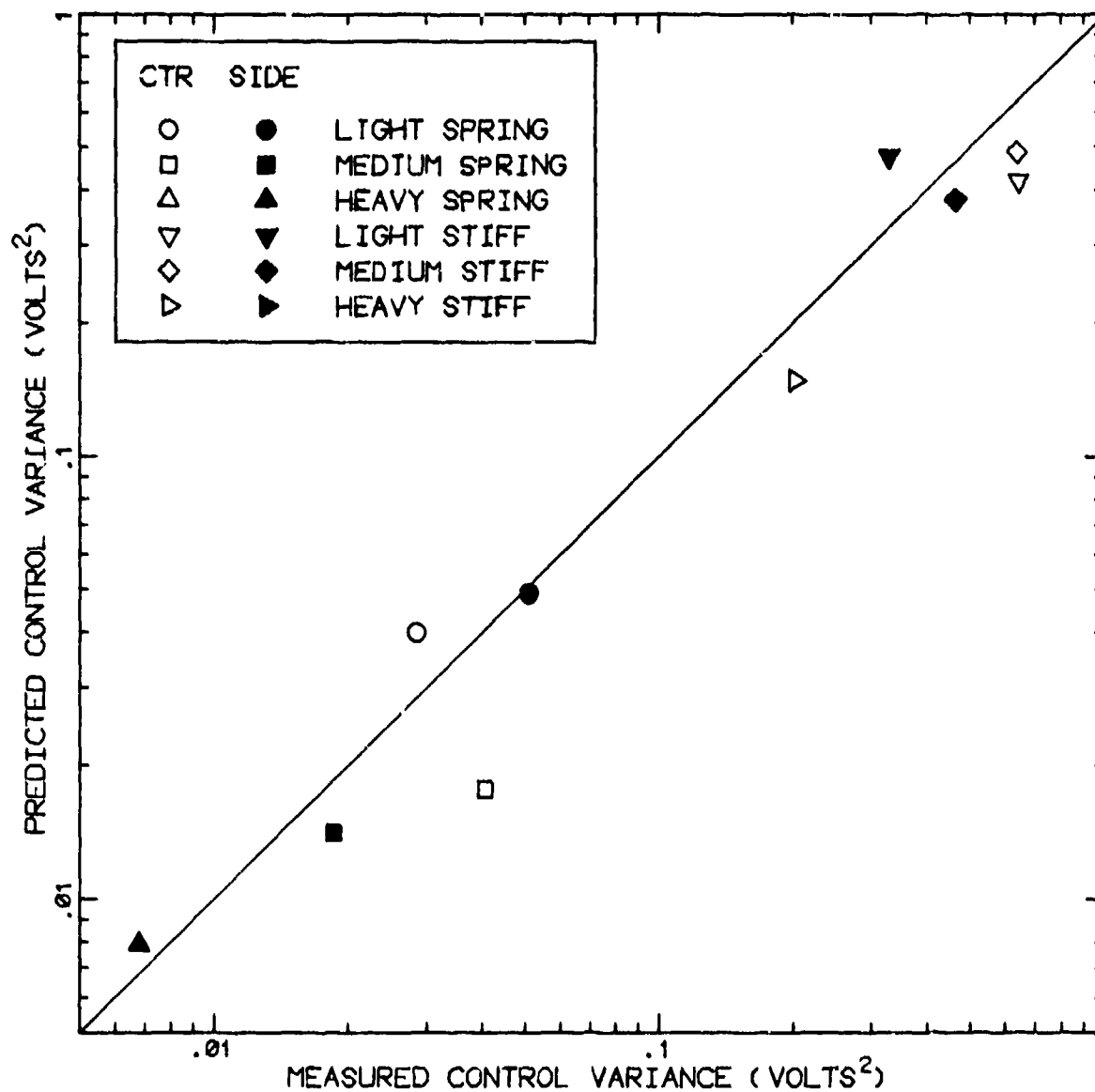
Figure B-4. Comparison of Predicted and Measured Vibration-Correlated Control Scores

B-18

Constant levels were recorded on analog tape for each of the tracking variables, and calibration of these signals proceeded without difficulty. Since the accelerometers could not be subjected to a constant acceleration for a sufficient length of time, however, it was not possible to record the desired constant calibration voltages on analog tape. Instead, all accelerometers were subjected to sinusoidal vibration at 10 Hz, and this information was used during playback to generate constant calibration levels.

Calibration of acceleration signals was considered unreliable for Experiments 1 and 2 because (a) calibration signals were not "clean", and (b) transformation of the sinusoidal calibration signal to a d.c. level was not sufficiently sophisticated. For these experiments, we simply examined the sinusoidal calibration signal visually by playback into an oscilloscope, and used the analog computer to generate d.c. voltages equal to plus and minus the zero-to-peak amplitude of the sinusoid. Accuracy of this procedure was hindered by the presence of significant low-frequency noise on the 10 Hz sinusoid that was recorded on analog tape, and the short duration of the calibration signal prohibited much in the way of electronic filtering. We therefore felt that acceleration signals obtained in these two experiments were subject to possible significant errors with regard to determining the scale factor and should not be used for analysis.

The reliability of calibration was greatly improved in subsequent experiments by providing signals less corrupted by noise and of longer duration, and by using an electronic filtering technique to determine the required constant calibration levels. Each calibration sinusoid was processed by a low-

pass filter to reduce the possible low-frequency noise corruption (including d-c bias), and the filter output was rectified to yield a voltage equal to the zero-peak swing of the sinusoid.

B.3.2 Experimental Results

Describing functions relating shoulder acceleration to platform acceleration are shown for the six stick configurations in Figure B-5. These results reflect measures obtained from the center, side, or average of center and side locations, according to the availability of the data (see Table B-1). Since no consistent differences are observed across stick configuration, we are justified in coalescing these data into a single average describing function, also shown in the same figure. The smooth curve represents an analytic approximation to the average shoulder/platform describing function having the form

$$\frac{\alpha_s}{\alpha_p}(s) = \frac{1 + (B/K)s}{1 + (B/K)s + (\frac{M}{K})s^2}$$

where $B/K = .033$ seconds and $M/K = .0012$ seconds^2.

Elbow/shoulder describing functions are shown for all stick configurations in Figure B-6. Except perhaps for some high-frequency phase differences associated with the stiff sticks, the elbow appears to respond in phase with the shoulder but at a slightly greater amplitude. By averaging across the five frequency points and across the six sticks we find that the amplitude of the elbow response is about 1.4 dB greater than the shoulder response. This is a somewhat lesser difference than indicated by the rms acceleration scores shown in Table B-3, where the average ratio of rms elbow score to rms shoulder score
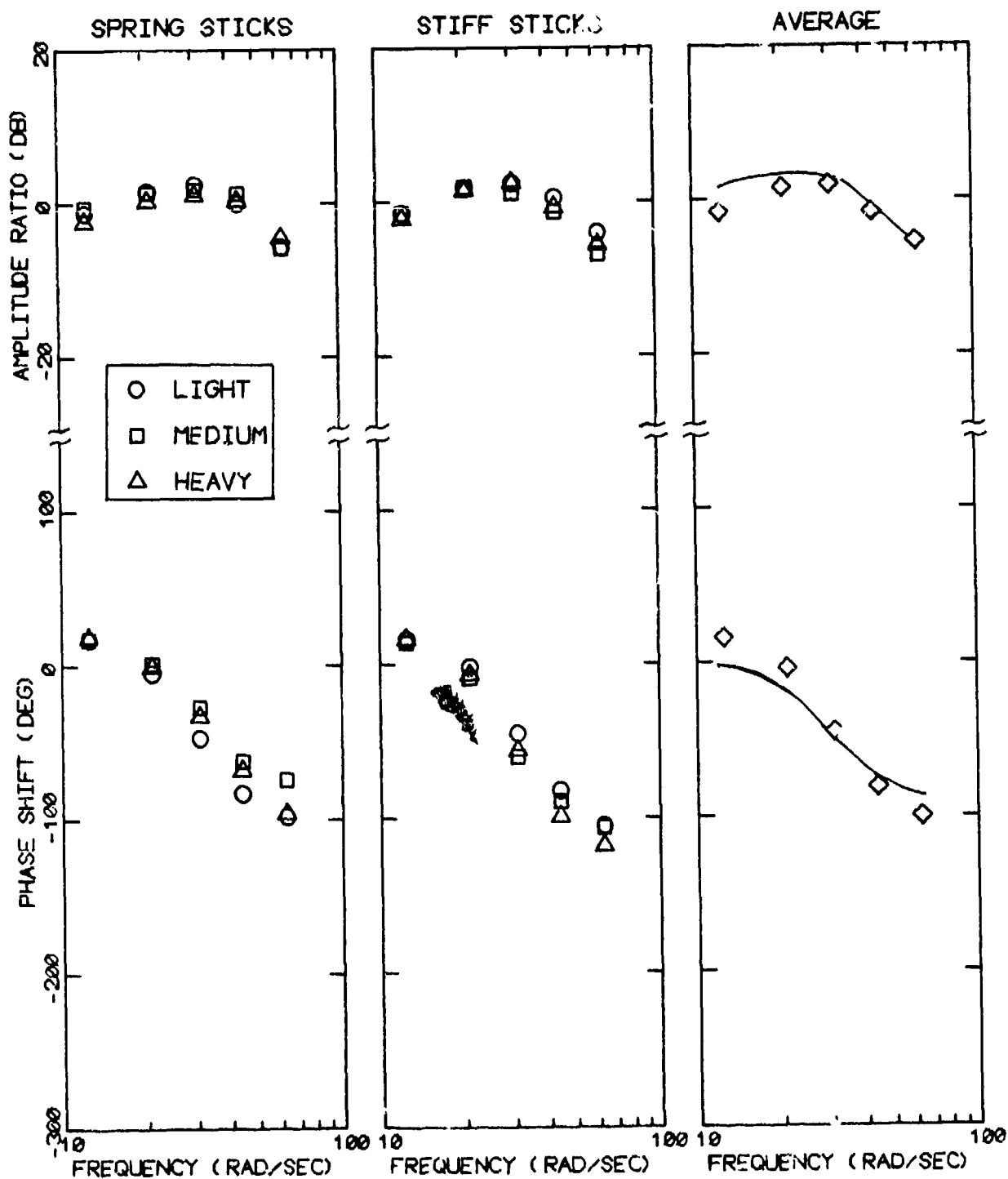
Figure B-5. Shoulder/Platform Describing Functions
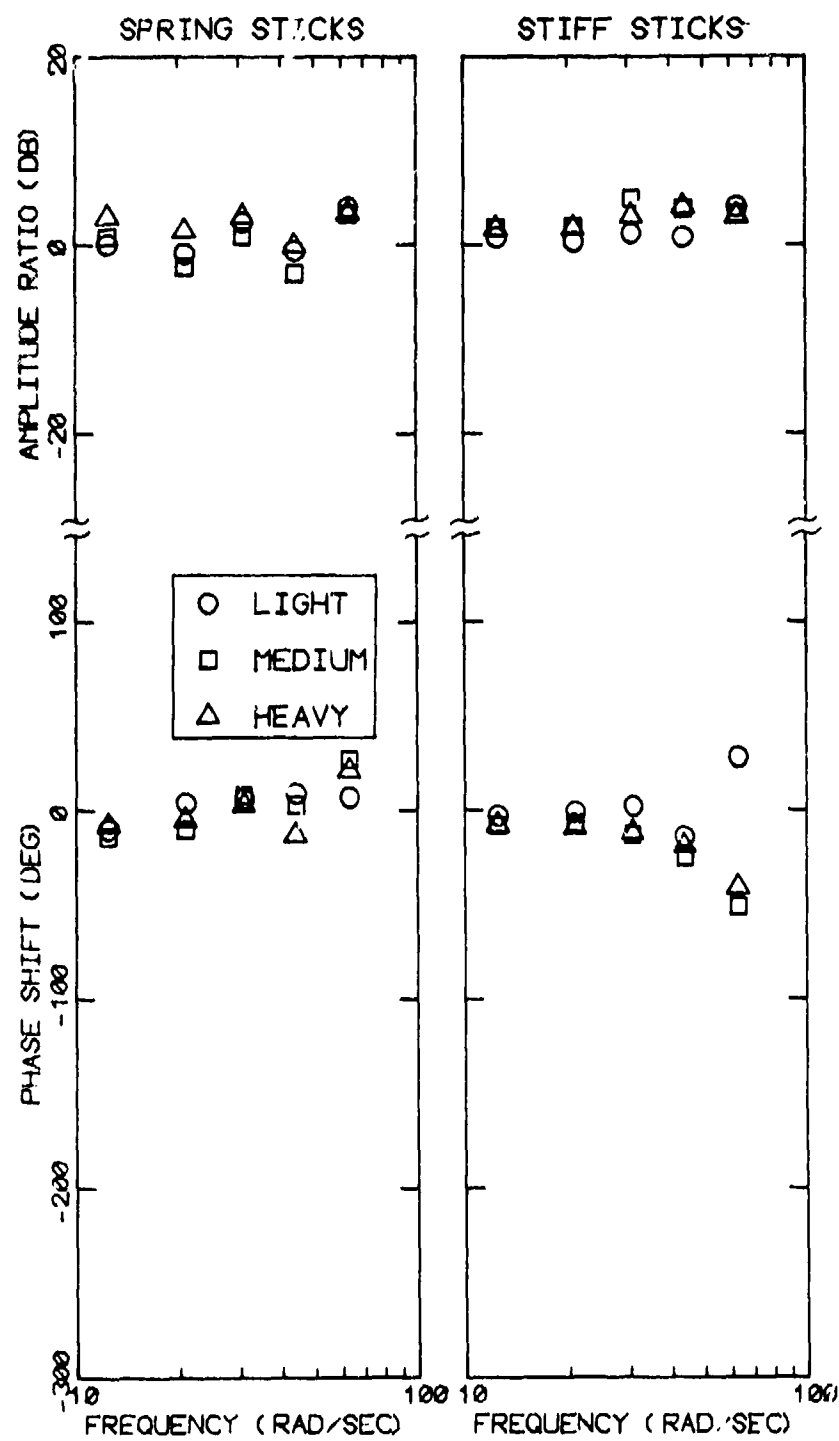
Figure B-6. Average Elbow/Shoulder Describing Functions

B-22

is about 1.4 (a difference of about 3 dB). The data of Figure B-6 are based entirely on the components of shoulder and elbow response that are linearly correlated with the platform vibration. As shown previously in Table A-2, a larger fraction of the elbow response is uncorrelated with platform motion, which may account for the greater difference in rms acceleration scores.

B.4   Head Motion

Measurements obtained from the inboard and outboard bitebar accelerometers were used to compute describing functions relating translational and rotational response of the head to platform acceleration. Relative motion between the head point-of-regard and the display was also computed from these measures. Computational techniques and experimental results are described below.

B.4.1 Analysis Procedures

The measurement situation is diagrammed in Figure B-7.

Let D = the viewing distance, inches

       S = separation between the inboard and outboard accelerometers, inches

       Z_i = vertical displacement of the inboard bitebar, inches

       Z_o = vertical displacement of the outboard bitebar, inches

       Z_h = vertical displacement of the head point-of-regard, inches, obtained by projecting the line of the two accelerometers to the plane of the display

       θ = angle of head rotation, radians
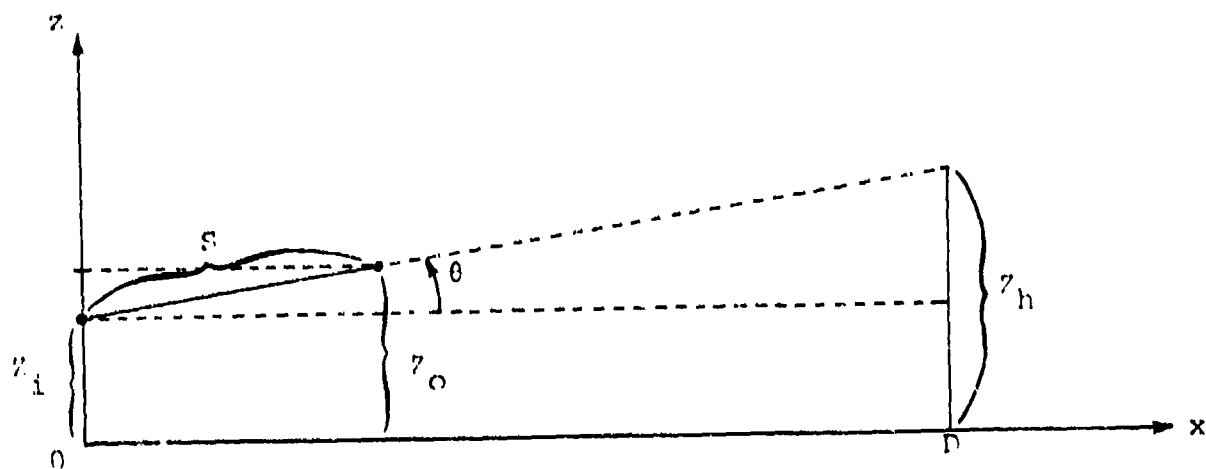
Figure B-7. Measurement of Head Translation and Rotation

For small angles of rotation, the following approximations are valid:

$$\theta \simeq \frac{z_o - z_i}{S} \simeq \frac{z_h - z_i}{D} \tag{B-4}$$

$$\alpha_\theta \simeq 386.4 \, \frac{(\alpha_o - \alpha_i)}{S} \simeq 386.4 \, \frac{(\alpha_h - \alpha_i)}{D} \tag{B-5}$$

where α_i, α_o, and α_h denote vertical accelerations of the inboard accelerometer, outboard accelerometer, and the head point-of-regard in g; and α_θ denotes rotational acceleration of the head in rad/sec^2.

Measurements at our disposal were the outputs of the inboard and outboard accelerometers. These signals were Fourier transformed to provide the following describing functions: (a) $\frac{\alpha_i}{\alpha_p}$, relating acceleration of the inboard accelerometer to platform accelerometer, and (b) $\frac{\alpha_o}{\alpha_i}$, relating acceleration of the outboard accelerometer to that of the inboard accelerometer. Both these quantities are dimensionless.

Translation of the head was considered equivalent to translation of the inboard bitebar, and the relationship between head rotation and platform acceleration was computed in terms of measureable quantities by appropriate manipulation of equation (B-5). Thus,

$$\frac{\alpha_h}{\alpha_p} = \frac{\alpha_i}{\alpha_p} \tag{B-6}$$

$$\frac{\alpha_\theta}{\alpha_p} = \frac{386.4}{S} \left(\frac{\alpha_o}{\alpha_i} - 1 \right) \frac{\alpha_i}{\alpha_p} \tag{B-7}$$

where $\dfrac{\alpha_i}{\alpha_p}$ is a dimensionless quantity and $\dfrac{\alpha_\theta}{\alpha_p}$ has units of $(\text{rad/sec}^2)/g$.

Relative motion between the head point-of-regard and the display was computed as follows. First, we manipulate the identity shown in equation (B-5) to yield the following expression for head point-of-regard acceleration:

$$\alpha_h = \alpha_i + \frac{D}{S}(\alpha_o - \alpha_i)$$

We then compute the describing function relating acceleration of the head point-of-regard to platform acceleration in terms of measureable quantities:

$$\frac{\alpha_h}{\alpha_p} = \frac{\alpha_i}{\alpha_p} + \frac{D}{S}\left(\frac{\alpha_o}{\alpha_i} - 1\right)\frac{\alpha_i}{\alpha_p}$$

Finally, we note that the display is attached rigidly to the platform, and the spectrum acceleration of the head point-of-regard with respect to the display is given as

$$\phi\alpha_{dh}\alpha_{dh} = \left|\frac{\alpha_h}{\alpha_p} - 1\right|^2 \phi\alpha_p\alpha_p$$

$$\phi\alpha_{dh}\alpha_{dh} = \left|\left[1 + \frac{D}{S}\left(\frac{\alpha_o}{\alpha_i} - 1\right)\right]\frac{\alpha_i}{\alpha_p} - 1\right|^2 \phi\alpha_p\alpha_p \qquad (B-8)$$

where $\phi\alpha_{dh}\alpha_{dh}$ is the relative acceleration of the head point-of-regard in inches/sec^2 and $\phi\alpha_p\alpha_p$ is the platform acceleration in g. Appropriate integrations of this spectral quantity yield mean-squared displacement and velocity of the head point-of-regard relative to the display.

B.4.2 Experimental Results

Describing functions relating inboard bitebar acceleration
to platform acceleration are shown in Figure B-8 for the six stick
configurations; describing functions relating outboard to inboard
bitebar accelerations are shown in Figure B-9. Results obtained
from side and center locations have been combined where possible.

The bitebar/platform describing functions are virtually
identical for the six stick configurations; hence, we may consider
the average describing function (also shown in Figure B-8).
Figure B-9 shows that the describing functions relating outboard
to inboard bitebar acceleration are nearly identical for four
of the stick configurations (all but heavy spring and heavy
stiff). These transfer functions are essentially flat with
near-unity gain and are averaged together in Figure B-9c. The
remaining describing functions show an amplitude variation of
about 4 dB across the measurement range. It is not clear why
these transfers should differ from the others, and in Section
B.4.3 we discuss the possibility of measurement error.

Describing functions relating head rotational acceleration
to platform acceleration were computed from the preceding measures
as indicated by equation (B-7). These describing functions are
shown for each of the six stick configurations in Figure B-10;
also shown in this figure is the average over four configurations
(all but heavy spring and heavy stiff). Zero dB indicates
1 deg/sec^2 head rotation per g of platform acceleration.

The curves shown in Figure B-10 display appreciably greater
frequency dependency than do the describing functions presented in
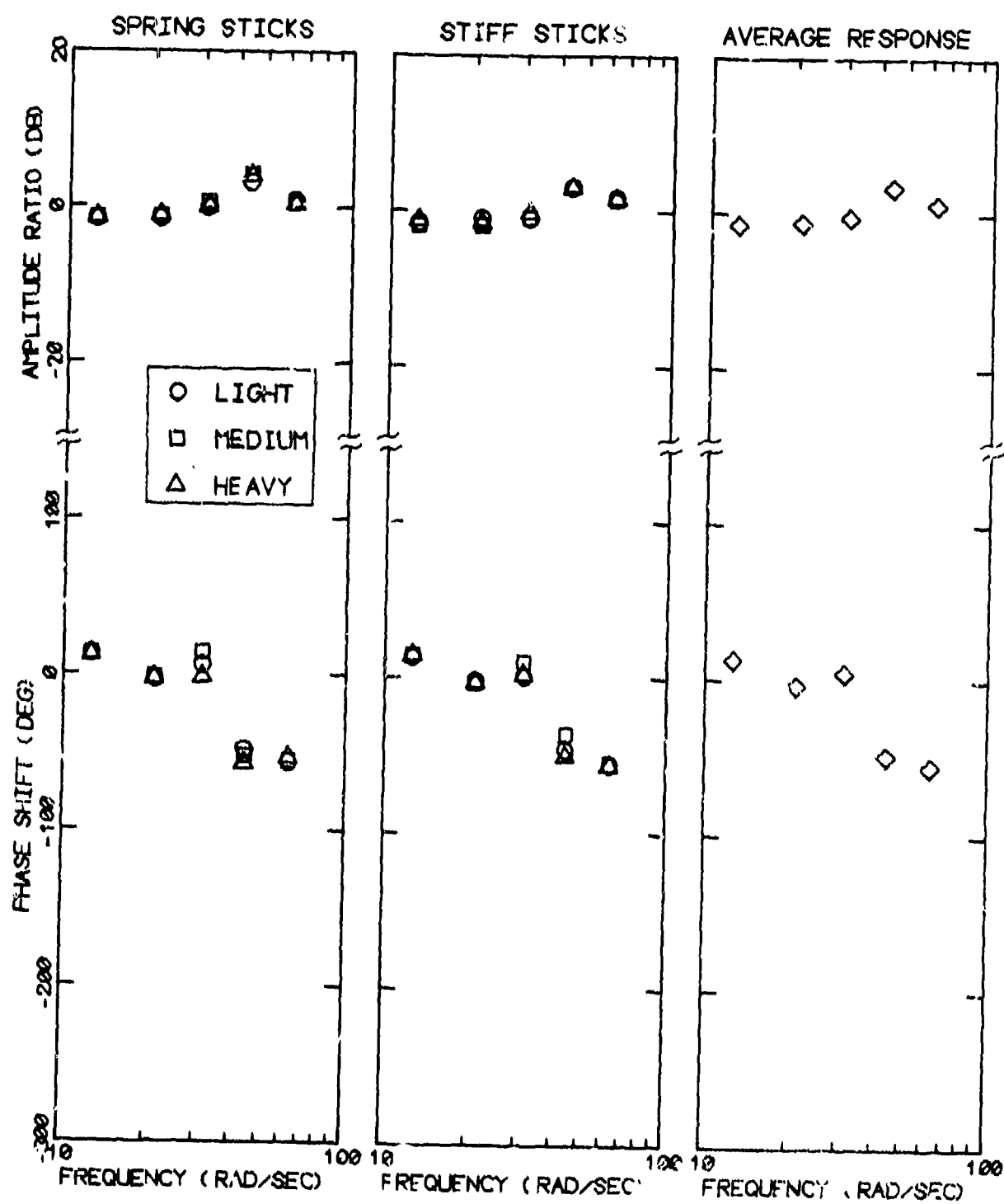the preceding two graphs. The apparent cause of the large swings

Figure B-8.   Describing Functions Relating Acceleration of Inboard Bitebar to Platform Acceleration
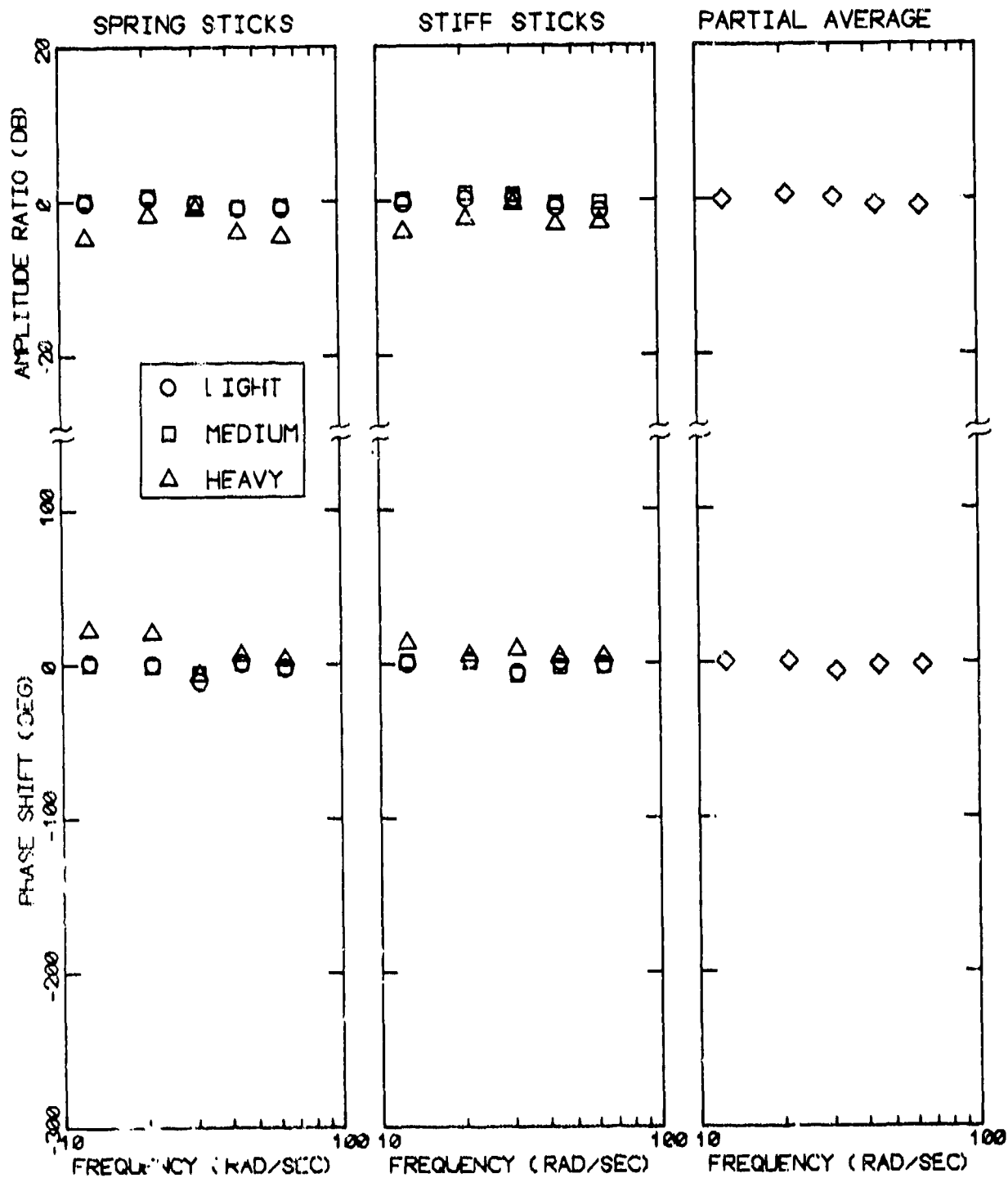
Figure B-9. Describing Functions Relating Outboard to Inboard Bitebar Acceleration
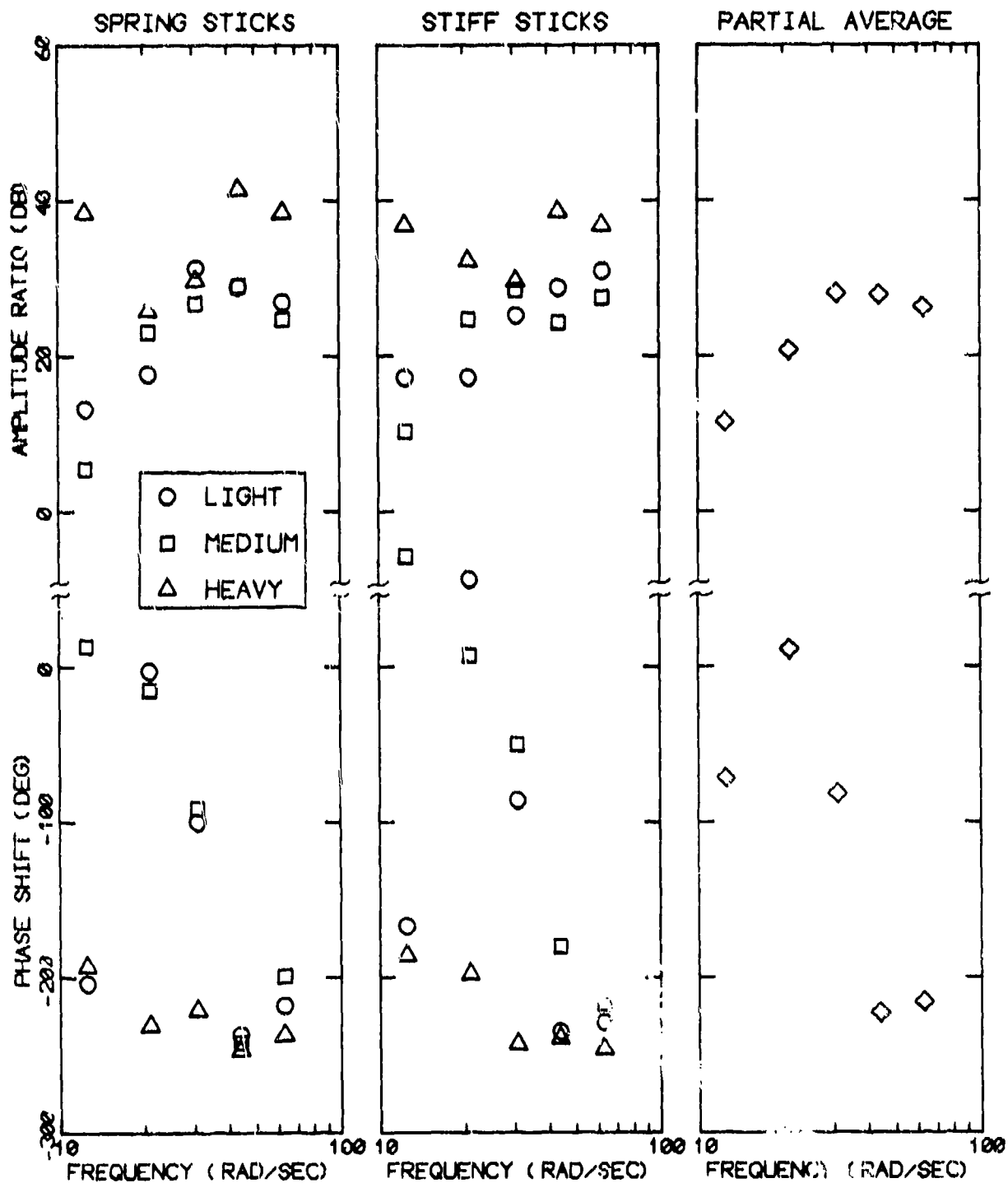
Figure B-10.   Describing Functions Relating Head Rotation to Platform

in both amplitude and phase is that the inboard and outboard
accelerometers are subjected to nearly the same acceleration,
for the most part. As these accelerations approach identity in
amplitude and phase, the describing function α_o/α_i will approach
zero amplitude (i.e., a large negative dB value) and may change
by 180 degrees, as can be seen from inspection of equation (B-7).

Equation (B-8) was used to compute the spectrum of the
acceleration of the head point-of-regard with respect to the
display. Appropriate frequency-weighting and integration of
this spectrum provided estimates of relative rms displacement
and rms velocity of the head point-of-regard.

Estimated displacement and velocity quantities for the head
point-of-regard are shown in Table B-5a. As might be expected
from the describing functions relating head rotation to platform
vibration, values predicted for the heavy spring and heavy stiff
sticks were considerably greater than corresponding measures
predicted for the remaining four configurations. Data provided by
the heavy spring and stiff sticks were considered anomalous, as
explained below, and only data from the remaining sticks was used
for further analysis.

The spectrum of the acceleration of the eye point-of-regard,
relative to the display, was estimated by simply ignoring the
components of spectrum for head motion below 4 Hz. (That is, we
assumed the oculomotor system would compensate for head motion
below this frequency.) Frequency-weighting and integration were
then carried out to obtain rms displacement and velocity.
The results of this analysis, conducted for four of the six stick
configurations, are shown in Table B-5b. The average rms dis-
placement was normalized with respect to the display gain to obtain
a suitable visual noise parameter for subsequent model analysis.

Table B-5

Estimated Rms Motion Quantities of Eye and
Head Point-of-Regard Relative to the Display

Device	Rms Motion	
	Displacement (inches)	Velocity (inches/sec)

a. Head Point-of-Regard

Light Spring	.218	4.35
Medium Spring	.132	3.0
Heavy Spring	2.01	27.4
Light Stiff	.232	3.73
Medium Stiff	.191	3.90
Heavy Stiff	1.66	21.9

b. Eye Point-of-Regard

Light Spring	.117	3.81
Medium Spring	.064	2.23
Light Stiff	.067	2.51
Medium Stiff	.083	2.84
Average	.083	2.85

B.4.3   Investigation of Possible Measurement Error

As every attempt had been made to maintain a constant bio-
dynamic environment throughout the experimental program, the
extremely large head motions (relative to the display) observed
for the heavy spring and heavy stiff stick configurations were
quite unexpected. Consequently, additional analysis was under-
taken to determine whether or not these results might be the
result of possible measurement error (where "measurement error"
includes all sources of error in the experimental, recording,
and analysis procedures).

Suspicious as to the reliability of the data were aroused
by the fact that data for the heavy spring and heavy stiff stick
configurations were obtained from the same subexperiment (Experi-
ment 7), where the stiff stick was at center location and the
spring stick at the side. Accordingly, we proceeded to analyze
the results of the subsequent experiment, in which the same
sticks were used with their locations reversed. The objective
here was to determine whether or not there was a consistent
relation between head motion and control-stick design. If such
a consistency were to be observed (i.e., if Experiment 8 showed
the same behavior as Experiment 7), we would assume that the
subjects had changed their posture when manipulating these control
devices and that such postural changes resulted in larger vibration-
induced head motion. Alternatively, if the results of Experiment 8
were similar to the results of the earlier experiments, we would
question the validity of the results of Experiment 7.

Data from Experiment 8 were not obtained in time to ?
digitization and analysis of the type performed on preceding
subexperiments. Therefore, a simple check was performed on the
data of Experiments 7 and 8 as well as on data from an earlier
subexperiment (Experiment 6).

Mean-squared deviational scores were computed for the inboard
bitebar acceleration and for the difference between inboard and out-
board accelerations. (A large difference score implies large head
rotations.) Signals were high-pass filtered to eliminate possible
d-c bias from the recorded signals. The primary variable of
interest was the ratio of the difference score to the score obtained
from the inboard accelerometer.

As expected from the foregoing analysis, the ratio score
obtained from the data of Experiment 7 was, on the average, appre-
ciably higher than the score computed from data of Experiment 6.
The data of Experiment 8, however, confirmed the results of
Experiment 6 (medium spring and medium stiff sticks). Accordingly,
we concluded that some form of measurement error must have been
present in Experiment 7 with regard to the signals obtained from
either or both of the bitebar accelerometers, and these data were
ignored in subsequent analysis.

APPENDIX C

ANALYSIS OF TRACKING PERFORMANCE

Tracking performance in both static and vibration conditions is analyzed in some detail in this Appendix, and comparisons are presented between experimental data and model output. Rms error and control scores are analyzed first, followed by analysis of frequency-domain measures.

Preliminary analysis of performance scores was performed on the tracking scores obtained from four subjects to explore possible effects of stick location on tracking performance. Analysis of variance revealed no statistically significant effects. Accordingly, the bulk of the analysis of performance scores — and all analysis of frequency-domain measures — was performed on averages (where possible) of measures obtained from the two stick locations.

C.1   Rms Performance Scores

Rms error and control scores are shown for each of seven test subjects for static and vibration tracking in Table C-1. Also shown are average performance scores as well as standard deviations and standard errors computed across subjects.* All scores are in volts, referred to the analog simulator.

_____

*Definitions of statistical measures are given in Appendix A.

Table C-1

Rms Performance Scores for Tracking Variables

Stick	Individual Subjects							Statistics		
	CBH	PH	RM	DM	JP	AP	DS	Mean	SD	SE

a. Error, Static Tracking

Stick	CBH	PH	RM	DM	JP	AP	DS	Mean	SD	SE
Light Spring	.330	.330	.426	.446	.533	.588	.415	.438	.096	.036
Medium Spring	.331	.340	.507	.472	.546	.550	.446	.456	.090	.034
Heavy Spring	.418	.308	.491	.320	.483	.355	.497	.410	.083	.031
Light Stiff	.280	.248	.531	.344	.356	.418	.336	.359	.093	.035
Medium Stiff	.262	.244	.539	.319	.314	.443	.318	.348	.105	.040
Heavy Stiff	.320	.210	.369	.244	.350	.302	.345	.306	.059	.018

b. Error, Vibration Tracking

Stick	CBH	PH	RM	DM	JP	AP	DS	Mean	SD	SE
Light Spring	.442	.560	.608	.494	.823	.798	.546	.610	.147	.055
Medium Spring	.435	.522	.679	.502	.687	.652	.536	.573	.099	.037
Heavy Spring	.508	.424	.548	.403	.651	.452	.616	.515	.095	.036
Light Stiff	.471	.495	.647	.480	.545	.630	.472	.534	.076	.029
Medium Stiff	.480	.452	.784	.480	.557	.650	.488	.556	.121	.046
Heavy Stiff	.438	.417	.513	.426	.485	.358	.475	.445	.052	.019

c. Control, Static Tracking

Stick	CBH	PH	RM	DM	JP	AP	DS	Mean	SD	SE
Light Spring	.390	.418	.410	.361	.305	.350	.402	.377	.040	.015
Medium Spring	.392	.394	.499	.390	.301	.320	.374	.381	.064	.024
Heavy Spring	.389	.391	.341	.397	.338	.387	.294	.362	.039	.015
Light Stiff	.388	.384	.377	.359	.335	.332	.361	.362	.022	.008
Medium Stiff	.440	.374	.568	.408	.345	.340	.375	.407	.079	.030
Heavy Stiff	.401	.375	.376	.413	.350	.396	.356	.382	.026	.010

d. Control, Vibration Tracking

Stick	CBH	PH	RM	DM	JP	AP	DS	Mean	SD	SE
Light Spring	.600	.826	.346	.454	.474	.450	.544	.528	.154	.058
Medium Spring	.610	.728	1.07	.430	.322	.350	.460	.568	.265	.100
Heavy Spring	.447	.620	.476	.529	.359	.461	.312	.458	.102	.039
Light Stiff	1.12	1.12	.832	.938	1.47	.848	.810	1.02	.236	.089
Medium Stiff	1.24	1.18	1.29	.938	1.57	.923	.863	1.14	.252	.095
Heavy Stiff	.622	.997	.791	.882	.633	.615	.881	.774	.154	.058

All scores are in volts.

Average performance scores are shown in meaningful physical units as well as in volts in Table C-2. Also shown are the ratios obtained by dividing each error and control score obtained under vibration conditions by the corresponding performance measure obtained in the static condition.

The ratios presented in Table C-2c show that, on balance, vibration caused proportionately larger increases in performance scores for the stiff-stick configurations than for the spring sticks. On the average, spring-stick error scores increased by about 30%, whereas stiff-stick scores increased by about 50%. Larger differences were observed for the effects of vibration on the rms control score. Vibration caused the control score to increase by about 30% on the average for the spring sticks, whereas this score increased by over a factor of 2 for the stiff sticks. Particularly large increases were observed for the light and medium stiff sticks, where, as we shall presently observe, vibration feedthrough accounted for a sizeable portion of the control activity.

Performance differences among the six stick configurations can best be observed from Figure C-1. Figure C-1a shows a somewhat lower rms error for the stiff sticks than for the spring sticks in the absence of vibration. Because of the proportionately greater effect that vibration has for the stiff sticks, however, this trend is essentially nullified under vibration conditions.

Figure C-1b reveals a nearly constant rms electrical control signal for the six sticks under static conditions. As noted above, considerable differences across sticks are shown for the control score under vibration conditions.

Table C-2

Average Rms Performance Scores

Variable	Stick					
	Spring			Stiff		
	Light	Med	Heavy	Light	Med	Heavy

a. Static

		Light	Med	Heavy	Light	Med	Heavy
Error	(volts)	.438	.456	.410	.359	.348	.306
Error	(inches)	.082	.086	.077	.067	.065	.060
Control	(volts)	.377	.381	.362	.362	.407	.382
Control	(inches)	.151	.152	.145	.0105	.0035	.0013
Control	(pounds)	.302	1.07	1.74	.398	.448	.764

b. Vibration

		Light	Med	Heavy	Light	Med	Heavy
Error	(volts)	.610	.573	.515	.534	.556	.445
Error	(inches)	.114	.107	.097	.100	.104	.083
Control	(volts)	.528	.568	.458	1.02	1.14	.774
Control	(inches)	.211	.227	.183	.0290	.0097	.0026
Control	(pounds)	.422	1.59	2.20	1.12	1.25	1.55

c. Ratio of Vibration Score to Static Score

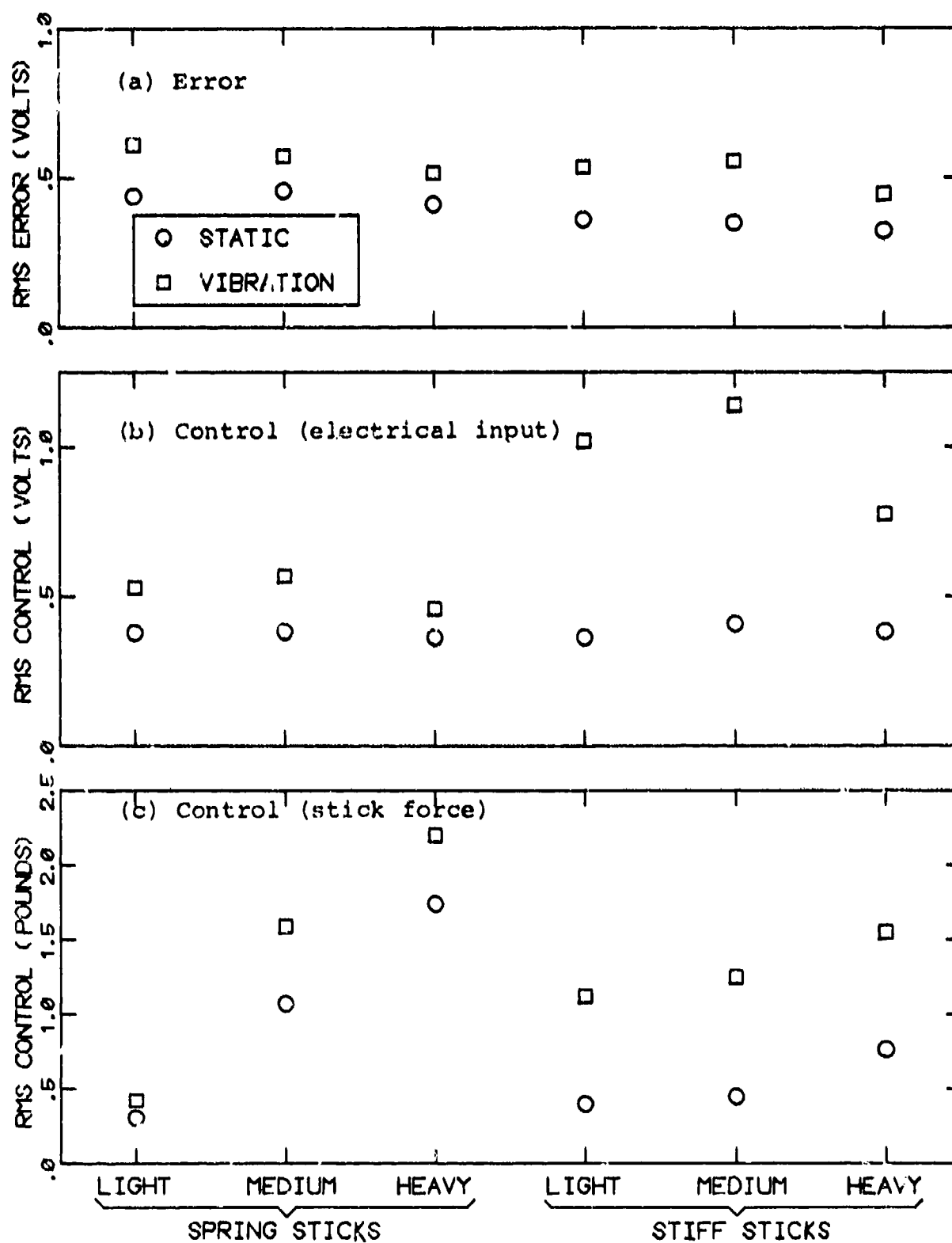|	Light	Med	Heavy	Light	Med	Heavy
Error	1.39	1.25	1.25	1.49	1.60	1.38
Control	1.40	1.50	1.26	3.56	2.81	2.02

Figure C-1.   Effect of Stick Design and Vibration on
               RMS Performance Scores

Figure C-1c shows that the actual control force applied to the stick varies widely from stick-to-stick for both static and vibration tracking. These differences, at least for static tracking, reflect pilot adaptation to the electrical control gain. For example, as the spring gradient is increased for the spring sticks, the effective control gain (in terms of volts/pound) is reduced, and the pilot must increase his rms control force to maintain constant control effectiveness.

Analysis of variance of the rms error and (electrical) control scores is summarized in Table C-3. Analysis across all experimental conditions, summarized in Table C-3a, reveals strong vibration-stick interactions for both error and control scores (significant at the 0.001 level). That is, we can attach statistical significance to the observation noted above; namely, that the increase in performance score due to vibration is different for the various stick configurations. Significant subject-vibration and stick-subject interactions are also found from analysis of the error score.

Because of the significant interactions, the analysis of variance has not for the most part revealed strongly significant main effects. Differences in both error and control score due to vibration are significant only at the 0.05 level, and stick configuration has a significant effect (0.05 level) only on the error score. These results do not imply that vibration and stick design have no highly significant effects on tracking performance, but that these effects should be explored singly rather than in combination.

Table C-3

Summary of Analysis of Variance

a. All Stick Configurations, Static and Vibration Tracking

Variable	Source of Difference					
	Vibr.	Stick	Subj.	Vibr. X Stick	Vibr. X Subj.	Stick X Subj.
Error	.05	.05	.001	.001	.01	.001
Control	.05	-	.05	.001	-	-

b. All Sticks, With or Without Vibration

Conditions	Variable	Source of Difference	
		Stick	Subject
Static	Error	.001	.001
	Control	-	.01
Vibration	Error	.01	.001
	Control	.001	-

c. One Stick Configuration, Static and Vibration

Stick	Variable	Source of Difference	
		Vibration	Subject
Medium Spring	Error	.01	.01
	Control	-	-
Medium Stiff	Error	.001	.001
	Control	.001	-

Table C-3b summarizes the results of analysis of variance performed on the performance measures for static tracking alone and for vibration tracking alone. We now find that stick design has a highly significant effect on rms error in both static and vibration conditions, whereas the effect on rms control is significant only for vibration tracking.

Analysis of variance of the data obtained from two of the stick configurations considered individually is summarized in Table C-3c. The effects of vibration on tracking error are now observed to be highly significant (.01 level or lower) for both the spring and the stiff stick. A significant effect on rms control score is observed only for the stiff stick.

Figure C-2 shows the average error and control variance scores partitioned into input-correlated, vibration-correlated, and remnant components, where "remnant" is defined as signal power correlated with neither tracking nor vibration inputs. Vibration-correlated power contributed less than 10% to the total error variance for all stick configurations. The relative contribution to total control variance, however, varied widely with the sticks. Vibration-related power was small for the spring sticks, but it accounted for almost half of the control variance for the light and medium heavy sticks. About 25% of the control variance was vibration-correlated when the heavy stiff stick was used.

Differences in electrical control gain account for the different relative contributions of vibration feedthrough observed for the stiff-stick configurations. Because of hardware limitations, the gain of the heavy stiff stick was about half of that of the other two stiff sticks. The variance of the vibration-correlated portion
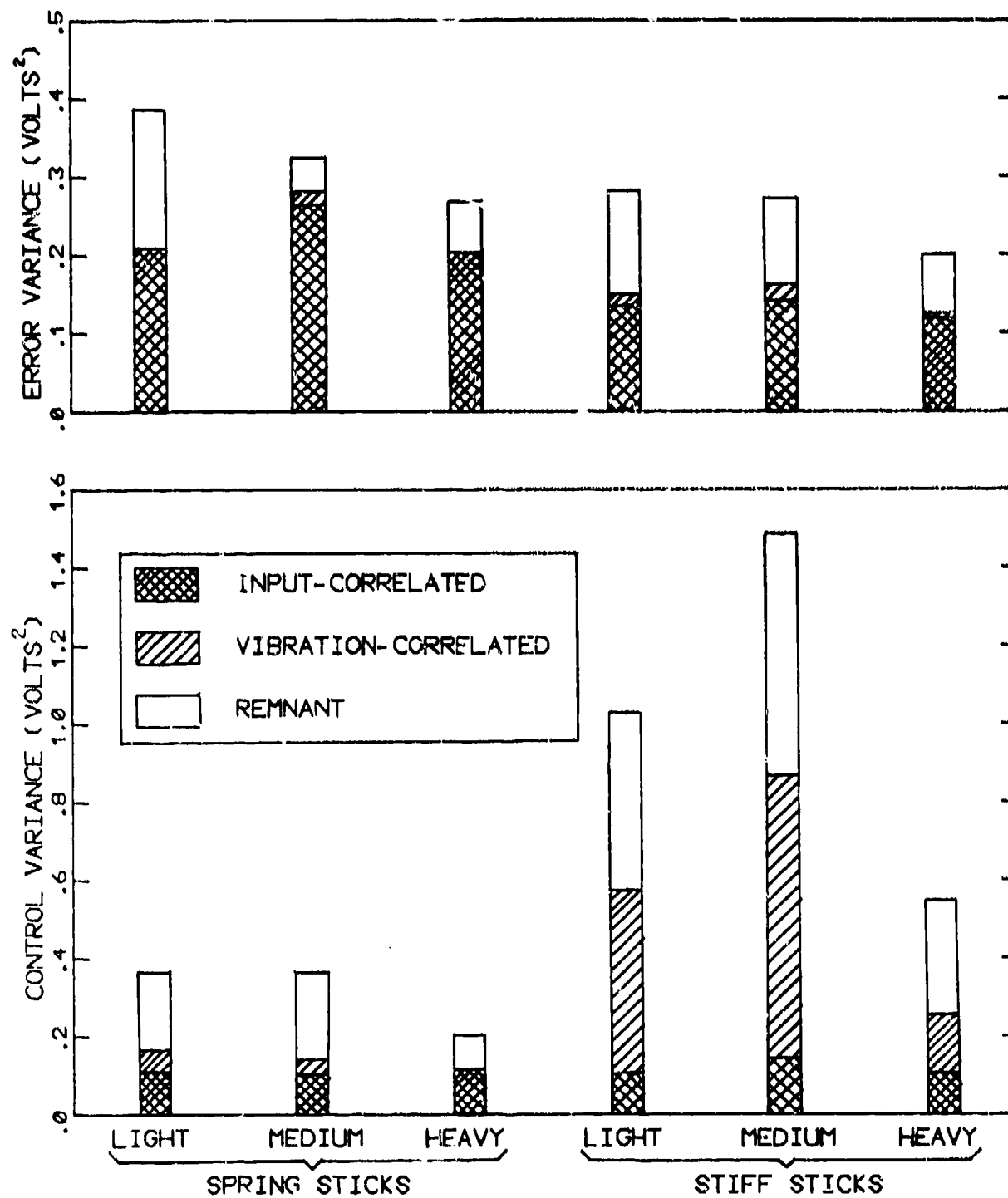
C-8

Figure C-2. Partitioning of Variance Scores

C-9

of the control power, measured as voltage output of the control
device, was therefore reduced by a factor of nearly four. The
portion of the control output related to tracking (including
remnant) varied less across the stiff sticks, since the pilots
increased their control forces to compensate for the reduced
control gain. Hence, the lower proportional contribution of
feedthrough seen for the heavy stiff stick.

Differences in the composition of control power between
spring and stiff sticks reflect differences in stick impedance
as well as control gain. The reader is referred to the main
text of this report for further discussion of the interaction
between stick parameters and performance measures.

C.2   Frequency-Domain Measures

Frequency-domain measures for each of the six stick confi-
gurations are shown in Figures C-3 through C-8 for tracking under
static and vibration conditions. Each figure contains a pilot
describing function relating control output (in volts) to tracking
error (in volts). Also shown in each figure is a spectrum derived
by dividing the remnant-related component of control power (at a
given input frequency) by the input-correlated component of control
power.* This quantity provides an indication of the pilot's signal/
noise capabilities and is needed for testing models for remnant.
We shall refer to this spectrum as the "ratio spectrum".

_____

*The ratio is based on what the input-correlated and remnant spectra
would be if the tracking input spectrum were continuous rather than
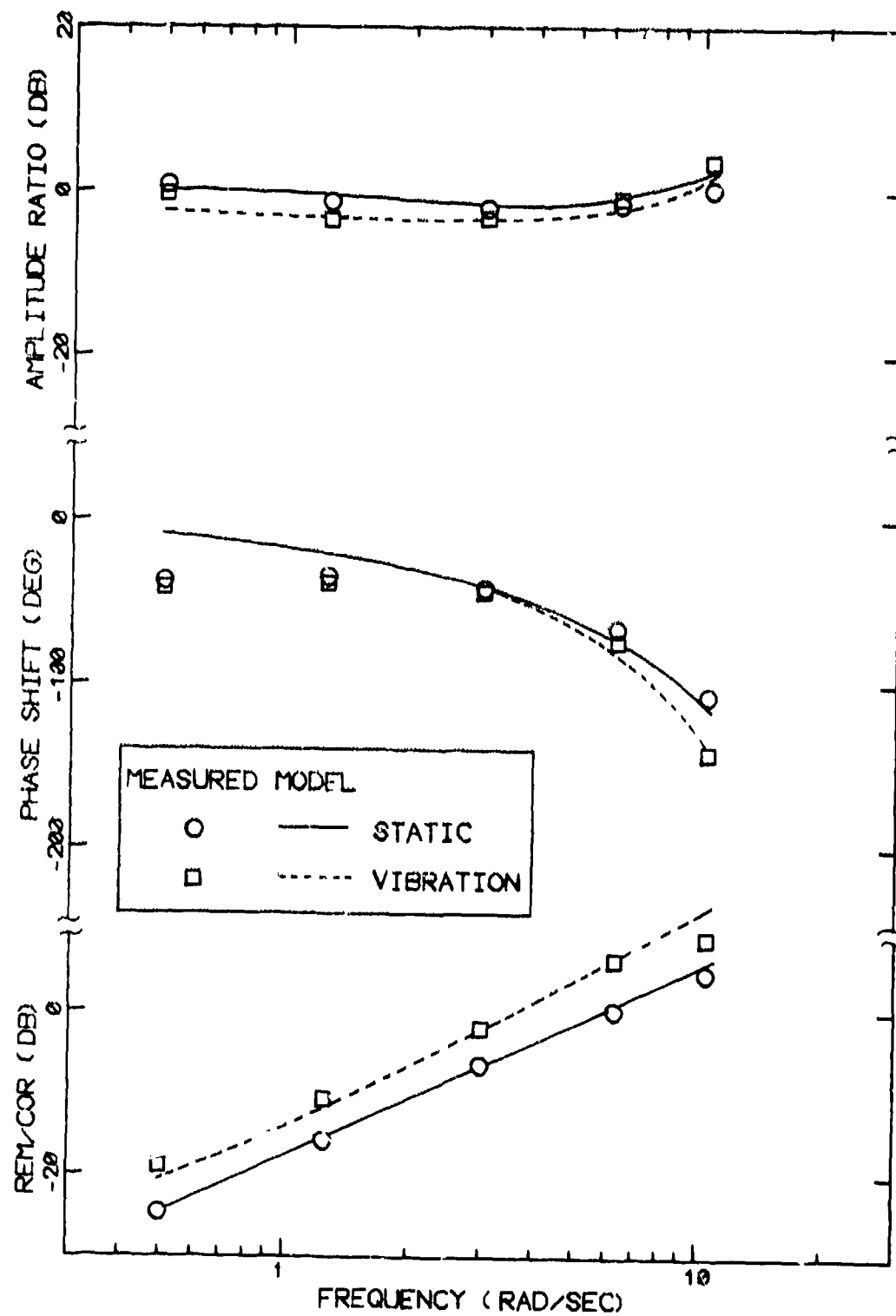sums-of-sinusoids. Details of this computation are given in
Appendix A.

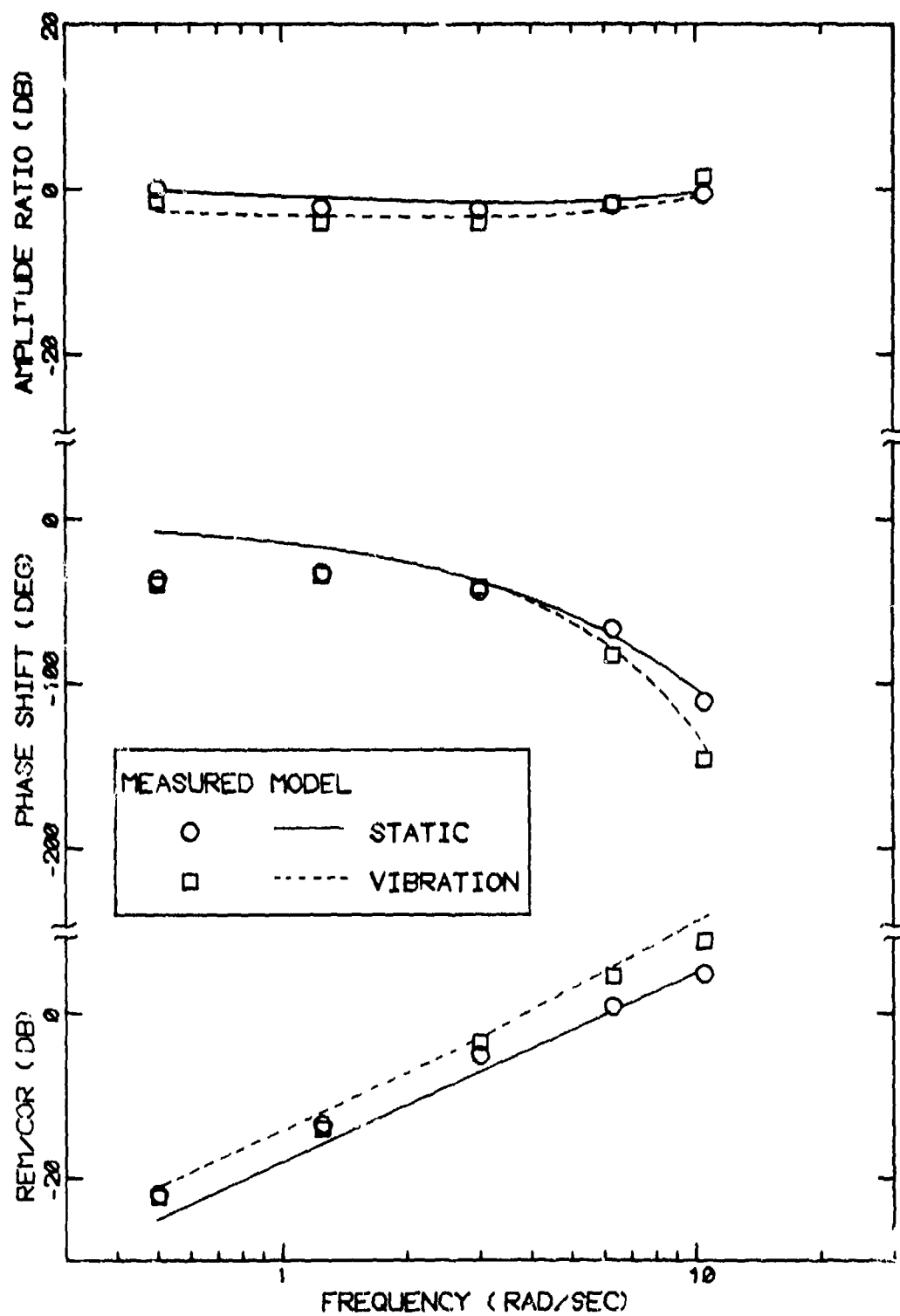Figure C-3. Frequency-Domain Measures for Light Spring Stick

C-11

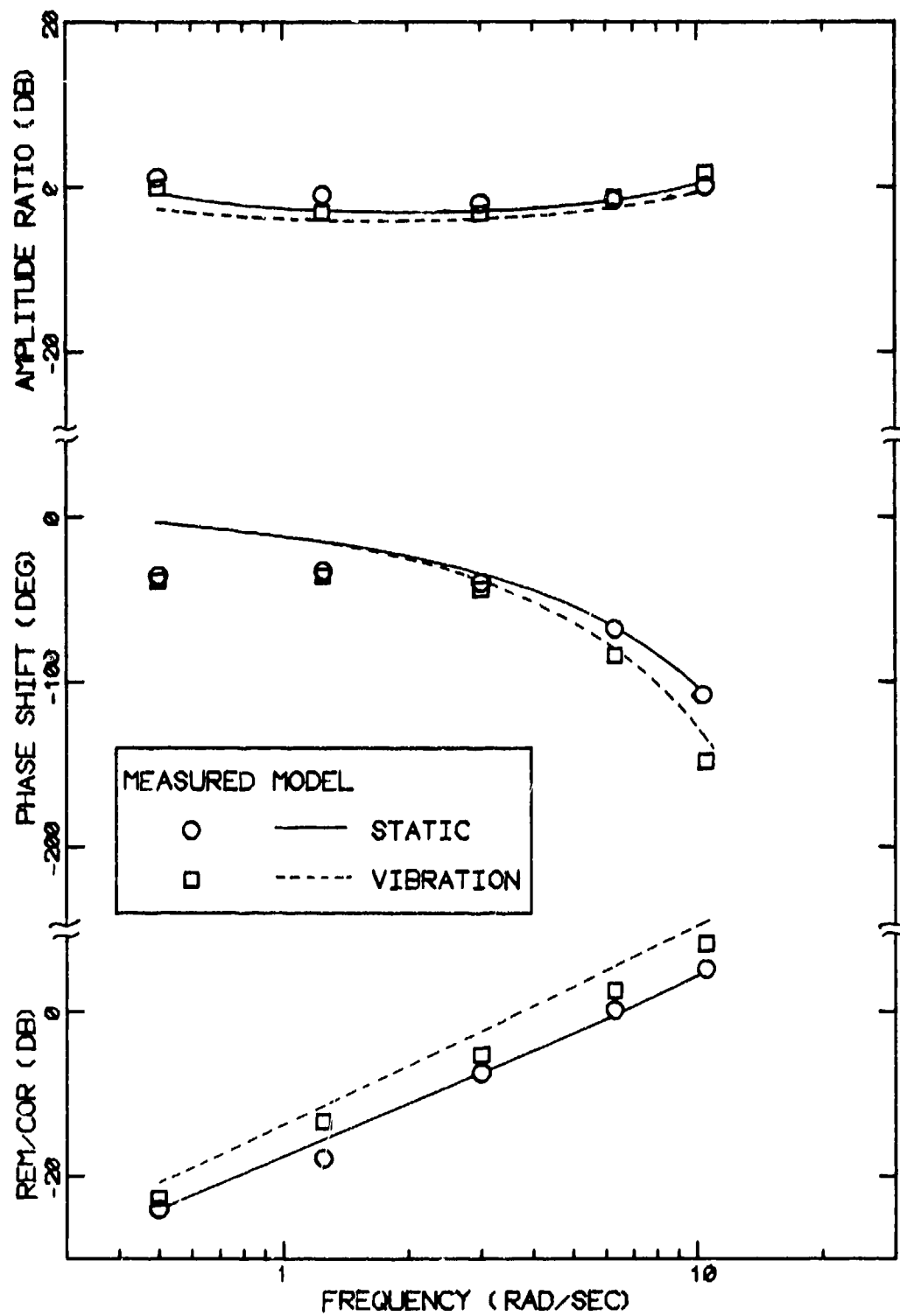Figure C-4.   Frequency-Domain Measures for Medium Spring Stick

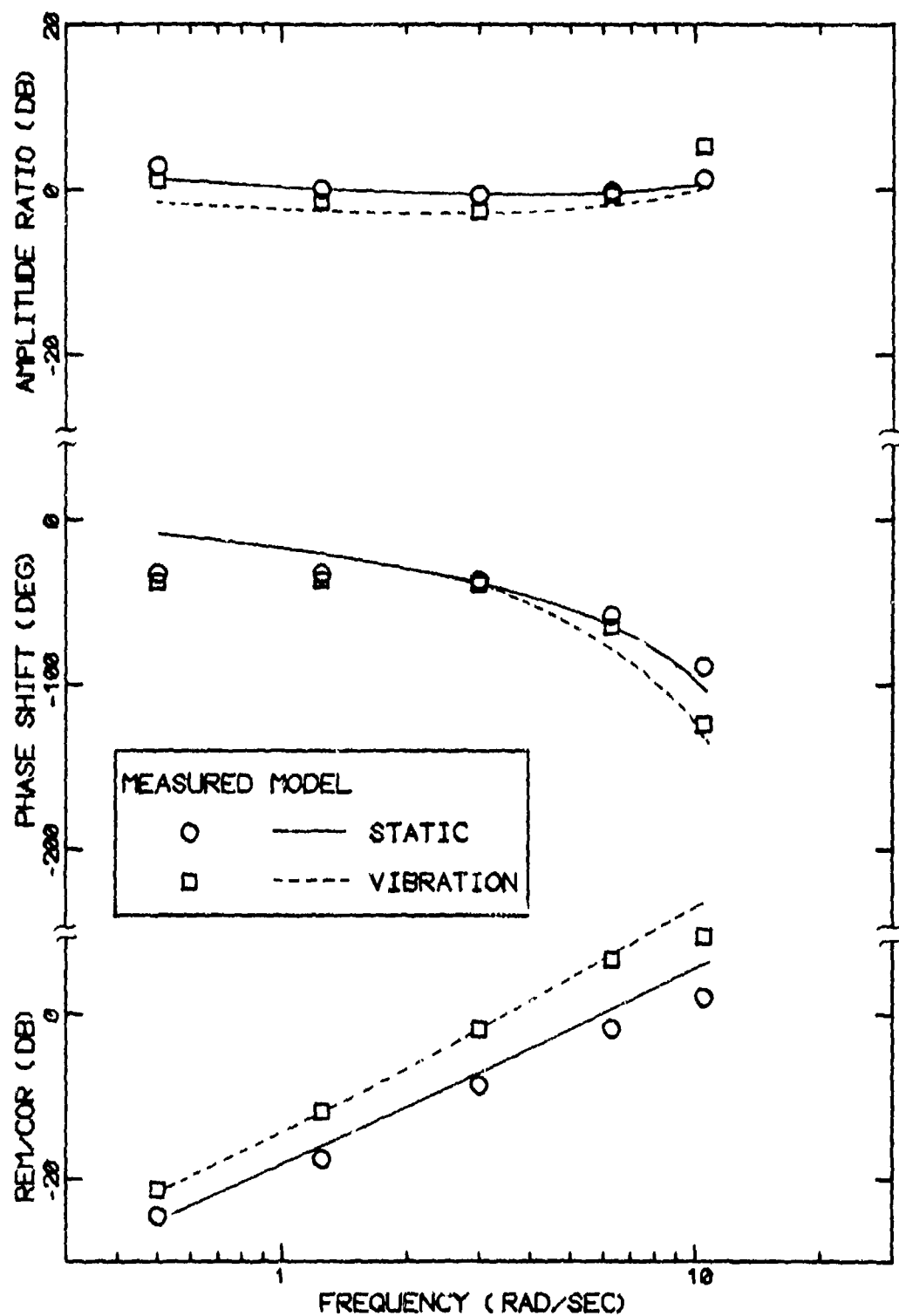Figure C-5. Frequency-Domain Measures for Heavy Spring Stick

C-13

Figure C-6. Frequency-Domain Measures for Light Stiff Stick
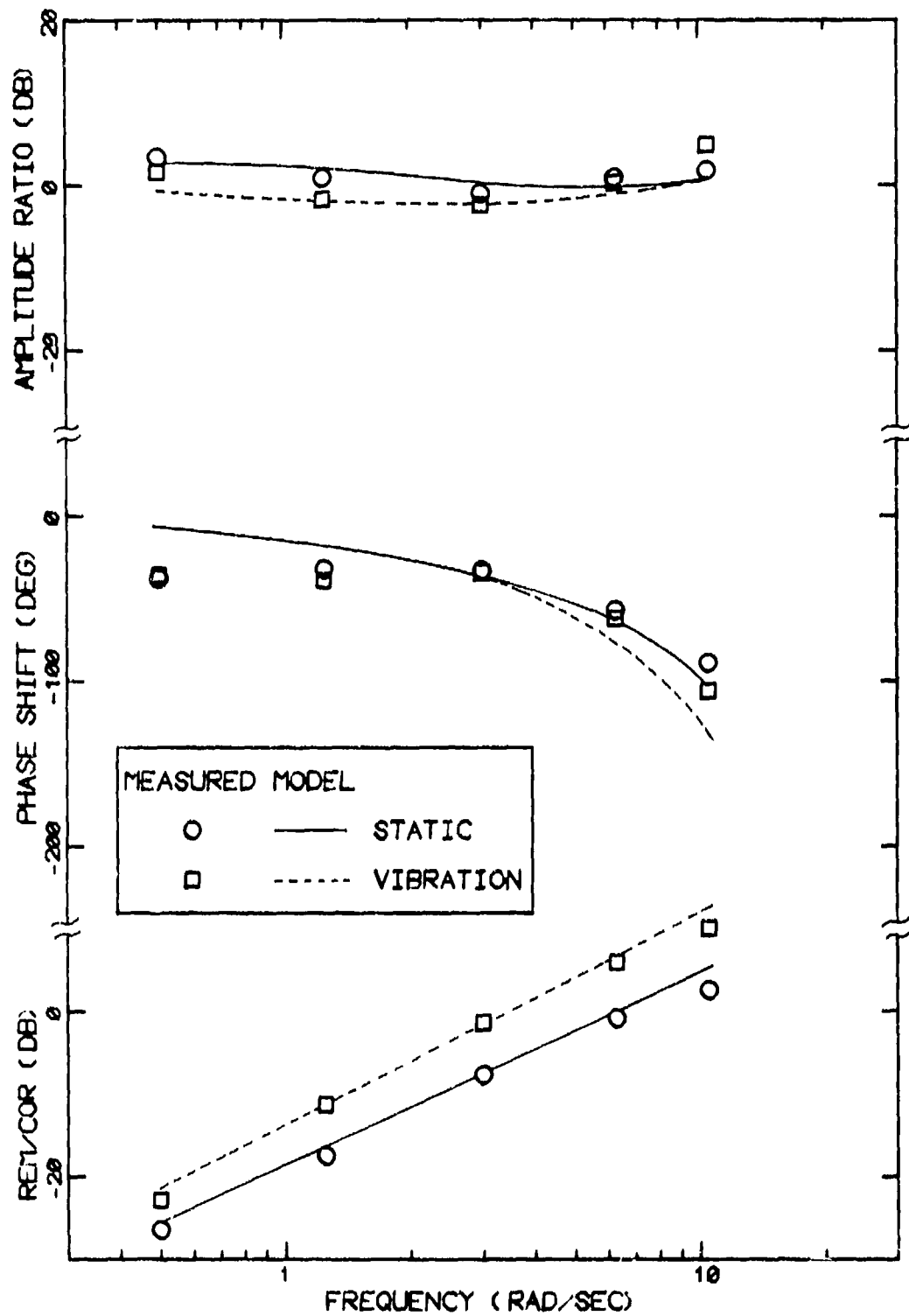
C-14

Figure C-7. Frequency-Domain Measures for Medium Stiff Stick
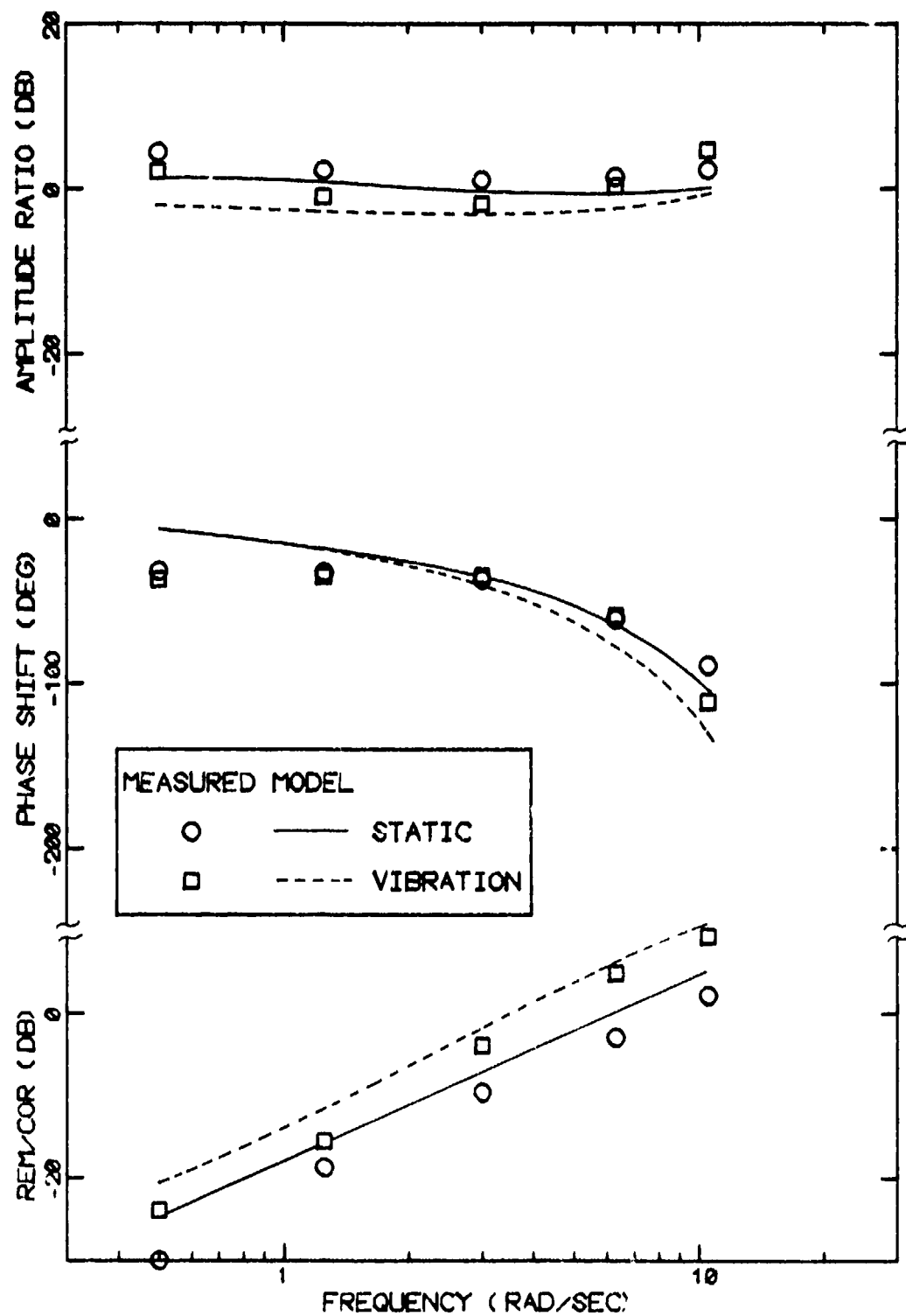
C-15

Figure C-8. Frequency-Domain Measures for Heavy Stiff Stick

Model results are compared with experimental describing functions and ratio spectra in these figures. The model results do not necessarily represent the best match to the data obtained in a given control situation. Rather, we felt that the results of the modeling effort would be more readily interpreted if an acceptable match to the entire body of data could be obtained with a minimum set of parameter values. Therefore, a single set of parameter values was found which best matched the data obtained from the six stick configurations under static conditions. A second set of parameter values was found for the vibration data, with the number of parameters re-evaluated kept to a minimum.

Three changes of parameter values were needed to account for the effects of vibration on tracking performance: (a) an increase in pilot time delay from 0.15 to 0.2 seconds, (b) a ten-fold increase in motor noise/signal ratio, and (c) the introduction of a residual observation noise associated with perception of tracking error. Values for all pilot-related model parameters are shown in Table C-4 for static and vibration conditions. Additional details on the modeling effort — including the procedure for differentiating among possible sources of vibration-related interference — are given in Appendix D.

Data from the six control-stick configurations show similar changes due to vibration. The following trends are observed: (a) the amplitude ratio is decreased by about 2-3 dB at the lowest three input frequencies (0.5, 1.25, and 3 rad/sec), is basically unaffected at 6.3 Hz, and increases 2-4 dB at the highest input frequency (10.5 rad/sec); phase lag is unaffected at lower frequencies, but shows an increase of 15-40 degrees at the highest input frequency; the ratio spectrum shows an overall average increase of about 5 dB with no consistent change in frequency-dependency. For the most part, these effects are mimicked quite well by the model results.

C-17

Table C-4

Values for Pilot-Related Model Parameters

Parameter	Parameter Value	
	Static	Vibration
Cost Functional*	$J = \sigma_e^2 + .03\ \sigma_u^2 + g\sigma_{\dot{u}}^2$	
Time Delay (seconds)	0.15	0.20
Motor Noise/Signal Ratio	0.004	0.04
Observation Noise/Signal Ratio	0.025(-21dB)	0.025(-21dB)
Displacement Threshold (volts)	0.135	0.135
Velocity Threshold (volts/sec)	0.54	0.54
Displacement Residual Noise (volts)	0.0	0.44
Velocity Residual Noise (volts/sec)	0.0	0.0

*Error and control in volts, "g' chosen to provide a motor time
constant of 0.1 seconds.

The describing function results are summarized in terms of gain-crossover frequency and phase margin in Table C-5. For the most part, gain-crossover increased with increasing stick stiffness, ranging from about 3-5 rad/sec for static tracking. Gain-crossover decreased under vibration for all stick configurations, with the average decrease being about 1.0 rad/sec for the spring sticks and 1.4 rad/sec for the stiff sticks. Phase margin increased under vibration by about 10 degrees on the average.

T-tests were performed on the data contained in Table C-5 to determine the statistical significance of vibration-related performance differences. In addition, analysis of variance was performed on the ratio spectrum at a single frequency (3 rad/sec). Table C-6 shows that the effects of vibration on gain crossover, phase margin, and the ratio of remnant to correlated control power were significant at the 0.01 level or better.

Table C-5

Effect of Vibration on Derived Performance Measures

Environment	Stick					
	Spring			Stiff		
	Light	Medium	Heavy	Light	Medium	Heavy

a. Gain-Crossover Frequency, rad/sec

	Light	Medium	Heavy	Light	Medium	Heavy
Static	3.2	3.0	3.3	4.0	4.5	4.9
Vibration	2.4	1.7	2.4	2.8	3.0	3.5

b. Phase Margin, degrees

	Light	Medium	Heavy	Light	Medium	Heavy
Static	47	47	48	47	46	40
Vibration	52	66	53	53	56	52

Table C-6

Summary of Tests for Statistical Significance

Variable	Statistical Test	Significance Level
Gain-Crossover Frequency	t-test	0.001
Phase Margin	t-test	0.01
$\Phi cc_r/\Phi cc_i$	analysis of variance	0.01

APPENDIX D

MODEL ANALYSIS

The important results of the model analysis have been summarized in preceding sections of this report. In this Appendix, we describe some of the tests that were performed to quantify certain model parameters and to differentiate among potential vibration-related interference effects.

D.1 State-Variable Representation of the System

A flow diagram of the control system (including stick-plus-hand dynamics) is diagrammed in the main text in Figure 12. The following identities are made in deriving a state-variable representation for this system:

$$x_1 = \text{tracking input (a first-order noise process)}$$

$$x_2 = \text{tracking error}$$

$$x_3 = \text{electrical control signal}$$

$$x_4 = \dot{x}_3$$

$$y_1 = \text{tracking error}$$

$$y_2 = \dot{y}_1/4$$

$$y_3 = x_3$$

where all state and display variables are in volts.

With the (theoretical) tracking input assumed to be a first-order noise process having a break frequency of 2 rad/sec, the following set of matrix equations defines system dynamics:

$$
\begin{bmatrix} \dot{x}_1 \\ \dot{x}_2 \\ \dot{x}_3 \\ \dot{x}_4 \end{bmatrix} = \begin{bmatrix} -2.0 & 0 & 0 & 0 \\ 2.0 & 0 & 4.0 & 0 \\ 0 & 0 & 0 & 1.0 \\ 0 & 0 & -386.4\, K_s/M & -386.4\, B/M \end{bmatrix} \cdot \begin{bmatrix} x_1 \\ x_2 \\ x_3 \\ x_4 \end{bmatrix} + \begin{bmatrix} 0 \\ 0 \\ 0 \\ 386.4\, K_e/M \end{bmatrix} u + \begin{bmatrix} 2.0 \\ 0 \\ 0 \\ 0 \end{bmatrix} w
$$

$$
\begin{bmatrix} y_1 \\ y_2 \\ y_3 \end{bmatrix} = \begin{bmatrix} 0 & 1.0 & 0 & 0 \\ 0.5 & 0 & 1.0 & 0 \\ 0 & 0 & 1.0 & 0 \end{bmatrix} \cdot \begin{bmatrix} x_1 \\ x_2 \\ x_3 \\ x_4 \end{bmatrix}
$$

where

w = white noise process with covariance equal to the variance of the input x_1

K_s = stick spring gradient, pounds/inch

B_s = stick damping, pounds/(inch/sec)

M = combined mass of stick and forearm, pounds

The display vector defined for this problem is somewhat non-standard in that (a) the display quantity y_2 is equal to one-fourth the error rate, rather than simply the error rate, and (b) the pilot's control input x_3 is included in the display vector. The reason for using one-fourth the error rate in this problem is that this quantity corresponds directly to one of the problem

D-2

variables recorded during the analog simulation. Model analysis is unaffected, except that threshold and rms residual noise levels associated with error rate should be divided by 4.

The third display quantity is included to allow us to determine the pilot describing function. As presently implemented, the model can predict describing functions between any display quantity and the "theoretical" control variable, which, for this problem, is the control force "F" (see Figure 12. Therefore, we must first predict the describing functions between error and force input and between electrical input and force input. We then cascade these describing functions to yield the desired describing function relating electrical control input to tracking error, which may then be compared with the corresponding measurement derived from the experimental data.

D.2   Static Tracking

Model analysis was first performed on the data obtained in the absence of vibration. A single set of model parameters was derived to provide a good overall match to the data obtained from all six control-stick configurations. The goal (not always achieved) was to match the measured rms error and control scores to within 10% and to match pilot describing functions and "ratio spectra" (ratio of remnant to input-correlated stick power) with 1 or 2 dB.

Determination of certain specific model parameters is described below.

D.2.1 Effective Control Intertia

We first attempted to predict the effects of stick design
on tracking performance using only the stick mass as the variable
"M" in the problem formulation. This approach, however, did not
allow the model to predict performance differences observed for
the various control configurations. Much better correspondence
to experimental results was obtained when M was increased to
include the mass of the forearm (as given in Allen et al. [7]).

D.2.2 Cost Weignting Coefficients

Initial modeling was attempted with a "cost" determined as
in previous analysis of single-variable systems [1, 2]; namely,
with cost equal to a weighted sum of mean-squared tracking error
and mean-squared control rate, where the relative weighting was
chosen to yield a motor time constant of about 0.1 seconds.
Reasonably small matching errors were found for most of the control
configurations, but the predicted error for the heavy spring stick
was about 23% below that found experimentally.

Since the control forces required by this control configu-
ration were greater than those required by the remaining five
configurations, we felt that the pilot's unwillingness to generate
large control forces might have been important in this case.
Therefore, a cost on control force was added to the total cost
expression, with the associated weighting factor chosen to provide
a good match to the heavy spring data. (The weighting on control
rate was readjusted to maintain the motor time constant at 0.1
seconds.) Because of the lesser control forces required by the
other control sticks, the match between model output and experi-
mental measurement was little effected in these cases by the

addition of the cost weighting on control force. Accordingly, the augmented cost expression was used for the remainder of the model analysis.

D.3   Vibration Tracking

Having "calibrated" pilot-related model parameters for static tracking, we then attempted to match the data obtained in vibration conditions. Our goal was again to obtain a good overall match to all six control sticks with a consistent set of model parameters and to do so with as few parameter changes as possible.

D.3.1 Modeling Visual Effects

Having estimated relative rms displacement and velocity of the eye-point-of-regard with regard to the display (Section B.4), tests were performed to determine the best way of representing the effects of blur in terms of parameters of the tracking model. These tests were made for the heavy spring stick configuration.

For our first test, we simply assumed that the effect of blurring was to render velocity information useless. This hypothesis was modeled by associating a very large noise/signal ratio with velocity perception. Other model parameters remained unchanged. Although a reasonably good match was obtained for tracking error and pilot describing function, the frequency-dependency of the ratio spectrum was not reproduced. The model predicted too little remnant power at low frequencies and too much at high frequencies.

For the second test, we set the rms residual noise associated with displacement perception equal to the average estimated rms eye-display displacement; similarly, residual noise on rate perception was equated to the estimated rms relative velocity. The results were essentially the same as in the first test, with the same gross mismatch between predicted and measured ratio spectra.

Finally, displacement residual noise was defined as in the second test, and rate residual noise was set to zero (i.e., we assumed no degradation in rate perception). This model change alone produced an insufficient increase in tracking error and control activity to account for the effects of vibration. Good results were obtained in conjunction with other parameter changes, however, and this treatment of visual effects was adopted for the model validation tests shown in the text of this report.

D.3.2 Other Non-Motor Related Effects

Attempts were made to account for the effects of vibration through re-adjustment of the observation noise/signal ratio. This model parameter is believed to reflect primarily central-processing limitations, although certain visual effects could also show up as a change in this parameter. Again, the model was tested against data from the heavy spring stick experiment.

With the remaining model parameters unchanged from the static situation, observation noise/signal ratio was increased to match the rms error obtained during vibration. A reasonably good match was obtained to pilot gain; however, the predicted ratio spectrum increased by about 2 dB more than was observed experimentally. We therefore concluded that changing observation noise alone could not account adequately for the effects of vibration on tracking performance.

D-6

D.3.3 Motor-Related Effects

Three motor-related model parameters were explored: (a)
motor time constant, (b) time delay, and (c) motor noise. Decreasing
the motor tire constant (i.e., increasing the weighting coefficient
on control rate) did not yield effects consistent with those
observed experimentally. For example, the predicted rms control
score decreased, whereas the data showed about a 25% increase for
the heavy spring configuration. In addition, a poor match was
obtained to the frequency-domain results at high frequencies.
Consequently, we concluded that vibration had no significant
effect on this parameter, and the motor time constant was hence-
forth kept at 0.1 second.

With residual noise determined as described in D.3.1 and
with other parameter values appropriate to static tracking,
changes in time delay and motor noise were explored. An
acceptable match to the vibration results could not be obtained
through a change in only one of these parameters. Although we
could not precisely allocate the effects of vibration between
these two parameters, a good match to the data was obtained
with a time delay of 0.2 seconds and a motor noise/signal ratio
of 0.027 (motor noise variance divided by the variance of the
predicted control force). (Corresponding parameter values for
static tracking were 0.15 seconds and .0036, respectively.)

Model results were then tested against data obtained from
the remaining five control configurations to find the set of
parameter values that would provide the best overall match.
Residual noise and time delay were quantified as described
above, and motor noise/signal ratio was increased to 0.04 to
provide a better overall match. Remaining parameter values were
the same as used in matching static tracking results.

D.3.4 Relation of Motor Noise to Control Variance

It was suggested in a recent analysis of lateral-axis vibration that the motor noise varies in fixed proportion to the total control variance, where "total" variance is defined as the control variance related to tracking (including remnant) plus the effects of vibration feedthrough [10].

The spring-stick data do not appear to support this hypothesis. On the average, vibration caused the total variance to increase by about a factor of 2 (i.e., 3 dB). Model analysis shows that an increase in motor noise variance of greater than 10 dB is needed to account for the difference between vibration and static tracking. We therefore tentatively conclude that, while the motor noise may vary with control activity, the ratio of motor noise variance to control variance is influenced by the vibration environment.

APPENDIX - E ANTHROPOMETRIC RELATIONSHIPS

A series of 15 anthropometric dimensions were measured on the subjects used in this study. These measurements were made to determine the comparability of the body-size distribution of the test subjects with the body size distribution of rated Air Force men and to provide the basis for seeking relationships between body-size characteristics of the subject and effects of vibration on their performance. This latter objective will be pursued when a sample adequate for the required analyses is available.

SELECTED ANTHROPOMETRY OF SUBJECTS
IN THIS STUDY AND RATED AIR FORCE OFFICERS

	This Study			AF Rated Officers (1967)		
	$\overline{X}$	SD	N	$\overline{X}$	SD	N
Age*	32.6	7.2	8	29.5	6.3	2420
Weight	78.6	7.0	8	78.7	9.7	2420
Stature	175.5	6.1	8	177.3	6.2	2420
Sitting Height	91.8	2.7	8	93.2	3.2	2420
Thumb-Tip Reach	80.6	5.7	8	80.3	4.0	2420

*Age in years, weight in kilograms, all other dimensions in centimeters.

APPENDIX F
REFERENCES

1. Kleinman, D. L., S. Baron and W. H. Levison, "An Optimal-
   Control Model of Human Response, Part 1: Theory and Validation,"
   Automatica, Vol. 6, pp. 357-369 (1970).

2. Kleinman, D. L., S. Baron and W. H. Levison, "A Control Theoretic
   Approach to Manned-Vehicle Systems Analysis," IEEE Trans. on
   Auto. Control, Vol. AC-16, No. 6 (December 1971).

3. Baron, S. and W. H. Levison, "A Manned Control Theory Analysis
   of Vertical Situation Displays for STOL Aircraft,"
   NASA CR-114620 (April 1973).

4. Levison, W. H., "The Effects of Display Gain and Signal
   Bandwidth on Human Controller Remnant," Wright-Patterson Air
   Force Base, AMRL-TR-70-93 (March 1971).

5 Kleinman, D. L. and S. Baron, "Analytic Evaluation of Display
   Requirements for Approach to Landing," NASA CR-1952 (November
   1971).

6. Air Force Office of Scientific Research, Contract No.
   F44620-73-C-0075.

7. Allen, R. W., Jex, Henry R. and R. E. Magdaleno, "Manual Control
   Performance and Dynamic Response During Sinusoidal Vibration,"
   AMRL-TR-73-78, Systems Technology, Inc., 13766 South Hawthorne
   Blvd, Hawthorne, California. October 1973.

8. Magdaleno, R. E., Allen, R. W. and Henry R. Jex, "Vertical
   Vibration Interference on a Pitch Attitude Control Task,"
   in the Proceedings of the Tenth Annual Conference on Manual
   Control. Air Force Institute of Technology, Air Force
   Flight Dynamics Laboratory, Wright-Patterson Air Force Base,
   Ohio. (9-11 April 1974).

9. Meiry, Jacob L., "Vestibular and Proprioceptive Stabilization of Eye Movements," in Paul Bach-Y-Rita, Carter C. Collins, and Jane E. Hyde (eds.), The Control of Eye Movements, Academic Press, N. Y., 1971, pp. 483-496.

10. Levison, William H.; "Analysis of Vibration-Induced Pilot Remnant," BBN Report No. 2608, Final Report,(August 1973). Under Contract No. F33615-71-C-1207.

11. Levison, W. H., J. I. Elkind and J. L. Ward, "Studies of Multi-variable Manual Control Systems: A Model for Task Interference," NASA CR-1746 (May 1971).

12. Cooley, J. W., J. W. Tukey, "An Algorithm for the Machine Calculation of Complex Fourier Series," Mathematics of Computation 10, No. 90, pp. 297-301,(April 1965).